

1-1-1995

A study of bistable behavior and parameter variation in dark molecular clouds

Robert Lee Vaughn
University of Nevada, Las Vegas

Follow this and additional works at: <https://digitalscholarship.unlv.edu/rtds>

Repository Citation

Vaughn, Robert Lee, "A study of bistable behavior and parameter variation in dark molecular clouds" (1995). *UNLV Retrospective Theses & Dissertations*. 2991.
<http://dx.doi.org/10.25669/ofx5-ue20>

This Dissertation is protected by copyright and/or related rights. It has been brought to you by Digital Scholarship@UNLV with permission from the rights-holder(s). You are free to use this Dissertation in any way that is permitted by the copyright and related rights legislation that applies to your use. For other uses you need to obtain permission from the rights-holder(s) directly, unless additional rights are indicated by a Creative Commons license in the record and/or on the work itself.

This Dissertation has been accepted for inclusion in UNLV Retrospective Theses & Dissertations by an authorized administrator of Digital Scholarship@UNLV. For more information, please contact digitalscholarship@unlv.edu.

INFORMATION TO USERS

This manuscript has been reproduced from the microfilm master. UMI films the text directly from the original or copy submitted. Thus, some thesis and dissertation copies are in typewriter face, while others may be from any type of computer printer.

The quality of this reproduction is dependent upon the quality of the copy submitted. Broken or indistinct print, colored or poor quality illustrations and photographs, print bleedthrough, substandard margins, and improper alignment can adversely affect reproduction.

In the unlikely event that the author did not send UMI a complete manuscript and there are missing pages, these will be noted. Also, if unauthorized copyright material had to be removed, a note will indicate the deletion.

Oversize materials (e.g., maps, drawings, charts) are reproduced by sectioning the original, beginning at the upper left-hand corner and continuing from left to right in equal sections with small overlaps. Each original is also photographed in one exposure and is included in reduced form at the back of the book.

Photographs included in the original manuscript have been reproduced xerographically in this copy. Higher quality 6" x 9" black and white photographic prints are available for any photographs or illustrations appearing in this copy for an additional charge. Contact UMI directly to order.

UMI

A Bell & Howell Information Company
300 North Zeeb Road, Ann Arbor, MI 48106-1346 USA
313/761-4700 800/521-0600



A STUDY OF BISTABLE BEHAVIOR AND PARAMETER
VARIATION IN DARK MOLECULAR
CLOUDS

by

Robert L. Vaughn

A dissertation submitted in partial fulfillment
of the requirements for the degree of

Doctor of Philosophy

in

Physics

Department of Physics
University of Nevada, Las Vegas
December 1995

UMI Number: 9614369

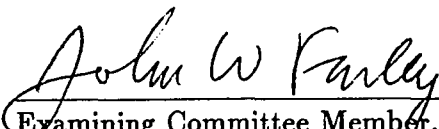
UMI Microform 9614369
Copyright 1996, by UMI Company. All rights reserved.

**This microform edition is protected against unauthorized
copying under Title 17, United States Code.**

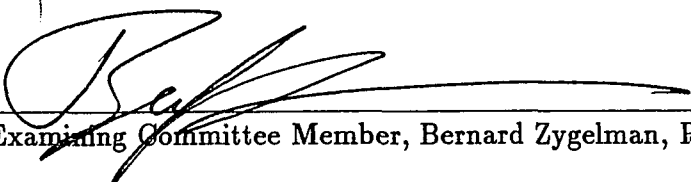
UMI
300 North Zeeb Road
Ann Arbor, MI 48103

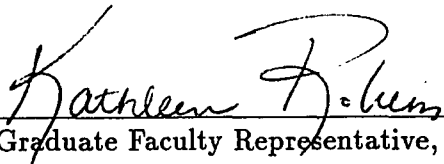
The Thesis of Robert Vaughn for Degree of Ph.D. in Physics is approved.

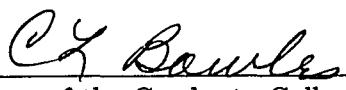
 11/14/95
Chairperson, Stephen Lepp, Ph.D.

 11/15/95
Examining Committee Member, John Farley, Ph.D.

 11/17/95
Examining Committee Member, Jim Selser, Ph.D.

 11/20/95
Examining Committee Member, Bernard Zygelman, Ph.D.

 11-15-95
Graduate Faculty Representative, Kathleen Robins, Ph.D.

 11-20-95
Interim Dean of the Graduate College Cheryl L. Bowles, Ed.D.

University of Nevada, Las Vegas
December 1995

ABSTRACT

A study of Bistable Behavior and Parameter Variation in Dark Molecular Clouds. investigates the phenomenon of bistability and its relation to phase transitions, derives an analytical model of fractional ionization and does a parameter study. Specifically, this investigation focuses on several different types of phenomena that are associated with the modeling of giant and dark molecular clouds. The chemical model of a molecular cloud consists of a set of stiff coupled differential equations. Each differential equation represents the the rate of change of the abundance of a chemical species in the molecular cloud. Analytical approximations to the fractional ionization are presented.

The models are found to have bistable solutions for a range of temperatures and densities. The range over which the bistable solutions exist are shown to dependent on; cosmic-ray ionization rate, elemental abundances, grain population and chemical reaction rate coefficients.

A parameter study over a range of temperatures and densities which have been inferred for the interstellar medium. The results of this study are compared to observed chemical abundances in the Taurus Molecular Cloud 1, L134, the Orion Ridge and Sagittarius B2. We examine the study for trace species which are particularly good

indicators of temperature and density. For example, H_2O is a useful probe for determining temperature and OH is a useful probe for determining density. In addition we have mapped out the water, molecular oxygen, atomic carbon and carbon monoxide abundances that will be compared to observations made by the Submillimeter Wave Astronomy Satellite (SWAS).

TABLE OF CONTENTS

ABSTRACT	iii
LIST OF FIGURES	vii
LIST OF TABLES	ix
ACKNOWLEDGMENT	vi
CHAPTER 1 ASTROPHYSICAL MODELING	1
Early Results 1926-1962	2
Discovery of Molecules and Molecular Clouds	3
The First Chemical Model 1973	5
The evolution of chemical models 1977-1990	7
Problems which Motivated the Investigation	8
Synopsis of Dissertation	11
CHAPTER 2 GIANT AND DARK MOLECULAR CLOUDS	12
The Morphology of Molecular Clouds	14
The Orion Complex	15
The Giant Complex Sgr B2	15
The TMC1	18
Grains	18
Synthesis of Molecular Hydrogen on Grains	20
Cosmic Rays and Molecular Clouds	22
Cosmic Ray Induced Ultraviolet Photons	22
The Heating and Cooling of Cold Clouds	23
The Heating Process	23
The Cooling Process	24
Heating of Cold Dark Clouds	26
The Cooling Process of Dark Clouds	26
CHAPTER 3 GAS PHASE REACTIONS IN MOLECULAR CLOUDS	28
Reaction Rate Coefficients	29

Cosmic Ray Ionization	30
Radiative Recombination	30
Dissociative Recombination	31
Ion-molecule reactions	31
Charge Transfer	32
Neutral-Neutral	33
Radiative Association	33
Mutual Neutralization	34
Radiative attachment	35
Summary	35
CHAPTER 4 GENERAL MOLECULAR CLOUD CHEMISTRY	36
Initiation Chemistry in Dark Clouds	36
Helium	38
Destruction of H_3^+	38
Oxygen Carbon Chemistry	39
Oxygen Chemistry	39
Nitrogen Chemistry	41
Production of Hydrocarbons	42
Production of Methane	43
Production of Acetaldehyde	43
Production of Methanol	43
Production of Methyl Cyanide	43
Production of Methyl Amine	44
Production of Carbon Chains	44
Synthesis C_2H_2	44
Synthesis C_4H	45
Effect of Ionic Helium	45
Sulfur Chemistry	46
Chemistry of Metals	47
Effects of Large Molecules	47
Long Chained Molecules	48
Summary	49
CHAPTER 5 THE GAS PHASE CHEMICAL MODEL	50
Model Construction	51
Chemical Rates	51
Cosmic Ray or Photo Reactions	52
Binary Reaction	52
A General Expression for the Rate for a Species Y	53
A Toy Model	56
The Full Model	58
Reaction Rate Coefficients for the UMIST Ratefile	59

Two Bodied Reactions Rate Coefficients	61
Cosmic Ray Ionization Rate	61
Photoionization	62
Induced Cosmic Ray Ionization	62
Elemental Abundances	63
Initial Conditions	64
Stiff differential equations	65
Data Structures	66
Description of the Data Structure	67
Creation of the Data Structure	68
Description of LSODA.F	68
Description of LINPACK	69
CHAPTER 6 BISTABILITY	71
Fractional Ionization	72
Phase Transitions	73
Procedure to Find a Bistable Region	74
The Bistability Diagram	77
The Cusp Catastrophe	81
Summary	83
CHAPTER 7 PHASE TRANSITIONS IN MOLECULAR CLOUDS	85
The slope of the fractional ionization	85
The General Chemistry of the LIP and the HIP	86
Mathematical Conditions for the HIP and LIP	92
The Amount of Metal Necessary to Maintain the HIP in TMC1	97
The Addition of Electron Rich Sources	99
Hydrogen Oxygen Chemistry	99
Carbon Oxygen Chemistry	103
Sulphur Chemistry	107
Metals	110
<i>He</i> ⁺ and <i>C</i> ⁺	112
Nitrogen	113
Silicon Chemistry	116
Hydrocarbon Chemistry	116
Summary	118
CHAPTER 8 BISTABILITY AND PARAMETER VARIATION	122
The Bistable Region	122
Elemental Abundances	123
Effects of Oxygen on the bistable region	123
Effects of Carbon on a Bistable Region	125
Nitrogen	126
Effects of Sulfur	128

Effect of Metals	129
Silicon	132
Effects of Cosmic Ray Ionization	132
Effects of Dissociative Recombination	134
Variation of Temperature and Density	136
Effects of Large Molecules	136
Summary	140
CHAPTER 9 APPROXIMATIONS OF THE FRACTIONAL IONIZATION ..	143
No metals	143
Oppenheimers Fractional Ionization Equation	145
The Effect of Cosmic Ray Induced Photons	152
Summary	158
CHAPTER 10 A PARAMETER STUDY	159
Selection of a Parameter Set	159
Results on Grid Boundary	160
Effects of low number densities on the abundance	160
Effects of temperatures above 300 K	162
Analysis of Variance of the Grid	163
OH as a Probe of Density	165
Comparison of Model with Observations	166
Taurus Molecular Cloud TMC1	167
L134	169
Orion Ridge and Sgr B2	169
Representive Results of the Parameter Study	172
Summary	173
CHAPTER 11 CONCLUSIONS	175
Bistability	175
Chemistry as a Probe of Physical Conditions	176
The Model of Interstellar Clouds	177
REFERENCES	178

LIST OF FIGURES

Figure 1 The NH_3 Contours of an Interstellar Clouds	16
Figure 2 The Orion Complex	17
Figure 3 The TMC Cloud	19
Figure 4 Phase Transition for H_2O Molecule	74
Figure 5 This Graph illustrates the phase transition	75
Figure 6 The phase transition for $50-3000\text{ cm}^{-3}$	76
Figure 7 The phase transition $3000-50\text{ cm}^{-3}$	76
Figure 8 Superposition Figs. 6 and 7 Note the Bistable Region	77
Figure 9 Points in the Bistable Region	78
Figure 10 Graph of a Cusp Catastrophe	82
Figure 11 Traversing the Cusp Catastrophe	83
Figure 12 The ratio H_3^+ to H^+	90
Figure 13 H_3^+ at Phase Transition.....	90
Figure 14 Major Atomic ions C^+, H^+, S^+ for HIP and LIP	91
Figure 15 Behavior of Molecular Ions.....	93
Figure 16 Behavior of Molecules HIP and LIP	93
Figure 17 HIP Reaction Networks for the Hydrogen Oxygen Chemistry	101
Figure 18 LIP Reaction Networks for the Hydrogen Oxygen Chemistry	102
Figure 19 HIP Reaction Networks for the Carbon Oxygen Chemistry	105
Figure 20 LIP Reaction Networks for the Carbon Oxygen Chemistry	106
Figure 21 Behavior of S near the Phase Transition	108
Figure 22 Behavior of S+ and SO near the Phase Transition	109
Figure 23 Behavior of S, S+, and SO near the Phase Transition	109
Figure 24 LIP Reaction Networks for the NO Chemistry	114
Figure 25 HIP Reaction Networks for the NO Chemistry	115
Figure 26 LIP Reaction Networks for the Hydrocarbon Chemistry	119
Figure 27 HIP Reaction Networks for the Hydrocarbon Chemistry	120
Figure 28 Note as O is enhanced the Bistable Region Disappears	124
Figure 29 Note as O is depleted the Bistable Region Shrinks	125
Figure 30 Note as C is enhanced the Bistable Region Disappears.....	126
Figure 31 Note as C is Depleted the Bistable Region Disappears.....	127
Figure 32 Effect of Nitrogen for abundances 1.0 0.5 and 2	127
Figure 33 Effect of Sulphur on the Bistable Region	128
Figure 34 The Bistable Region exist at low n with only H He C N O present ...	129

Figure 34 Effect of small sulphur depletions on the bistable region	130
Figure 35 As Mg initial abundance is increased the hysteresis loops shifts	130
Figure 36 Extreme Enhancement of Mg	131
Figure 37 Note of hysteresis loop shrinks metallic abundance increases	131
Figure 38 In this example the loop is small indicating the HIP will dominate ..	132
Figure 39 Silicon will behave like a metal for large enhancements	132
Figure 40 Effect of doubling the ionization rate sulphur density= 10^6	133
Figure 41 Note the effect of increasing the cosmic ray ionization rate	134
Figure 42 Increasing the Dissociative Recombination Rate	135
Figure 43 Surface Plot of Temperature and Number Density	137
Figure 44 Disappearance of Bistability as n_{LM} increases	141

LIST OF TABLES

Table 1 Observed and Calculated Molecular Abundances	7
Table 2 Properties of Molecular Regions in the Interstellar Medium	13
Table 3 Cooling Wavelength for Various Species	25
Table 4 Various Reactions that Occurring inside Interstellar Clouds	29
Table 5 Table of Species in the UMIST Ratefile	60
Table 6 Cloud Abundances and Solar Abundances	64
Table 7 Rates for H_3^+ in HIP and LIP	94
Table 8 Rates for Electrons in HIP and LIP	94
Table 9 Hydrogen Oxygen Abundances at HIP and LIP	103
Table 10 Oxygen and Carbon Species At High and Low Ionization	104
Table 11 Sulphur High and Low Ionization	108
Table 12 Metals at High and Low Ionization	111
Table 13 Silicon and Magnesium at High and Low Ionization	116
Table 14 Abundances of Selected Hydrocarbons n=1450	121
Table 15 Dissociative Recombination Rates and Investigators	135
Table 16 Third Most Abundant Species	160
Table 17 OH Abundances	166
Table 18 The HCN to HNC Ratio $\frac{HCN}{HNC}$	167
Table 19 TMC1 Abundnaces	168
Table 20 L134 Abundnaces	169
Table 21 Orion Ridge Abundnaces	170
Table 22 Sgr B2 Abundnaces	171
Table 23 Parameter Study: T=10 K, T=50 K and T=200 K n=10 ²	172
Table 24 Parameter Study: T=10 K, T=50 K and T=200 K n=10 ⁴	173
Table 25 Parameter Study: T=10 K, T=50 K and T=200 K n=10 ⁶	174

ACKNOWLEDGMENTS

I would like to thank the University of Nevada Las Vegas and the Department of Physics for the opportunity to study Physics. I would like to thank John Farley for inviting me to Las Vegas in 1992 and Steve Lepp for being my advisor. I would like to thank my wife Wei Xia (Wishy) for her patience. I appreciate the computer assistance from Terry Gibbons and John Kilburg. I would like to thank David Miller for proofreading comments. Finally, I would like to thank to NSF EPSCoR and NASA for support.

Chapter 1

Astrochemical Modeling

Astrochemical research entered its modern period in 1963 with the discovery of the OH radical. The combined efforts of radio and optical astronomers, coupled with those of theoretical astrophysicists and experimentalist, have lead to a rich understanding of the chemical processes occurring within dark interstellar clouds.

Models of the gas-phase chemistry in astrophysics, are now sufficiently sophisticated to accommodate 5000 reactions and 500 species. These models are capable of giving reasonable estimates for the abundances of a variety of chemical species. Thus it is possible to check the predictive power of some of the models. However, there are still problems associated with gas phase models which require further investigation.

This investigation will address the problem of bistable solutions and their associated phase transitions, an analytical approximation for the fractional ionization and a parameter study. This chapter will review the important literature which lead to the discovery of bistability in dark cloud models.

The final section of this chapter gives a brief outline of the dissertation.

Early Results 1926-1962

The existence of interstellar molecules was originally suggested by A.S.Eddington in the Barkerian Lectures (Eddington 1926). Eddington's speculations were confirmed by the discovery of four unknown spectral lines by Merrill in 1934. These lines were identified and are associated with CH^+ , CH , and CN . An attempt to calculate molecular abundance from the intensity of spectral lines was made by Swings and Rosenfeld in 1937. The problem with the Swings and Rosenfeld model was that their assumption was based on the existence of thermodynamic equilibrium. Their model used the Boltzmann Distribution to obtain the ratio of population in excited states to ground states. This would allow them to predict abundance by using $\frac{n_i}{n_0} = \exp(-\frac{\Delta E}{kT})$.

However, the interstellar medium is not in equilibrium. Equilibrium conditions do not exist because the diffuse clouds where these molecules are observed is at 100K, while the ultraviolet photons have energies of 10-20 eV. Since there are 11606 degrees Kelvin per electron volt, the temperature of the photons is greater than the temperature of the cloud.

Despite their unsuccessful attempt to compute abundances they proposed a continuing search for diatomics in the interstellar medium (Swings and Rosenfeld 1937). The first reported attempt to do gas phase chemistry in a non-equilibrium state was by Kramers and ter Haar (1946). They constructed a gas phase model which used specific rate constants to account for the formation and destruction of CH and CH^+ (Kramers and ter Haar 1946). Bates and Spitzer (1951) improved the Kramers Model

by computing more reliable rate coefficients.

The generally accepted theory until the mid-1960's was that the interstellar medium was too hostile to allow molecules to exist for an extended period of time. This conclusion was reasonable since only three stable species CH , CH^+ and CN had been detected. Most scientists were convinced that it was possible for large molecules to be formed on interstellar dust, but they also believed these molecules would be short-lived because of the intense radiation which was associated with the interstellar medium.

Discovery of Molecules and Molecular Clouds

A revolutionary discovery occurred in 1963 with the observation of the two ground state transitions of the hydroxyl radical OH . By using techniques of microwave absorption, Weintraub was able to identify two new transitions in the microwave spectrum (Weintraub, Barrett, Meeks and Henry 1963). Weintraub's discovery was important for two reasons: it provided incontrovertible evidence that supported the existence of molecules in dark clouds and it was responsible for the creation of a new observational method for detecting microwave spectral lines (Weintraub 1963).

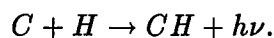
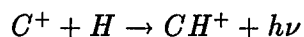
Research into interstellar clouds intensified after 1968, centimeter and millimeter observations led to the discovery of more than 30 molecules. In particular, the detection of microwave transitions in the late sixties led to the discovery of ammonia NH_3 , water vapor H_2O , and formaldehyde H_2CO in the cores of dark clouds. The discovery of molecules in dark clouds motivated astrophysicists to reexamine their

assumption that molecules are rapidly destroyed in the interstellar medium.

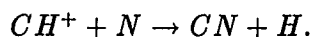
In the early 1970's, analysis of absorption lines in the ultraviolet region led to the discovery of H_2 , HD and CO . Much of the data for these discoveries was accumulated using rockets and the Copernicus satellite. Concurrent observations of atomic hydrogen illustrated that atomic hydrogen was converted into molecular hydrogen in regions of obscuration. By the end of 1971 over 21 molecular species had been detected in the dark interstellar clouds (Litvak 1972).

The major question at the beginning of the 1970's was how to account for the large number of molecules. The observation of an increasing number of molecules led Solomon and Klemperer (1972) to suspect that the existence of diatomics could be explained by standard chemical reactions. Using high quality data provided by Herbig (1970) they proceeded to calculate rate coefficients for various gas phase chemical reactions which produce diatomics.

Solomon and Klemperer (1972) also suggested mechanisms to explain the formation of CH^+ , CH and CN . Their work used radiative association to explain the formation of CH^+ and CH :



They also showed that CN could be formed by the ion-molecule reaction:



Before, Solomon and Klemperer's research, dense interstellar clouds were thought to be too cold to allow chemical reactions to occur. Solomon and Klemperer (1972) realized that electronic reactions between ions and neutral species can be very rapid at low temperatures. They were able to calculate a set of rate constants which provided some explanation as to why molecules form in dark interstellar clouds.

The First Chemical Model 1973

Herbst and Klemperer (1973) were the first to define a chemical model of a dark interstellar cloud. The method used by Herbst and Klemperer was to model chemical networks as a system of kinetic equations. Herbst and Klemperer set up 35 differential equations, one for each species in the model. Their reaction set consisted of 100 reactions. The system of equations they used had a form similar to the following set of equations.

$$\frac{dX_1}{dt} = \Sigma k_r X_q X_r n - \Sigma k_{mn} X_n X_m n + \Sigma_i k_i X_i - \Sigma_j k_j X_j$$

$$\frac{dX_2}{dt} = \Sigma_{pr} k_{pr} X_q X_r n - \Sigma k_{mn} X_n X_m n + \Sigma_i k_i X_i - \Sigma_j k_j X_j$$

⋮

$$\frac{dX_{35}}{dt} = \Sigma_{pr} k_{pr} X_q X_r n - \Sigma k_{mn} X_n X_m n + \Sigma_i k_i X_i - \Sigma_j k_j X_j$$

Notice these equations are indexed in a generic form (refer to chapter 5 to obtain a detailed explanation of rate equation indexing). The X's represent the abundance

and the k 's are rates coefficients. To solve the system of the equations Herbst and Klemperer exploited the fact that at steady state equilibrium the derivatives are equal to zero. Thus, the set of equations may be expressed as follows.

$$\frac{dX_1}{dt} = \Sigma k_{p1} X_q X_r n - \Sigma k_{n1} X_n X_m n + \Sigma k_{i1} X_i - \Sigma k_{j1} X_j = 0$$

$$\frac{dX_2}{dt} = \Sigma k_{p2} X_q X_r n - \Sigma k_{n2} X_n X_m n + \Sigma k_{i2} X_i - \Sigma k_{j2} X_j = 0$$

⋮

$$\frac{dX_{35}}{dt} = \Sigma k_{p35} X_q X_r n - \Sigma k_{n35} X_n X_m n + \Sigma k_{i35} X_i - \Sigma k_{j35} X_j = 0.$$

By removing dependent equations from the above system and replacing them with equations of charge conservation and atomic nuclei conservation a set of 35 independent nonlinear equations is constructed. The method that Herbst and Klemperer is important because it is still useful for obtaining steady state solutions. The solutions to these nonlinear algebraic equations will be a vector containing the molecular abundances. Newton's method is generally used for solving such a system of equation. The above equations can be reformulated as a the problem in the matrix form.

$$\mathbf{f}(\mathbf{x}_n) = \mathbf{0} \tag{1.1}$$

where $\mathbf{f}(\mathbf{x}_n)$ is a matrix of the nonlinear functions that represent the set of equations.

The solution is computed using Newton's Method (Press 1991).

$$\mathbf{x}_{n+1} = \mathbf{x}_n - \frac{\mathbf{f}(\mathbf{x}_n)}{\mathbf{f}'(\mathbf{x}_n)} \tag{1.2}$$

Species	Observation	Calculation
<i>H</i>	20.72	20.73
<i>H₂</i>	20.62	20.62
<i>C</i>	15.56	15.60
<i>C⁺</i>	16.80-17.15	17.80
<i>N</i>	16.22-16.70	16.48
<i>HD</i>	14.20	14.25
CO	15.03-15.20	15.02
<i>CH⁺</i>	13.53	13.57
<i>CN</i>	12.94	12.75
<i>OH</i>	13.71	13.71

Table 1: Observed and Calculated Molecular Abundances. These abundances are given in terms of the logarithm of the column density (Black and Dalgarno 1977).

This process continues until some tolerance has been achieved. The tolerance is usually represented by the 1-norm.

$$\| \mathbf{x}_n - \mathbf{x}_{n-1} \| < \epsilon \quad (1.3)$$

Using this method Herbst and Klemperer were the first to obtain a steady state solution to the chemical model for a molecular cloud. Using a similar model led Black and Dalgarno (1977) calculated the abundances of ζ Ophiuchi. These results are listed in Table 1.

The evolution of chemical models 1977-1990

These early models have become the foundation of present interstellar gas phase chemical networks. During the late 1970's and early 1980's several investigations led to the development of more sophisticated and larger reaction networks. The main thrust of this effort is illustrated in several papers (e.g. Brown 1977; Iglesias,1977;

Suzuki 1979; Prasad and Huntress 1980 a,b; Rice and Brown 1981; Herbst 1983 Millar and Freeman 1984a,b; Leung,Hebrst and Huebner 1984; Brown and Rice 1986). These reaction networks contained approximately 1300 reactions (Millar 1990).

All of the reaction models mentioned above are based on the construction of large reaction libraries. Reaction libraries consist of a set parameters that allow the computation of rate constants for all of the molecular species in the network. The first large reaction set was assembled by Prasad and Huntress (1980). The Prasad and Huntress data set was modified by Brown and Rice (1986). They revised values of reaction cross sections so they could do analysis on the the influences of initial conditions on the predicted abundance. The last five years have been fruitful in the construction of reaction sets. Herbst and Leung (1989) constructed a library which contained 2548 reaction and 273 species.

Synopsis of Dissertation

A model of the chemistry occuring in molecular clouds was constructed. The model made use of the University of Manchester Institute of Science and Technology (UMIST) ratefile (Farquhar and Millar 1993). The UMIST chemistry was extended to include a population of small grains. This model calcuates the abundance of species for a given temperature, density, cosmic-ray ionization rate and elemental abundances. A parameter study was conducted in which the model was run over a range of temperatures and densities in order to systematically map out variations in trace species and determine which may be useful as a probe of temperature or

density. The parameter study is also useful for predicting abundance found by future observations as instruments become more sensitive. It also provides a map of expected water, molecular oxygen, atomic carbon and carbon monoxide abundances which may be observed by Submillimeter Wave Astronomy Satellite (SWAS).

Construction of the model required building a program which constructed and solved a set of ordinary differential equations. Because of the model was so large it was necessary to build a data structure to represent the system of equations. It was also necessary to build utility programs to check the equations for balance and to edit the reaction set. In the course of developing the model it was discovered that an analytic approximation for the fractional ionization was possible.

The model was also compared against measured abundances in clouds such as TMC1 (Friberg 1984), L134 (Swade 1987), Sgr B2 (Ziurys and Turner 1986) and the Orion Cloud Complex (Irvine, Goldsmith and Hjalmarson 1987).

During the development of the model it was found that for particular densities and temperatures more than one solution were possible. Such bistable regions have been seen before (Le Bourlot 1993). This study verifies the existence of such bistable regions in a more complete chemical model of interstellar clouds. The investigation was extended to determine how the bistable regions varied with changes in cosmic ray ionization rate, elemental abundances and grain population. The last required extending the UMIST ratefile to include reactions with a population of small grains. The reactions for this extension were obtained from Lepp (1987) and Greenberg (1994)

The bistable solutions found in this thesis are exciting because of the relation

between bistability and chemical chaos. The existence of chemical chaos was demonstrated in the laboratory 30 years ago by the Russian chemists Boris Belousov and Anatol Zhabotinskii (Scott 1991). This work has inspired investigators who study complex chemical systems to inquire whether chaotic type phenomena exist in these systems. Lepp has suggested that an example of a bistable solution is interesting because it may lead to an example of chemical chaos (Lepp 1994). It will be shown in chapter 6 that it might be theoretically possible to observe the B-Z process in interstellar clouds by formulating the problem in the context of catastrophe theory (Thom 1976). A B-Z reaction consist of as set chemical compunds which when combined may undergo self-sustained oscillations which can be periodic or chaotic. (Thompson 1982).

Outline of Dissertation

Chapter 2 provides a summary of the morphology and physical characteristics of the molecular cloud. Important chemical reactions that are occurring inside the cloud are reviewed in chapter 3. Chapter 4 provides a discussion of the various types of chemical process occurring inside the cloud. Chapter 5 presents a discussion which focuses on the construction of the mathematical model and the software that was used to determine the solution to the model. The development of a data structure to accommodate large systems of equations is also discussed in chapter 5.

Chapter 6 develops an algorithm which uses changing direction instead of changing initial abundance to detect bistable behavior. Chapter 6 also presents a theoretical

discussion about bistabilities and suggests that catastrophe theory is a mathematical model that may explain their qualitative behavior. Phase transitions and the different chemistries associated with them are discussed in Chapter 7. Chapter 8 presents a parameter study which investigates the variation of molecular abundances, variation of physical parameters, and the effects of large molecules on the bistability.

Chapter 9 derives analytical expressions for the fractional ionization. In particular, this chapter is motivated by work done by Oppenheimer and Dalgarno (1975). Their work is extended to include cosmic ray induced photoionization.

In Chapter 10, a parameter study is described and a comparison made of model abundances to measurements that have been made on existing molecular clouds. We focus on the Orion Cloud Complex, Sgr B2, TMC1 and L134.

Chapter 2

Giant and Dark Molecular Clouds

Giant molecular clouds and dark molecular clouds are the astrophysical objects modeled in this investigation. Giant molecular clouds are much larger than dark molecular clouds. Both are large enough so that uv and visible cannot penetrate to the center of the cloud. The giant molecular clouds are usually associated with active star formation such as massive OB stars and giant HII regions. Dark molecular clouds on the other hand are quiescent. By quiescent we mean the clouds do not appear to be forming stars.

Table 2 provides some data on the clouds mass, number density, temperature and line width. As their name implies, the giant molecular clouds have more mass and are larger than dark clouds. The giant molecular clouds tend to have higher temperatures, because they have heating sources such as embedded O and B stars. The giant molecular clouds are also more dynamic. The larger line widths implies more internal motion than a dark cloud.

In addition to molecular clouds there are diffuse clouds. **Diffuse Clouds** contain a large number of molecules and can be modeled using many of the techniques discussed in this work. They have a temperature of 100 K and a number density of 100

Cloud Complex Properties		
Cloud Type	Giant Molecular	Dark Cloud
Size(pc)	20-80	6-20
Number Density(cm^{-3})	100-300	100-1000
Mass(M_{\odot})	$8 \times 10^4 - 2 \times 10^6$	$10^3 - 10^4$
Line Width(km/sec)	6-15	1-3
Temperature(K)	7-15	≈ 10
Cloud Properties		
Cloud Type	Giant Molecular	Dark Cloud
Size(pc)	3-20	0.2-4
Number Density(cm^{-3})	$10^3 - 10^4$	$10^2 - 10^4$
Mass(M_{\odot})	$10^3 - 10^5$	5-500
Line Width(km/sec)	4-12	0.5-1.5
Temperature(K)	15-40	8-15
Properties of Molecular Cloud Cores		
Cloud Type	Giant Molecular	Dark Cloud
Size(pc)	0.5-3	0.1-0.4
Number Density(cm^{-3})	$10^4 - 10^6$	$10^4 - 10^5$
Mass(M_{\odot})	$10^1 - 10^3$	$10^{0.3} - 10^{10}$
Line Width(km/sec)	1-3	0.2-0.4
Temperature(K)	30-100	≈ 10

Table 2: Properties of Molecular Regions in the Interstellar Medium Notice that Table 2 categorizes the cloud into 3 regions. In general, it is accepted that cloud complex means a set of different clouds which are in the general vicinity of one another. The term cloud in this case applies to a specific region of the complex which appears to take on some structure. Finally, the term core deals with a centralized concentration of material within the cloud.

cm^{-3} . The dominant ions in diffuse clouds is C^+ . The most important feature which differentiates these clouds from dark and giant molecular clouds is that UV photons play a significant role in the chemistry. The models reflect this condition by assuming a visual extinction of $A_v = 1$ for diffuse clouds and a visual extinction of $A_v = 10$ for dark and giant molecular clouds.

The **Inter-cloud Medium** has a temperature of 10,000 K and a number density of $0.1cm^{-3}$. All atoms with an ionization potential less than 13.6 eV are ionized. These regions contain no molecules.

The Morphology of Molecular Clouds

A molecular cloud consists of a collection of interstellar dust and gas. The gas component of the mixture contains a substantial amount of molecules, while the remainder of the molecules exist in the form of ice on the surfaces of the grains. Observations of the $3.08\mu m$ absorption band suggest the existence of H_2O is condensed on the grain surface, while absorption bands of 4.62 and $4.67 \mu m$ suggest the existence of solid carbon monoxide condensed on the grain surface (Grim, Greenberg and Schutte 1988)

Much of what is known about molecular clouds is derived by maps and spectra of emission lines. The emission lines are in the millimeter and centimeter wavelength region of the electro-magnetic spectrum. For single dish radio telescopes maps of the cloud are constructed one pixel at a time. Carbon Monoxide (CO) and Ammonia (NH_3) are useful for determining cloud morphology because their microwave signa-

tures can be detected, allowing observers to map the clouds structure. Figures 1 and 2 provide illustration of these contour maps.

The most prominent rotational transition for the CO emission is from $J = 1$ to the $J = 0$. This transition is responsible for the 2.6 mm line. The ammonia line is produced by an inversion . The primary emission line occurs at a wave length of 1.3 cm. CO is used most of the time to obtain maps of the outer regions of the cloud while NH_3 is used as a probe of the cloud cores. Figure 2.1 and 2.2 provide illustrations of these contour maps.

The Orion Complex

The Orion Molecular Cloud Complex is the most extensively studied region containing molecules. This is because it is 1500 light years from the sun and is rich in millimeter and sub-millimeter emissions. Virtually all of these microwave emission originate from molecules. Chemical gradients have been detected with various regions of the Orion Complex. Examples of these regions are the hot core which has a temperature ranging from 30-200 K and a number density greater than 10^6 cm^{-3} and the ridge region which has a temperature of 30-100 K and a number density 10^4 cm^{-3} and 10^6 cm^{-3} (Goldsmith 1986).

The Giant Complex Sgr B2

The Sgr B2 cloud is located a distance of 8500 parsec from earth. It contains a core which has a diameter of 5-10 parsec. A large variety of molecules have been

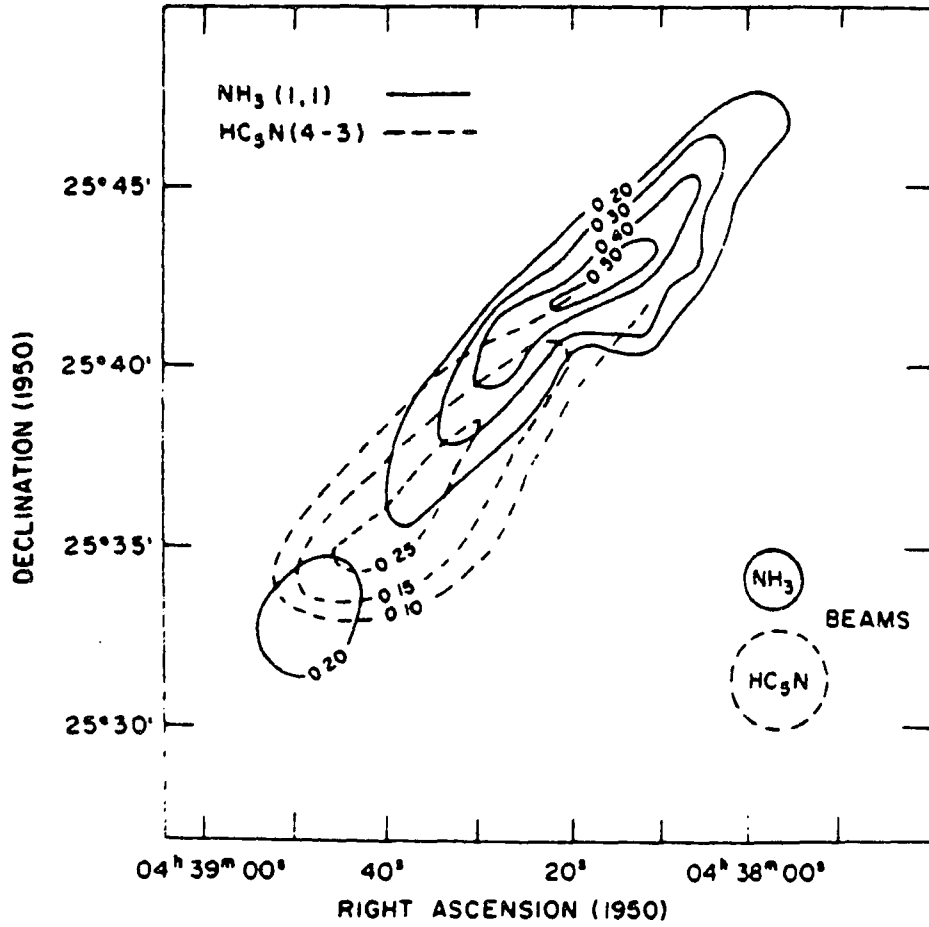


Figure 1: The NH_3 Contours of an Interstellar Clouds

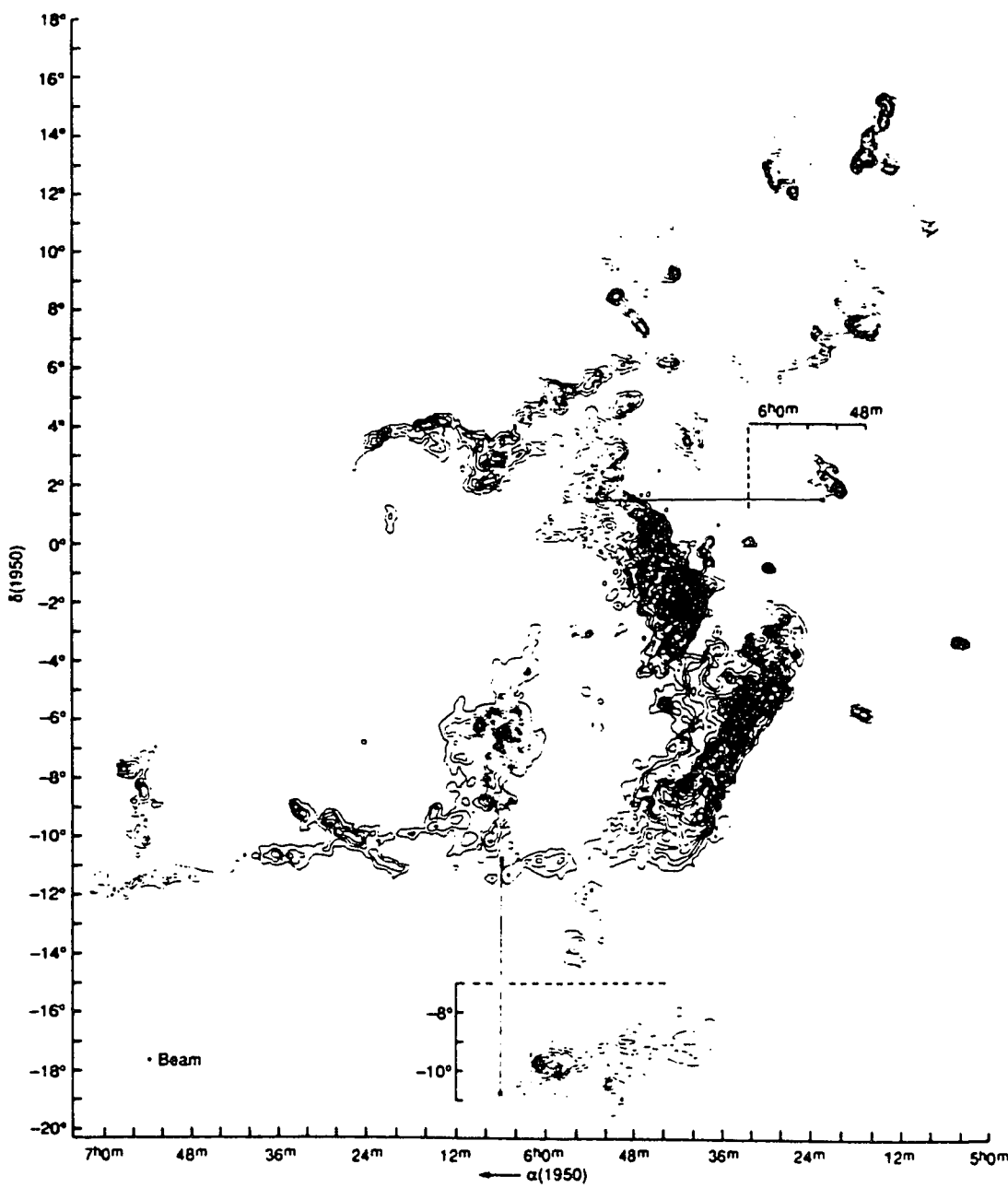


Figure 2: CO contours of The Orion Complex

discovered in this region. Observations indicate that this is a region of extensive star formation (Irvine et. al 1987). *CO* observation reveals an extended envelope with a mean number density of 5000 molecules per cubic centimeter (Scoville, Solomon and Penzias 1975).

TMC-1

The Taurus Molecular Cloud 1 or TMC-1 is about 115 parsecs from the earth. It is opaque to visible and ultraviolet radiation. Molecules observed in this cloud are characterized by low excitation temperature and narrow line widths. Not all interstellar molecules are observed in TMC-1; however, some of the largest molecules detected to date have been discovered in TMC-1. Figure 3 shows a map of TMC-1.

Observations indicate that the temperature of TMC-1 is 10K and it has a molecular density of $3 \times 10^4 \text{ cm}^{-3}$. The total mass of TMC-1 is one solar mass (Duley and Williams 1984).

Grains

The term grain is a general term which applies to a coagulation of matter. The relative abundance of grains is of the order of 2.2×10^{-12} (Spitzer 1951). Physical dimensions of the grain vary from $\frac{1}{10}$ to $\frac{1}{10000}$ of a micron. The size and the theory of the composition of the grains is currently a subject of scientific debate (Greenberg 1994). Current theory maintains that grains are created when a star enters the red giant phase and ejects its outer shell. Some grains are composed of silicates of aluminum, iron and magnesium. Others consist of carbon in the form of graphite or PAH's. It

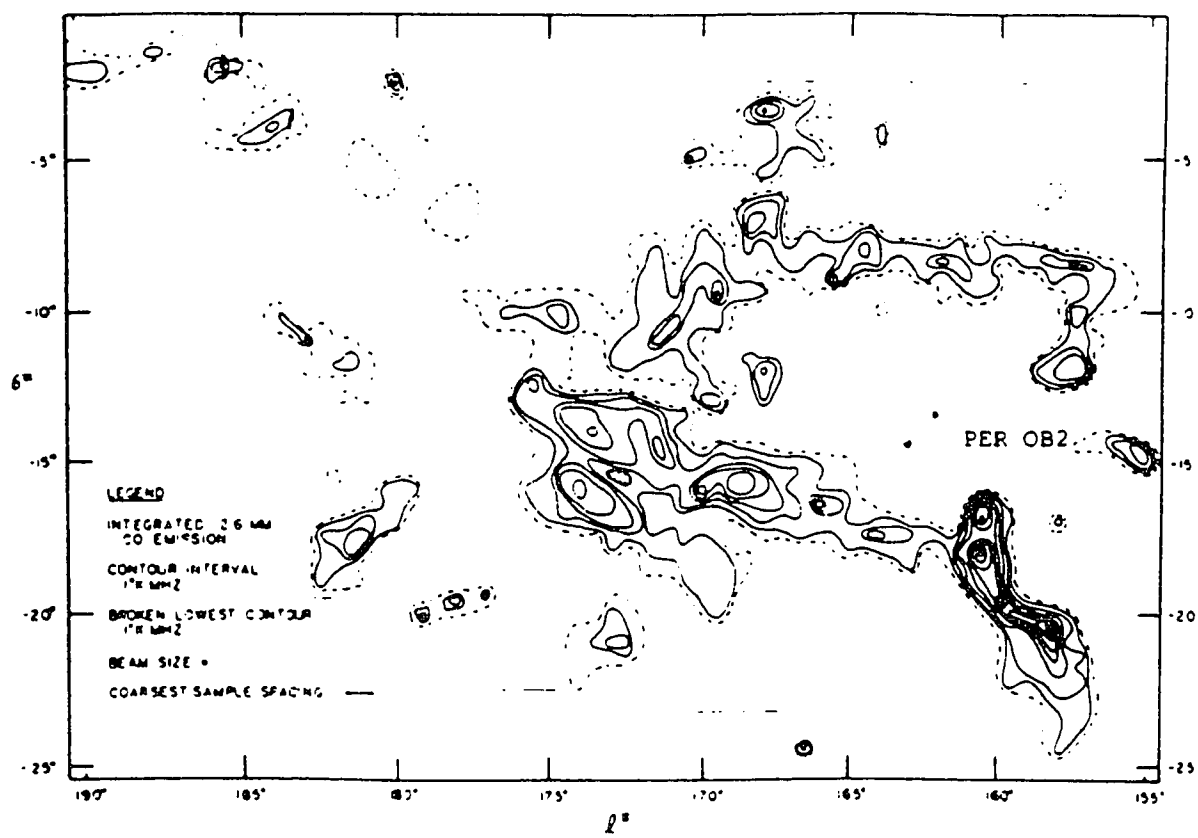


Figure 3: The TMC Cloud

is postulated that some of these grains are coated by ices which consist of water, ammonia and methane (Greenberg 1994). The Copernicus ultraviolet satellite has shown discovered regions of spectral signatures which correspond to silicon, iron and aluminum.

The effect of grains on the chemistry of dense interstellar clouds is crucial. Grains shield the cloud from ultraviolet radiation and provide sites for the formation of molecular hydrogen. Effects of the ultraviolet shielding result in an environment which is conducive to the formation of relatively large molecules. The grains also provide sites for charge transfer. Accumulation of carbon, oxygen, nitrogen and metals on the surface of the grains account for the formation of an accretion mantle.

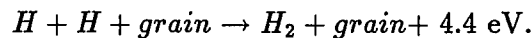
There are relatively a large abundance of complex molecules in the dark dense interstellar clouds. Stief (1972) demonstrated that dust in the outer layer of dark interstellar clouds attenuates the ambient Galactic ultraviolet radiation. Ultraviolet radiation is an important ingredient in the process of molecular destruction. Therefore, we must conclude that the presence of grains provides shielding and enhances the possibility of molecular survival. Observations of diffuse clouds tend to support this conclusion. Diffuse clouds, which lack grain shielding, show an absence of spectral signatures of large molecules.

Synthesis of Molecular Hydrogen on Grains

Atomic hydrogen is the major source of hydrogen molecules in dark dense molecular clouds. The rate of formation of molecular hydrogen by collisions with atomic hydro-

gen by radiative association is slow. The rate constant for this process is estimated to be between 10^{-29} and $10^{-31} \text{ cm}^3 \text{ s}^{-1}$ (Duley and Williams 1984). This low rate coefficient is too small to explain the amount of molecular hydrogen that is observed. It is assumed that H_2 is formed on the surface of grains. The grain acts as a catalyst and provides a site for the formation of molecular hydrogen.

The mechanism for H_2 formation can be summarized as follows. The hydrogen atom must collide with the grain to form a sufficiently strong H-grain bond, however the bond energy cannot be too large or the formation of H-grain bond will not occur. This hydrogen atom must remain on the grain surface until another hydrogen grain bond forms. The hydrogen atoms on the surface must have sufficient mobility on the surface so they can get sufficiently close to each other. As the molecules get close to each other the probability of tunneling increase enough to favor the formation of molecular hydrogen. The following reactions illustrates the synthesis of molecular hydrogen:



For this study the hydrogen formation rate coefficient is taken to be

$$k_g = 9.5 \times 10^{-18} \text{ cm}^3 \text{ sec}^{-1}$$

Millar (1991).

Cosmic Rays and Molecular Clouds

Cosmic rays (CRP) are a mixture of high energy protons, alpha particles, 1 percent heavy nuclei electrons and positrons. The relatively high abundance of heavy nuclei suggest that cosmic rays are formed in supernova or pulsars (Cowsik and Price 1971). Cosmic rays are important because they are sufficiently energetic to penetrate the interior of dense interstellar clouds and ionize molecular hydrogen. This process provides the mechanism that initiate the chemistry by ionization of the molecular hydrogen and atomic helium. Electrons produced for this ionization provide a source of heating for the cloud. It is estimated that the cosmic ray ionization rate is on the order of $10^{-17} \text{cm}^3 \text{s}^{-1}$ (Lepp 1992).

Cosmic Ray Induced Ultraviolet Photons

The interior of the dense interstellar cloud is efficiently shielded from ambient galactic ultraviolet radiation by dust. However the shielding of the visible and ambient ultraviolet radiation does not preclude the existence of ultraviolet radiation. Ultraviolet radiation is produced in dense molecular clouds by secondary electrons produced by the cosmic ray ionization (Prasad and Tarafdar 1983).

Cosmic-ray particles with energies between 10 Mev and 100 Mev ionize molecular hydrogen in the interior of the clouds and produce secondary electrons with an average energy of 30 eV (Cravens and Dalgarno 1978). The electrons lose their energy by exciting, dissociating and ionizing H_2 . The electrons which excite the molecular hydrogen are responsible for the generation of ultraviolet photons. These electrons

excite the Lyman band (90-170 nm) and Werner bands (90-130 nm) of H_2 . When the H_2 de-excites, ultraviolet photons are radiated.

The cosmic-ray induced photons have sufficient energy to ionize other species. The rate constant for reaction involving cosmic-ray induced photons have been calculated by Gredel, Lepp and Dalgarno (1987). Their rate coefficients have been incorporated into the UMIST Ratefile. The effect of cosmic ray induced ultraviolet photons on the chemistry and abundances of dense interstellar molecular clouds is discussed in this investigation.

The Heating and Cooling of Cold Clouds

The primary agent for the heating of molecules is cosmic ray radiation, while the cooling of the clouds occurs through radiation. This section explains some of the more important processes that are responsible for the energy balance of the molecular clouds. The last section explains this process for dark clouds.

The Heating Process

Several different types of mechanical and quantum processes account for the heating of interstellar clouds. In general, interstellar matter may be heated by a variety of different processes. Some of the dominant heating processes include cosmic ray ionization, diffuse interstellar starlight, the energy released in the grain formation of molecular hydrogen and gravitational compression. If the interstellar matter is near a star formation region, it can be heated directly or indirectly by stellar radiation.

The Cooling Process

The cooling process of dark dense interstellar clouds is a two-stage process. The first stage of the process involves the collision of atoms, molecules, electrons and ions. These collisions provide enough energy to excite the vibro-rotational levels of several molecules. These molecules de-excite through the process of spontaneous emission. They spontaneously emit microwaves which have energy of the order of 1.0×10^{-3} electron volts. It is interesting to note that these emissions, when detected by radio telescopes, can be used to map the cloud.

The molecular cloud temperatures are between 5 and 100 degrees Kelvin. This corresponds to an energy of approximately 10^{-3} eV. Hydrogen does not participate in the cooling process of cold clouds. This is because the excitation energies of the first excited state are too high. For atomic hydrogen the energies are given by $\frac{13.6}{n^2} eV$ and the threshold rotational excitation of molecular hydrogen is 450 K. It is interesting to note that the hot core in Orion has a temperature of 200K, which is well below the minimal threshold to excite molecular hydrogen.

In order for the cloud to cool, there must be some atoms or molecules with energy levels that are spaced sufficiently close to allow transitions that are energetically compatible with the kinetic temperatures. Carbon, oxygen, silicon and some diatomics have sufficiently low enough energy levels which will permit the cooling process. Table 3 list species that are important for this process.

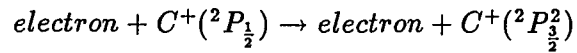
An illustrative example of the cooling process is ionic carbon in the excited state.

element	emission	transition μm
C^+	${}^2P_{3/2} \rightarrow {}^2P_{1/2}$	158 μm
C	${}^3P_1 \rightarrow {}^3P_0$	609 μm
C	${}^3P_2 \rightarrow {}^3P_1$	370 μm
C	${}^2P_{3/2} \rightarrow {}^2P_{1/2}$	63 μm
O	${}^3P_1 \rightarrow {}^3P_2$	63 μm
O	${}^3P_0 \rightarrow {}^3P_1$	146 μm
Si^+	${}^2P_{3/2} \rightarrow {}^2P_{1/2}$	35 μm
CO	$J = 1 \rightarrow J = 0$	2.6 mm

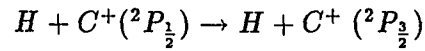
Table 3: Wavelength for transitions important in cooling molecular clouds.

Consider the collision of C^+ with an electron or a hydrogen atom. The ${}^2P_{1/2}$ level lies 64.0 μm below the $P_{3/2}$ level.

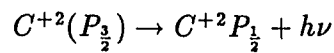
The C^+ ion is excited by either



or



These reactions extract thermal energy from the cloud by converting kinetic energy to radiation energy. The excited $C^+(P_{3/2})$ ion can radiate a photon at 156 μm in the spontaneous radiative transition.



Because the cross section of absorption is small the 156 μm photon will escape from the cloud (Dalgarno 1977).

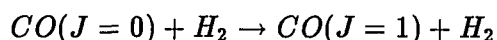
Heating of Cold Dark Clouds

The heating mechanism for dark dense quiescent clouds is restricted to the energy expelled from a cosmic ray ionization of H , H_2 or He . The energy emitted from H_2 formation is not significant in the heating process of dark clouds at low temperatures. Shielding by grains of dust and gas prevents visible and ultraviolet radiation from penetrating and heating the interior of the cloud.

The ionization of H , H_2 , or He produces energetic electrons. These electrons have a relatively high energy, that is dissipated through a series of inelastic collisions with molecular and atomic hydrogen. The process continues until the electron's energy is reduced to a point where elastic collisions with ambient electrons account for the remaining energy transfer.

The Cooling Process of Dark Clouds

Carbon monoxide is the primary cooling agent in the cold dark interstellar cloud. There are two reasons for this. First, carbon monoxide is the second most abundant molecule in the cloud (hydrogen being the most abundant). Second, carbon monoxide has a rotational de-excitation level for $J = 1 \rightarrow J = 0$, with an excitation threshold of 5 eV. Excited by collisions with H_2 molecules,



the $J = 1$ de-excites by the spontaneous emission of a photon of wavelength 2.6mm,



These emission lines are used by radio astronomers to map the cloud.

Chapter 3

Gas Phase Reactions in Molecular Clouds

There are several of different types of chemical reactions in the molecular clouds. The UMIST Ratefile (Farquhar and Millar 1993) catalogs 3715 of these reactions. In this chapter we explain briefly some of the mechanics and unique features of the gas phase reactions. There are several types of gas phase reactions that occur in the molecular cloud. Only two reactions out of a set of 3717 reactions are not gas phase reactions. These two reactions account for the production of molecular hydrogen on the surfaces of grains.

A summary of the important reaction types and their rate coefficients in the cloud are given in Table 4. This table is derived from the UMIST Ratefile (1992). The chapter reviews the definition of chemical rate coefficients then comments are made on each of the reaction type.

Reaction Type	Example	Rate Coefficient
C- Ray Ionization	$H_2 + crp \rightarrow H_2^+ + electron$	$10^{-17} s^{-1}$
Dissociative Recomb.	$H_3^+ + electron \rightarrow H_2 + H$	$5.5 \times 10^{-8} \sqrt{\frac{300}{T}} cm^3 s^{-1}$
Radiative Recombination.	$Si^+ + electron \rightarrow Si + h\nu$	$4.9 \times 10^{-12} \left(\frac{300}{T}\right)^{-0.6} cm^3 s^{-1}$
Charge Transfer	$He^+ + H \rightarrow He + H^+$	$1.9 \times 10^{-15} cm^3 s^{-1}$
Radiative Association	$C^+ + H \rightarrow CH^+ + photon$	$1.7 \times 10^{-17} cm^3 s^{-1}$
Ion-Molecule	$H_3^+ + CO \rightarrow HCO^+ + H_2$	$1.7 \times 10^{-9} cm^3 s^{-1}$
Neutral-Neutral	$CN + NO \rightarrow N_2 + CO$	$5.3 \times 10^{-13} - 10^{-11} cm^3 s^{-1}$
Mutual Neutral.	$C^+ + C^- \rightarrow 2C$	$2.3 \times 10^{-7} \sqrt{\frac{300}{T}} cm^3 s^{-1}$
Radiative Attachment	$H + electron \rightarrow H^- + h\nu$	$5.57 \times 10^{-17} \sqrt{\frac{300}{T}} cm^3 s^{-1}$

Table 4: Various Reactions that Occurring inside Interstellar Clouds

Reaction Rate Coefficients

Accurate determination of the rate coefficient is important in the construction of a robust kinetic model of a molecular cloud. It is difficult to recreate the environment of molecular clouds for an extended length of time. The rate coefficient can be measured in the laboratory or calculated using quantum mechanics. It is difficult to recreate the environment of molecular clouds in the laboratory. However, at the time of this investigation 900 out of 3715 rates have been measured experimentally. The decreasing cost of high speed computational devices will make quantum mechanical calculations less expensive.

The reaction rate coefficient is defined to be the average of the product of the cross section and the velocity:

$$K = \langle \sigma v \rangle \quad (3.1)$$

or

$$K = \int f(v)v\sigma dv. \quad (3.2)$$

where $f(v)$ is the probability distribution which defines the velocity distribution where v is the velocity, and σ is the total cross section. If the gas is thermalized the $f(v)$ is the Maxwellian velocity distribution:

$$f(v) = 4\pi v^2 \left(\frac{m}{2\pi kT}\right)^{\frac{-3}{2}} \exp\left(\frac{-mv^2}{2kT}\right) \quad (3.3)$$

where k is the Boltzmann Constant, m is the mass, T is the temperature and v is the magnitude of the velocity.

Cosmic Ray Ionization

The cosmic ray ionization of hydrogen and helium account for virtually all of the ionization in the molecular clouds. Most of the species in the cloud are composed of atomic and molecular hydrogen and atomic helium. Cosmic ray ionization of other species does not significantly effect the chemistry of the cloud because of their lower abundance. The rate coefficient for this study is $1.25 \times 10^{-17} \text{sec}^{-1}$.

Radiative Recombination

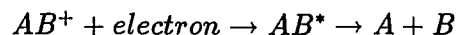
The radiative recombination is described by the reaction:



The surplus energy which is given off when the system forms a bound state. In dense molecular clouds the ionization is affected by the radiative recombination on atomic ions such as S^+ , Si^+ , or the metallic ions M^+ .

Dissociative Recombination

In the gas-phase many polyatomic and diatomic molecules are formed by dissociative recombination. The following generic reaction describes dissociative recombination.

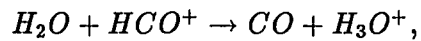


Current theory suggests that dissociative recombination can occur in two stages. Initially, the system which is composed of a free electron and a positive molecular ion combine to form a metastable state. This state will allow the electron to undergo a radiationless transition to form the metastable state AB^* . This results in a neutral molecule AB^* on a repulsive potential energy surface. The second stage involves the mutual repulsion of A and B. This system de-excites with A and B moving rapidly under the influence of mutual repulsion. A typical rate coefficient for this reaction is $10^{-7} \textit{ cm}^3\textit{ s}^{-1}$.

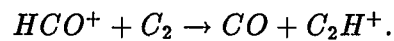
Ion-molecule reactions

Ion-Molecular reactions are the most frequently occurring reactions in the UMIST Ratefile. Ion-Molecule reactions have been studied extensively in the laboratory for temperature ranges from 300K-1000K. A majority of the reactions are exothermic and have a rate coefficient of $10^{-9} \textit{ cm}^3\textit{ s}^{-1}$. Ion-Molecular reactions occur because of long range attractive forces. These forces can cause the ion-molecular pair to spiral inwards toward each other until they collide. (Bates and Morgan 1987).

Polar species tend to react faster than non-polar species. To illustrate this point consider the reaction of the polar molecule water with the ion HCO^+ which has a rate coefficient of $2.5 \times 10^{-9} \text{ cm}^3\text{s}^{-1}$,



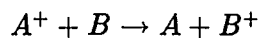
compared with the rate coefficient for the non-polar molecule C_2 which is $8.3 \times 10^{-10} \text{ cm}^3\text{s}^{-1}$,



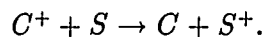
Notice that the rate coefficient of polar reactants is over 10 times faster than that of the non-polar molecules.

Charge Transfer

Charge transfer reaction can generally be expressed as follows.



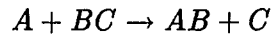
When an ion and a molecule approach each other there is a possibility of charge transfer occurring. If the energy of the interaction is sufficiently low the collision will not be adiabatic and the electron transfer cross section is low. An important charge transfer reaction for this investigation is:



The rate coefficient for this reaction is equal to $1.5 \times 10^{-9} \text{ cm}^3\text{s}^{-1}$. Charge transfer is the dominant process when the system is in the high ionization phase.

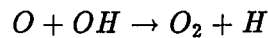
Neutral-Neutral

The neutral-neutral chemical process



is usually negligibly slow at low temperatures. This can be explained by the Rule of Hirschfelder (1941). Hirschfelder says the activation energy is about 5 percent of the energy of the broken bond. The chemistry of the dark interstellar clouds present many exceptions to this rule because the activation energy of atoms and free radicals (species contain a pair of unpaired electrons) may be very small or zero. The low temperature environments of cold interstellar clouds are dominated by reactions whose potential energy surfaces are without barriers. This explains why we expect to find these reactions occurring in the dark cloud (Graff 1989).

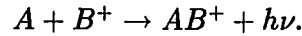
An important reaction involving the neutral-neutral process is



which has a rate coefficient of $k = 7.9 \times 10^{-11} \text{ cm}^3 \text{ s}^{-1}$. This reaction is important because it is the dominant pathway which converts atomic oxygen to molecular oxygen.

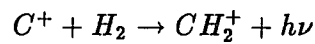
Radiative Association

If two species approach each other along an excited potential energy surface there exists the possibility of a radiative transition to a lower attractive potential surface. The energy radiated by the collision is sufficiently large to make the total energy of the two species system less than zero and a bound state is formed,



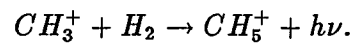
The reaction rate coefficient is of order 10^{-13} to $10^{-17} \text{ cm}^3 \text{ s}^{-1}$.

There are two reactions that are representative of radiative association which are important to the network of carbon chemistry. The following reaction provides a path for forming hydrocarbons.



The radiative association process is also crucial for the creation of methane, methanol, methyl cyanide, and methylamine. The CH_3 radical will form a complex via radiative association and this complex will be free to react with other species (see chapter 4) to produce various molecules.

For example, consider the production of methane. The production of the CH_5^+ molecular ion is important for the creation of methane CH_4 , H_2CO and many cyclohydrocarbons. CH_5^+ is produced as follows:

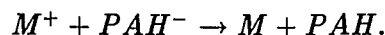
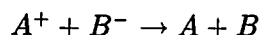


At 30K, Bates (1986) has shown the rate coefficient to be $2.7 \times 10^{-13} \text{ cm}^3 \text{ s}^{-1}$. The CH_5^+ complex reacts with CO to produce methane.

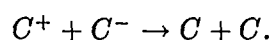


Mutual Neutralization

Mutual Neutralization provides a sink for many positive ions. Polycyclic Aromatic Hydrocarbons act to neutralize metals from the cloud.



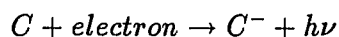
The rate coefficient for reactions of this type are on the order of $10^{-6} \sqrt{\frac{1}{T}} \text{ cm}^3 \text{ s}^{-1}$ (Omont 1986). For carbon ions Mutual Neutralization is given by:



The rate coefficient for this reaction is $1.29 \times 10^{-6} \text{ cm}^3 \text{ s}^{-1}$ for a temperature of 10K. Notice that these rate coefficient are relatively high. This is to be expected because opposite charges create large coulombic forces.

Radiative attachment

Radiative attachment is the process for the the creation of negative ions.



The rate for radiative attachment of this reaction is $3.0 \times 10^{-15} \text{ cm}^3 \text{ s}^{-1}$. When this process is compared to a process which undergoes charge transfer (rate coefficient $10^{-10} \text{ cm}^3 \text{ s}^{-1}$) it is relatively slow.

Summary

This chapter has introduced the major reactions which account for the gas phase chemistry of a large molecular cloud. The various processes may be characterized by the rate at which they occur. However, the abundance of the species also contributes to the rate. By considering the effects of the rate coefficients and abundances it is possible to make intelligent conjectures of the steady state solution as to the model.

Chapter 4

General Molecular Cloud Chemistry

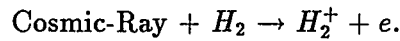
Giant molecular clouds and dark dense clouds are capable of synthesizing complicated molecules. The visual extinction coefficient for giant and dark clouds are about $A_v = 10$, thus there are virtually no ultraviolet photons available to participate in chemical reactions. The ambient galactic ultraviolet radiation, which is associated with the destruction of chemical bonds, is shielded by grains. The absence of galactic ultraviolet radiation means molecular abundances are determined by ion-molecule reactions. This allows large molecules to form.

This chapter reviews some of the important chemical reactions occurring in the dark and giant molecular clouds. The reactions presented are chosen because they represent the creation or the destruction of a species which is important to understanding the chemistry of the cloud.

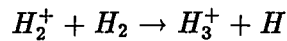
Initiation Chemistry in Dark Clouds

Dark molecular clouds and giant molecular clouds have dust grains which make them opaque to ultraviolet and visible radiation. However, dark and giant molecular clouds are partially transparent to cosmic-rays. Cosmic-rays provide the source of

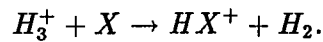
energy to initiate the chemistry of the cloud. Cosmic-rays will ionize primarily hydrogen molecules and helium atoms because they are most abundant. The process which drives the dark and giant cloud chemistry is the ionization of molecular hydrogen by cosmic-rays.



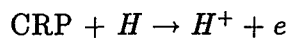
The H_2^+ is quick to react with the molecular hydrogen to produce H_3^+



The H_3^+ ion is the most important ion in the cloud. This is because H_3^+ can react rapidly with any species X , which has a proton affinity greater than molecular hydrogen H_2 ,



The chemistry of a dark interstellar cloud is to a minor extent dependent on the cosmic ray ionization of atomic hydrogen and helium. Atomic hydrogen is ionized by the reaction:

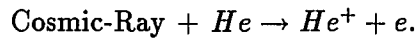


The H^+ ion recombines with an electron with a rate of coefficient of $k_e = 3.5 \times 10^{-12} \sqrt{(300/T)^3} \text{ cm}^3 \text{ s}^{-1}$ (Millar and Farquhar 1993). This is the value from the University of Manchester rate file of rate coefficients. This will be referred to as the UMIST Ratefile throughout the remaining part of this investigation (Millar and

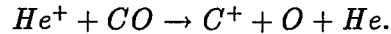
Farquhar 1993). Notice at $T=10\text{K}$ $k_e = 4.48 \times 10^{-11} \text{ cm}^3 \text{ s}^{-1}$ is relatively slow when compared with the dissociative recombination of H_3^+ with electrons. These rate constants are of the order of 10^{-8} to $10^{-7} \text{ cm}^3 \text{ s}^{-1}$, depending on the temperature.

Helium

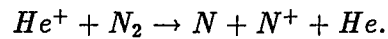
The helium chemistry initiated by the reaction



The existence of the helium ion is important for cloud chemistry because of its high ionization potential it can charge transfer and destroy many molecules. For example it can react with CO to dissociate it and produce C^+ and O ,

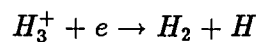


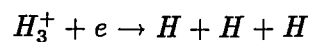
The ionized helium can also dissociate N_2 ,



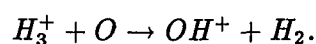
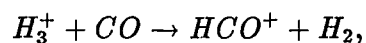
Destruction of H_3^+

There are two processes that significantly effect the rate at which H_3^+ is dissipated in the molecular cloud: dissociative recombination and proton transfer. Dissociative recombination removes electrons from the cloud and creates molecular and atomic hydrogen.





Larsson (1995) has performed experiments which suggest the branching ratios are 0.2 to 0.8 respectively. Another way that H_3^+ is removed from the cloud is via the process of proton transfer. Two of the predominant reactions are:

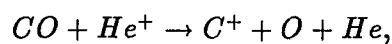
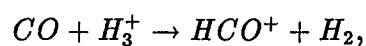


Oxygen Carbon Chemistry

Oxygen and carbon play a central role in the chemistry of dark interstellar clouds. This section will describe several important reactions associated with CO and O_2 . Carbon monoxide is created by the reaction

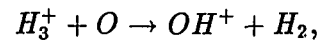


The ion-molecule reaction is the major method for the destruction of CO . The major reactions removing CO are:

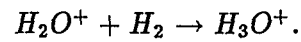
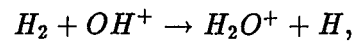


Oxygen Chemistry

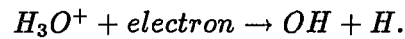
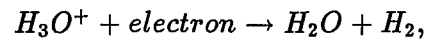
Another important reaction sequence is the sequence which produces the water molecule and the hydroxyl radical. The sequence is initiated with the formation of the OH^+ ion,



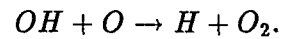
which reacts quickly with H_2 to form H_3O^+ ,



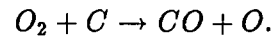
The dissociative recombination of H_3O^+ produces either a water molecule H_2O or an OH radical by dissociative recombination,



This reaction will be discussed more in Chapter 7. Molecular oxygen is primarily formed by the reaction,

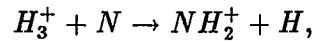


and molecular oxygen is primarily destroyed by the reaction,

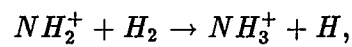
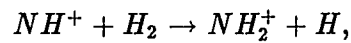
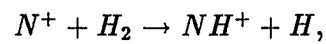


Nitrogen Chemistry

The chemistry of nitrogen can be initiated by H_3^+ ,

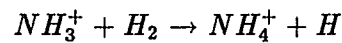


or by the nitrogen ion through the reaction sequence:



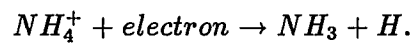
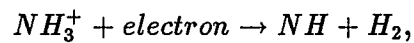
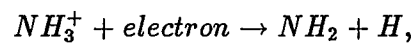
which are all fast with rate coefficients greater than $10^{-10} \text{ cm}^3 \text{ s}^{-1}$ (Farquhar 1995).

The next reaction in this sequence is slow

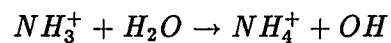


with rate coefficient $k = 2.0 \times 10^{-12} \text{ cm}^3 \text{ s}^{-1}$.

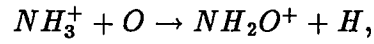
NH_3^+ and NH_4^+ via dissociative recombination with electrons produce:



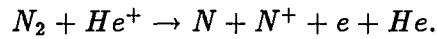
The NH_3^+ ion can also react with other species:



and



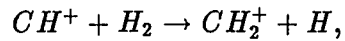
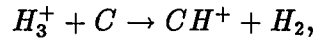
to produce more complicated molecules. Molecular nitrogen can be destroyed by helium ions



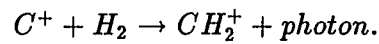
Production of Hydrocarbons

A large variety of hydrocarbons have been detected in molecular clouds. The size of hydrocarbon molecules detected include molecules which have 10 or more atoms. This section highlights some of the important reactions that occur in molecular clouds.

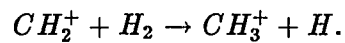
The hydrocarbon chemistry is initiated by



or by

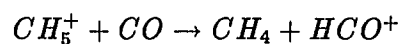
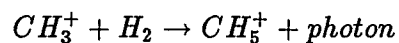


CH_2^+ quickly reacts with H_2 to form $CH_3^+ + H$,

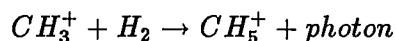


CH_3^+ is an important step in the formation of methanol (CH_3OH), methane (CH_4), methyl cyanide (CH_3CN) and methyl aldehyde (CH_3COH). This section presents the chemical pathways necessary to synthesize these compounds. It is interesting to note that radiative association participates in the first step of all of these reactions. Reactions involving radiative association tend to be relatively slow.

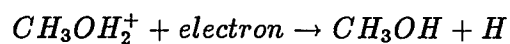
Production of Methane



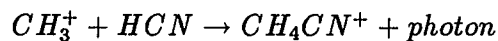
Production of Acetaldehyde

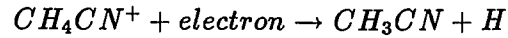


Methanol

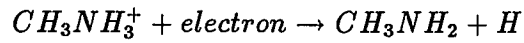


Production of Methyl Cyanide





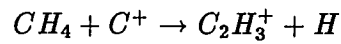
Production of Methyl Amine



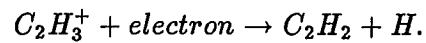
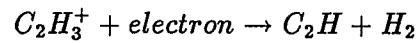
Production of Carbon Chains

The formation of larger molecules is initiated by reactions of C^+ with CH_4 . When a simple hydrocarbon such as methane has been produced, it is possible to utilize this molecule to produce more complicated species. Consider the following two reaction pathways which lead to the production of C_2H_2 and C_4H .

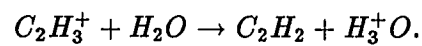
Synthesis of C_2H_2



this reaction will undergo dissociative recombination and will form one of two species

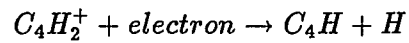
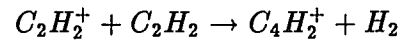


Proton transfer to water is can also produce C_2H_2



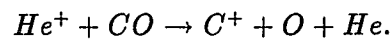
Synthesis of C_4H

Notice that C_2H_2 is crucial for the production of C_4H .

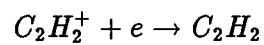
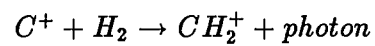


Effect of Helium Ions

The most important species for the initiation of the chemistry is H_3^+ . However helium ions are also important because they can react with stable neutral species. In particular they can react with CO to produce a carbon ion



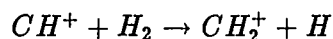
Ionized carbon will participate in the carbon chemistry by reacting with atomic and molecular hydrogen through radiative association.



The CH^+ is rapidly removed by



and by

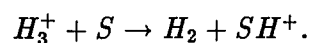


The last reaction is fast at room temperature and low temperatures. Large abundances of molecular hydrogen in comparison with the abundance of electrons favors the formation of CH_2^+ .

One reason ionized carbon is important is because it will react with methane to make precursor ions of acetylene, C_2H_2 and the ethyl radical, C_2H .

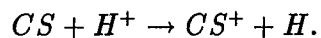
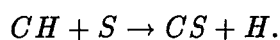
Sulfur Chemistry

Atomic sulphur reacts with H_3^+



But sequential reactions of SH^+ and SH_2^+ with H_2 are endothermic

Sulphur can react with CH to form CS. Once the CS is formed it can act as a site for charge transfer.

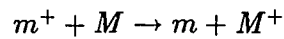


or



Chemistry of Metals

The primary function of metals in the dark interstellar clouds is to provide sites for the transfer of charge. As the cloud approaches a steady state the metallic ions Na , Mg and Fe will remove charge from large molecules.



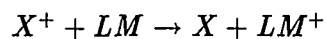
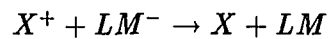
where m represents a charge molecule and M is Mg , Na or Fe .

The net effect of this process is in the behavior of the fractional ionization. This process will be examined in detail in Chapter 7.

Effects of Large Molecules

The effects of large molecules on the chemistry of the dark interstellar cloud chemistry can be quite dramatic. Without large molecules the molecular ions are removed by dissociative recombination and charge transfer to metals.

However, the large molecules provide sites for the accumulation of charge particles. When large molecules are incorporated into the reaction networks molecular ions are removed by mutual neutralization with the LM^- (Lepp and Dalgarno 1986).



and

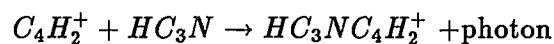
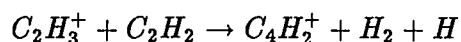
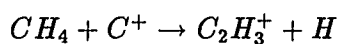




Large molecules, when added to the gas-phase chemistry, have a dramatic effect on the fractional ionization. Electrons will transfer to the large molecules and the fractional ionization will decrease. The effects of large molecules will be analyzed in detail in chapter 8.

Long Chained Molecules

One of the major discoveries of molecular astrophysics has been in detection of large molecules in certain molecular clouds. The existence of these large molecules confirms that interior regions of the cloud are shielded from destructive processes such as photoionization. This section will illustrate how a long chained molecule of length 9 can be formed. (Prasad et. al. 1987)



Processes similar to this form reaction pathways that explain the formation of molecules with up to 13 atoms (Irvine 1987).

Summary

This chapter has reviewed important reactions and species that participate in the dark and giant molecular cloud chemistry. The simple molecules are ionized to provide a starting point for the creation of highly reactive ions such as H_3^+ . These species may then react in a variety of ways to create molecular functional groups that can participate in the synthesis of larger molecules.

Chapter 5

The Gas Phase Chemical Model

Quantitative models of gas phase chemical networks provide the astrophysicist with a powerful method for calculating the abundance of chemical species found in molecular and dark clouds. Typically, the models have between 150 and 400 coupled stiff nonlinear differential equations. Efficient solutions of these systems require the investigator to apply sophisticated computing techniques. These techniques include subroutines which can solve stiff differential equations and data structures which are capable of isomorphically representing the system of equations. The objective of this chapter is to present a comprehensive and rigorous discussion which will focus on the construction of these models.

This chapter is divided into 3 parts. The first part will focus on the mathematics that are necessary to construct chemical models. The second section will address how the UMIST Ratefile (Millar 1990) and cosmic abundances factor into the construction of a model. The final section will focus on algorithms and software which produce solutions to the chemical model.

Model Construction

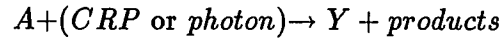
Analysis of the reaction networks associated with the UMIST Ratefile (Farquhar and Millar 1993) can be performed by considering and photo, cosmic-ray and binary reactions. The contributions of formation and destruction reactions will be discussed in the first part of this section. Next the construction of a general rate equation will be presented for some arbitrary species Y . Finally, a toy model will be presented to illustrate how a simple system may be constructed from a small reaction set. This will provide the reader with a clear idea as to how the full model is constructed.

Chemical Rates

The rate at which a reaction occurs is the product of the rate coefficient and the abundances of the species involved. The UMIST Ratefile (Farquhar and Millar 1993) provides information about reactions and rate coefficients. The following question must be answered in order to construct a kinetic model of the interstellar cloud chemistry: given a species Y , which belongs to some of the reactions in the molecular cloud, how is a rate equation constructed for Y ? Once this problem is solved in general, then, the reaction network can be constructed. The answer requires an explanation on how to express the first and second order expressions for the formation and destruction of the species Y .

Cosmic Ray or Photo reactions

Cosmic ray or photo reactions change one species into another. A cosmic-ray or photo reaction which forms Y is:



The contribution to the chemical rate can be expressed as:

$$\frac{dn_Y}{dt} = k_A n_A \text{cm}^3 \text{s}^{-1} \quad (5.1)$$

where n_A is the number density of A in units of cm^{-3} and k_A is the rate coefficient in units of s^{-1} . The rate of formation is in units of $\text{cm}^{-3} \text{s}^{-1}$.

A cosmic ray or photo reaction which removes Y is:



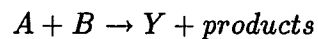
The contribution to the rate of change in n_Y is:

$$\frac{dn_Y}{dt} = -k_Y n_Y \text{cm}^3 \text{s}^{-1}. \quad (5.2)$$

Where n_Y is the number density of Y in units of cm^{-3} and k_Y will be the rate coefficient in units of s^{-1} . The rate will be given in units of $\text{cm}^3 \text{s}^{-1}$.

Binary Reaction

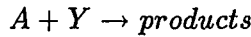
The formation of Y from two species A and B occurs as follows:



The rate is given by:

$$\frac{dn_Y}{dt} = k_{AB}n_A n_B cm^3 s^{-1}. \quad (5.3)$$

Where n_A is the number density of A in units of cm^{-3} and n_B is the number density of B in units of cm^{-3} . The rate coefficient k_{AB} will be in units of $cm^3 s^{-1}$. The rate Y is formed will be in units of $cm^{-3} s^{-1}$. When Y is destroyed in a binary reaction it must react with another species A. This reaction is illustrated as:



The rate is given by:

$$\frac{dn_Y}{dt} = -k_{AY}n_A n_Y cm^3 s^{-1} \quad (5.4)$$

Where n_A is the number density of A in units of cm^{-3} and n_Y is the number density of Y in units of cm^{-3} . The rate coefficient k_{AY} has units of $cm^3 s^{-1}$. The rate of destruction has units of $cm^3 s^{-1}$.

A General Expression of the Rate for a Species Y

The UMIST Ratefile (Millar 1992) consist of reactions with photons, cosmic rays and binary reactions. By selecting a particular species Y and performing summations over all other species in the UMIST Ratefile it is possible to obtain an expression for the rate of Y in units of $cm^{-3} s^{-1}$. Let

$$\frac{dn_Y^{1+}}{dt} = \text{photo and cosmic-ray formation rate for all species}$$

$$\frac{dn_Y^{2+}}{dt} = \text{binary formation rate for all species}$$

$$\frac{dn_Y^{1-}}{dt} = \text{photo and cosmic-ray destruction rate for all species}$$

$$\frac{dn_Y^{2-}}{dt} = \text{binary destruction rate for all species}$$

The rate for species Y will be defined as:

$$\frac{dn_Y}{dt} = \frac{dn_Y^{1+}}{dt} + \frac{dn_Y^{2+}}{dt} + \frac{dn_Y^{1-}}{dt} + \frac{dn_Y^{2-}}{dt} \quad (5.5)$$

The expression for all photo and cosmic-ray reactions which contribute to the rate of the formation of Y is given by the :

$$\frac{dn_Y^{1+}}{dt} = \sum_A k_A n_A cm^3 s^{-1}. \quad (5.6)$$

where n_A is the number density of A in cm^{-3} and k_A is the rate coefficient in units of sec^{-1} of photo-process and cosmic ray processes which lead to the formation of Y .

The expression for all binary process terms which contribute to the formation rate of Y is given by the expression:

$$\frac{dn_Y^{2+}}{dt} = \sum_A \sum_B k_{AB} n_A n_B cm^3 s^{-1}. \quad (5.7)$$

Where k_{AB} is the rate of the binary process leading to the formation of Y in units of $cm^3 s^{-1}$. And n_A and n_B are the number densities of A and B in units of cm^{-3} .

The expression for all binary reactions contribution to the destruction rate for Y is given by the expression:

$$\frac{dn_Y^{2-}}{dt} = -n_Y \sum_A k_{AY} n_A cm^3 s^{-1}, \quad (5.8)$$

where k_A is the rate of the binary process leading to the formation of Y in units of $cm^3 s^{-1}$. And n_A and n_Y are the number densities of A and Y in units of cm^{-3} , and finally, the expression represents the rate in which the photo and cosmic-ray process destroys n_Y

$$\frac{dn_Y^{1-}}{dt} = -n_Y \sum_Y k_x cm^3 s^{-1}, \quad (5.9)$$

where k_Y is the rate for the photo and cosmic-ray destruction of Y in units of sec^{-1} and n_Y is the number density of Y in units of cm^{-3} .

The sum of these terms is the the time derivative of n_Y .

$$\frac{dn_Y}{dt} = \sum_A \sum_B k_{AB} n_A n_B + \sum_A k_A n_A - n_Y \sum_A k_{AY} n_A - n_Y \sum_Y k_Y \quad (5.10)$$

The terms of the rate equation can be summarized as follows:

n_A, n_B and n_Y are the number densities (cm^{-3})

k_{AB} is the binary rate constant for formation of Y ($cm^{-3} sec^{-1}$),

k_{AY} is the binary rate constant for destruction of Y ($cm^{-3} sec^{-1}$),

k_Y is the rate coefficient for the photo or cosmic-ray Y (sec^{-1}), and

k_A is the rate coefficient for the photo or cosmic-ray formation of Y sec^{-1} .

The rate equation for Y can be written in terms of the relative abundance by dividing by the number density for hydrogen nuclei $n = 2n_{H_2} + n_H$.

$$\frac{dX}{dt} = \sum_A \sum_B k_{AB} X_A X_B n + \sum_A k_A X_A - X_Y \sum_A k_{AY} X_A n - X_Y \sum_X k_Y \quad (5.11)$$

where

$$X_Y = \frac{n_y}{n} \quad (5.12)$$

and

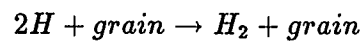
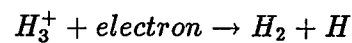
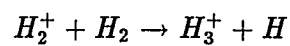
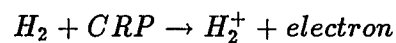
$$X_A = \frac{n_A}{n} \quad (5.13)$$

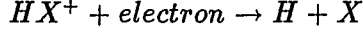
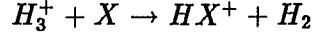
This is done in the actual model to scale the results.

A Toy Model

The full model for the reaction network used in this investigation contained 3717 reactions, 389 species and 12 atoms. Examination of a how a simple model is constructed will provide some insight into the procedure and methodology associated with construction of a large and more complicated network. This investigation designates this simple model as a *Toy Model*.

We will begin the explanation as to how to construct a reaction set by first considering a set of 6 reactions. The rate equations for this reaction set will serve to illustrate how the large chemical networks are created. We consider the following reaction set:





We now construct the rate equations for the above reaction set.

$$\frac{d[H_2]}{dt} = -\zeta[H_2] - k_2[H_2][H_2^+] + k_e[H_3^+][e] + 2k_g n[H] + k_M[H_3^+][X] \quad (5.14)$$

$$\frac{d[H_2^+]}{dt} = -k_2[H_2][H_2^+] + \zeta[H_2] \quad (5.15)$$

$$\frac{d[H_3^+]}{dt} = k_2[H_2][H_2^+] - k_e[H_3^+][n_e] - k_M[H_3^+][X] \quad (5.16)$$

$$\frac{d[H]}{dt} = k_2[H_2][H_2^+] - k_e[H_3^+][e] - 2k_g[H]n \quad (5.17)$$

$$\frac{d[e]}{dt} = \zeta[H_2] - K_e[H_3^+][e] - K_{X2}[HX^+][e] \quad (5.18)$$

$$\frac{d[X]}{dt} = -K_{X1}[H_3^+][X] + K_{X2}[HX^+][e] \quad (5.19)$$

We now rewrite equations 1-6 in terms of the relative abundances. To accomplish this we divide both sides of the equations by n , where n is equal to the number of hydrogen nuclei $n = n_H + 2n_{H_2}$ and the relative abundance of some species m is defined to be $X_m = \frac{[m]}{n}$.

$$\frac{dX_{H_2}}{dt} = -\zeta X_{H_2} - k_2 X_{H_2} X_{H_2^+} n + k_e X_{H_3^+} X_e n + 2k_g X_H n \quad (5.20)$$

$$\frac{dX_{H_2^+}}{dt} = -k_2 X_{H_2} X_{H_2^+} n + \zeta X_{H_2} \quad (5.21)$$

$$\frac{dX_{H_3^+}}{dt} = k_2 X_{H_2} X_{H_2^+} n + k_e X_{H_3^+} X_e n - k_M X_{H_3^+} X_M n \quad (5.22)$$

$$\frac{dX_H}{dt} = k_2 X_{H_2} X_{H_2+n} - k_e X_{H_3+X_e} n - 2k_g X_H n \quad (5.23)$$

$$\frac{dX_e}{dt} = \zeta X_{H_2} - k_e X_{H_3+X_e} - K_{X_2} X_{HX+X_e} \quad (5.24)$$

$$\frac{dX_x}{dt} = -K_{X_1} X_{H_3+X_x} n + K_{X_2} X_{HX+X_e} n \quad (5.25)$$

Where X can represent a variety of different molecules i.e O, CO, OH, H_2O

The Full Model

Complexity is the only difference between the full model and the toy model. The full model incorporates 3717 reactions into 389 rate equations. The construction of the full model is analogous to the construction of the toy model. The problem is that construction of the full model must be done by the computer to avoid mistakes.

Mathematical representation of the model can be expressed as follows.

$$\frac{dn_{Y_1}}{dt} = \sum_A \sum_B k_{AB} n_A n_B + \sum_A k_A n_A - n_{Y_1} \sum_A k_{A_1} n_A - n_{Y_1} \sum_{Y_1} k_{Y_1}$$

$$\frac{dn_{Y_2}}{dt} = \sum_A \sum_B k_{AB} n_A n_B + \sum_A k_A n_A - n_{Y_2} \sum_A k_{AY_2} n_A - n_{Y_2} \sum_{Y_2} k_{Y_2}$$

⋮

$$\frac{dn_{Y_{389}}}{dt} = \sum_A \sum_B k_{AB} n_A n_B + \sum_A k_A n_A - n_{Y_{389}} \sum_A k_{AY_{389}} n_A - n_{Y_{389}} \sum_{Y_{389}} k_{Y_{389}}$$

This system of equations can be written in terms of the fractional abundance. This representation is important because this is what the programs compute.

$$\begin{aligned}
\frac{dX_{Y_1}}{dt} &= \sum_A \sum_B k_{AB} X_A X_B n + \sum_A k_A X_A - X_{Y_1} \sum_A k_A X_A n - X_{Y_1} \sum_{X_{Y_1}} k_{Y_1} \\
\frac{dX_{Y_2}}{dt} &= \sum_A \sum_B k_{AB} X_A X_B n + \sum_A k_A X_A - X_{Y_2} \sum_A k_A X_A n - X_{Y_2} \sum_{X_{Y_2}} k_{Y_2} \\
&\vdots \\
\frac{dX_{Y_{389}}}{dt} &= \sum_A \sum_B k_{AB} X_A X_B n + \sum_A k_A X_A - X_{Y_{389}} \sum_A k_A X_A n - X_{Y_{389}} \sum_{X_{Y_{389}}} k_{Y_{389}}
\end{aligned}$$

Reaction Rate Coefficients for the UMIST Ratefile

The reaction rate coefficient determines how fast the reaction will occur. There are various parameters associated with each rate coefficient. The parameters are determined experimentally at high temperature. Since the dark interstellar clouds have temperatures between 7K and 15K, it is necessary to extrapolate the experimental results in order to estimate the rate coefficients. The form of the rate coefficients presented in the following sections is generally accepted to be correct. Many of the rate coefficients in the UMIST Ratefile (Farquhar and Millar 1993) are derived from extrapolations of experimental data. This method must be used because it is difficult to sustain the low temperatures in the laboratory. Current trends suggest that more powerful and less expensive computers could be used to compute more reliable rates theoretically.

h	he	o	c	n	s
p	mg	si	na	cl	fe
h2	h3+	h+	electr	h2+	h2cn
ch	hco	ch2	nh	ch3	nh2
ch4	oh	nh3	h2o	c2	co
no	h2co	hno	o2	o2h	h2s
h2o2	co2	n2o	ns	no2	so
ocs	s2	cn	n2	hs	cs
c2h	c2h2	hcn	c2h4	c3h	ocn
c4h	c5h	so2	c6h	c7h	c8h
c9h	he+	c+	ch2+	n+	ch3+
s+	hs+	h2s+	c3h2+	sih	sih2
sih3	ph	hpo	c3h2	c3h3	sic
pn	hcs	po	c5h2	ph2	c3
ccn	cco	hcsi	sin	cp	hcp
ch2ph	cc1	c4	c3n	clo	sic2
c3o	sinc	ccp	hccp	c5	sic3
c3p	c6	c5n	sic4	c4p	c7
c8	c7n	c9	c9	sio	c4h2
c6h2	c8h2	h-	c-	hnc	c2h3
c2h5	sih4	s-	hcl	c3h4	ch2cn
sich2	hns1	sich3	ch3cho	h2cs	h2sio
c2h5oh	ch3och3	hc3n	sic2h	h3c3n	sic2h2
c2s	c2h6co	sis	hcooch3	c5h4	hs2
sic3h	h3c4n	h2s2	c3s	hc5n	c4s
c7h2	c7h4	h3c6n	hc7n	c9h2	h3c8n
hc9n	ch3oh	ch3cn	ch2co	chooh	sio2
heh+	ch+	nh+	o+	o-	nh2+
ch4+	oh+	oh-	nh3+	ch5+	h2o+
nh4+	h3o+	na+	mg+	c2+	c2h+
cn+	cn-	c2h2+	hcn+	c2h3+	si+
n2+	co+	hcnh+	h2nc+	c2h4+	sih+
n2h+	hco+	hoc+	c2h5+	no+	sih2+
h2co+	p+	hno+	sih3+	h3co+	o2+
ph+	ph2+	sih4+	ph3+	o2h+	sih5+
ch3oh2+	cl+	h3s+	hcl+	c3+	h2cl+
c3h+	ccn+	c3h3+	sic+	c3h4+	hcsi+
c3h5+	ch3cn+	sin+	sich2+	cp+	hcp+
hnsi+	sich3+	sio+	pn+	cs+	co2+
sinh2+	sich4+	hcs+	hco2+	ns+	no2+
hpo+	so+	c4+	c4h+	c3n+	c4h2+
hc3n+	c4h3+	sic2+	sic2h+	c4h5+	sinc+
sic2h2+	sinch+	sic2h3+	pc2h+	fe+	sis+
c5+	c5h+	c4n+	c5h2+	hc4n+	c5h3+
c5h4+	so2+	h2c4n+	c5h5+	s2h+	hso2+
sic3h+	h3c4n+	h4c4n+	sic3h2+	c6+	c6h+
c6h2+	c6h3+	hc5n+	c6h5+	c7+	c7h+
c7h2+	c7h3+	c7h4+	c7h5+	h4c6n+	c8+
c8h+	c8h2+	c8h3+	c9+	c9h+	c9h2+
c9h3+	c9h4+	h4c8n+	c5n+	c7n+	c9n+
hc7n+	hc9n+	ch4n+	c2h6+	h2no+	ch3oh+
cnc+	ccnh+	c2o+	ch2cn+	hc2o+	c2ho+
nco+	ch2co+	h4c2n+	hnco+	ch3co+	ch3cho+
pnh2+	pnh+	pch4+	sioh+	c2h5o+	hpn+
pch3+	pnh2+	pnh3+	h2cs+	h2sio+	c2h5oh+
c2h6o+	cc1+	po+	hns+	h3cs+	h3sio+
chooh2+	c2h6oh+	c2h7o+	hso+	h2po+	h2cc1+
clo+	c2n2+	h2c3n+	c3o+	hc3o+	h4c3n+
c3h2o+	ccp+	h3c3o+	pc2h4+	c2s+	pc2h2+
pc2h3+	hc2s+	c2h6co+	c3h6oh+	ocs+	cooch4+
hsis+	hocs+	hsio2+	h5c2o2+	s2+	sic3+
h2s2+	h3s2+	pc3h+	c3s+	hc3s+	sic4+
h2c5n+	c6h4+	h3c5n+	sic4h+	c4p+	pc4h+
pc4h2+	c4s+	hc4s+	c8h4+	c8h5+	h2c7n+
h3c7n+	c9h5+	c10+	h2c9n+	h3c9n+	

Table 5: Table of Species in the Umist Ratefile

Two-Body Reactions Rate Coefficients

A majority of the reactions that occur in a molecular cloud are two bodied. The rates are fit to the following form:

$$k = \alpha(T/300)^\beta \exp(-\gamma/T) \text{cm}^3 \text{sec}^{-1} \quad (5.26)$$

where α , β and γ are parameters, from the UMIST Ratefile (Farquhar and Miller 1993). β is the parameter which indicates whether the rate depends on the temperature. When β vanishes, it implies the reaction is independent of the temperature. And γ is non-zero if the reaction is endothermic or has a barrier.

Cosmic Ray Ionization Rate

For direct cosmic ray ionization the rate coefficient is given by

$$k = \zeta \text{sec}^{-1}. \quad (5.27)$$

The exact value of the cosmic rate ionization ζ has not been determined. However, several observations and theoretical techniques have been used successfully to establish bounds for ζ . Earth bound measurements provided enough information to allow Spitzer(1968) to compute a lower limit of $\zeta = 6.8 \times 10^{-18} \text{s}^{-1}$. Shaver (1976) showed that analysis of the recombination lines of hydrogen and HI absorption measurements allows an estimate of the cosmic ray ionization rate. Shaver has computed ζ to be greater than $2 \times 10^{-17} \text{s}^{-1}$. The relationship between ζ and H_3^+ has been established (Lepp et. al. 1986). This method allowed ζ to be computed based on estimates

of OH . This is because OH is proportional to H_3^+ . A review of several methods of how to calculate the cosmic ray ionization rate led Lepp to conclude the average rate was $few \times 10^{-17} s^{-1}$ (Lepp 1992). The value of ζ suggested by Millar(1990) for the UMIST Ratefile was $1.2 \times 10^{-17} s^{-1}$. Because this value is consistent with Lepp's (1992) suggested rate (See Chapter2) it was used for the ζ in this study.

Photoionization

Dark clouds have a visual extinction, A_v , of greater than 4 mag. (Spitzer 1978). Some investigators use an A_v as high as 20.6 mag. (Shalabiea 1994). This investigation adopted a value of $A_v = 10$ for these models. This is the value that Millar suggest for the UMIST Ratefile(1990). For a photon reaction the rate coefficient is:

$$k = \alpha \exp(-\gamma A_v) \text{sec}^{-1} \quad (5.28)$$

where α and γ are parameters from the UMIST Ratefile.

Induced Cosmic Ray Ionization

Induced emission of ultraviolet photons is a consequence of the Prasad and Tarafdar process (1983). The electrons from the induced cosmic ray ionization excite molecular hydrogen to its Lyman and Werner bands. When these bands de-excite they provide an internal source of radiation. The albedo is important for this process because it is used to determine the rate of cosmic ray induced photo-dissociation (Lepp, Dalgarno and Sternberg 1987).

The extinction of radiation cross section is defined to be the sum of the absorption and scattering cross section.

$$\sigma_{ext} = \sigma_{abs} + \sigma_{sca} \quad (5.29)$$

The efficiency Q is defined to be

$$Q = \frac{\sigma}{A}. \quad (5.30)$$

where A is the area of the body scattering or absorbing the radiation. For dark clouds A will be the area of a grain. Equation(5.29) can be divided by the area A to yield an expression of the efficiencies.

$$Q_{ext} = Q_{abs} + Q_{sca} \quad (5.31)$$

$$\omega = \frac{Q_{sca}}{Q_{ext}} \quad (5.32)$$

The rate coefficient for cosmic-ray induced photoionization is proportional to (Miller 1991)

$$k = \frac{\alpha\zeta}{1 - \omega}. \quad (5.33)$$

where ζ is taken to be $1.2 \times 10^{-17} s^{-1}$, the cosmic ray ionization rate and the albedo is $\omega = 0.5$.

Elemental Abundances

The interstellar medium is composed of a majority of the elements in the periodic table. The abundances that are used in this investigation are based on the abundances

element	cloud abundance	solar abundance
H	1.0	1.0
He	1.4×10^{-1}	8.5×10^{-2}
C	7.3×10^{-5}	3.7×10^{-4}
O	1.76×10^{-4}	6.8×10^{-4}
N	2.14×10^{-5}	1.0×10^{-4}
S	2.0×10^{-6}	1.6×10^{-5}
P	3.0×10^{-9}	2.7×10^{-7}
Mg	3.0×10^{-9}	3.5×10^{-5}
Si	3.0×10^{-9}	3.5×10^{-5}
Na	2.0×10^{-9}	1.7×10^{-6}
Cl	3.0×10^{-9}	4.4×10^{-7}
Fe	3.0×10^{-9}	2.5×10^{-5}

Table 6: Cloud Abundances and Solar Abundances

that are used by Leung (1984). These abundances are listed in Table 5 along with the solar abundances. The abundances are used as a starting point for the parameter study.

Initial Conditions

Numerical solutions of any set of time dependent differential equations require a set of initial conditions. Contemporary research involving nonlinear systems of differential equations has generated several systems of differential equations where the final solution is sensitive to the initial conditions. It is important to explain how initial conditions are selected. The initial integration uses the cosmic depleted abundances for initial conditions as a bench mark in all calculations (Table 5.1). In this investigation the time dependent chemical model evolves under fixed parametric conditions such as constant temperature and/or constant number density. The chemical abundances

are allowed to evolve from the initial values until the steady state is reached.

Let the steady state solution be denoted by $X_{\frac{dx}{dt}=0}$. The steady state solution will be used as the initial condition for the next iteration in which the step size is decremented or incremented. This process continues until the steady state solution has been calculated over the desired range of the parameter space.

In general, given a system of differential equations:

$$\frac{dx}{dt} = f(x; \alpha). \quad (5.34)$$

Solve the system and obtain a solution x_n . Use this new solution as the initial value and integrate the system to obtain x_{n+1} . This process can be continued as long as desired. The advantage of this process is based on the idea that the new solution x_{n+1} will be within a neighborhood of x_n and will take less time to converge.

Stiff differential equations

Stiff differential equations are differential equations that are ill-posed in the computational sense. The notion of stiff is somewhat imprecise, but it communicates the idea that the solution has some components that change much more rapidly than others (Yakowitz and Szidarovzky 1986). Two common definitions are given below.

Definition One: A system of differential equations is said to be stiff on the interval $[0, T]$ if there exists a component of a solution of the system that has a variation on $[0, T]$ that is large compared to $1/T$.

Definition Two: A system is stiff if there exists more than one scale, with a great difference in size on which the solutions evolves. For instance, the system of

differential equations $y' = \mathbf{A}y$ where \mathbf{A} is a constant matrix with eigenvalues λ_i ; \mathbf{A} is stiff if

$$\max_i \lambda_i \mathbf{A} \gg \min_i \lambda_i \mathbf{A}$$

The rate coefficients associated with the chemistry of the dark interstellar cloud differ by several orders of magnitude. For example, the rate coefficient of the cosmic ray ionization is of the order of 10^{-17} s^{-1} whereas the rate coefficient of dissociative recombination of H_3^+ is of the order $10^{-8} \text{ cm}^3 \text{ s}^{-1}$. There are also great differences in the steady state abundances. For example, the fractional abundance of C_{10}^+ is 7.4×10^{-16} while the fractional ionization of hydrogen is 1. The large difference in the rate coefficients and the abundances indicates that there is the possibility that stiffness might be a problem. The use of conventional methods such as Runge Kutta or Adams Moulton becomes extremely time-consuming for this class of equation and can often lead to incorrect results.

This problem was avoided by adopting a differential equation solver called lsoda.f. Lsoda.f was developed by Livermore National Laboratories. This routine is necessary because the chemical network evolves along different time scales. The lsoda.f routine automatically adjusts its step size to account for the stiffness of the region it being integrated over. It achieves a high degree of stability with a larger step size because it is based on a backward difference Gear method.

Data Structures

The task of accurately representing a system of differential equations is going to

vary with the complexity of the system. Naturally, for small systems the selection of a computational representation is not as crucial as for large systems. However, as the system gets larger representations must be constructed by some computational procedure to ensure accuracy.

The evolution of the computer code in this study consisted of two stages. Stage one involved getting the program to integrate 50 or fewer of equations. The system of equations was represented as a 1-1 onto map of the fortran code. To accomplish this a program was written called jack.f which wrote two subroutines fex.f and jex.f. These two programs were used as external calls to lsoda.f. This method produced correct results. However when the size of the system exceeded 50 equations, the problem grew larger than the available memory.

The memory problem was solved by introducing a data structure. The data structure has relatively smaller memory requirements than the 1-1 onto representation. The idea that makes the data structure representation practical is that by using a small amount of memory you can store the large system of equations. The drawback is that every time the system of equations is called, the CPU must decode the data structure. Essentially, what is done is to trade off memory space for CPU time.

Description of the Data Structure

The data structure which is responsible for reconstructing the system of differential equations consists of 3 arrays. Array rate(n) is a double precision vector which contains the rate coefficients. The 2 dimensional array ivec(ic,nterms) is a list of all terms

in all equations. $Ivec(ic,1)$ constrains the rate coefficient index, $Ivec(ic,2)$ contains the multiplier and $Ivec(ic,3)$ and $Ivec(ic,4)$ contain the numerical indices of the species. The vector $numterm$ is a pointer to each equation. It contains the number of terms in each equation and its sum will equal the length of $ivec$. The arrays $Ivec$, $numterms$ and $rates$ are all stored in a common block. This block is accessed by $fex.f$ to construct the function. Every time the function is needed it must be computed using $fex.f$.

Creation of the Data Structure

The data structure is created by using an array of the strings. Each string contains a name of a molecule. This string is compared with each of the chemical reactions in the reaction list. The reaction list consists of at least three and a maximum of six species. If the string in the molecular list occurs in a position of the reaction list a flag is set which directs the program to increase the $nterm$ counter by 1. The program then sets $ivec(1,n)$ equal to the reaction number. This is important because this information will be used in the process to determine the rate coefficient. Next, the program determines the sign of the term. It does this by determining which side of the equations the species is located. Finally, the programs codes the reactions that are participating in the reaction. The code generated by this operation contains the pointer required to reproduce the function.

Description of LSODA.F

The reaction network is generated by the subroutine `EQTABLE`. `EQTABLE` reads in the rate file from the UMIST data set. `EQTABLE` then creates a data structure

which is isomorphic to the rate equations. The differential equations are recovered for calculation purposes by the subroutine `fex.f`. The UMIST set consisted of 389 molecular species and 3715 reactions (Farquhar and Miller 1993). `Lsoda` solves the initial value problem for stiff or non-stiff systems of first order ode-s,

$$\frac{dy}{dt} = f(t, y), \quad (5.35)$$

or, in component form,

$$\frac{dy(i)}{dt} = f(i) = f(i, t, y(1), y(2), \dots, y(neq)) \quad (i = 1, \dots, neq). \quad (5.36)$$

This is a variant version of the `lsoda` package. It switches automatically between stiff and non-stiff methods. This means that the user does not have to determine whether the problem is stiff or not, and the solver will automatically choose the appropriate method. It always starts with the non-stiff method. `Lsoda` uses a linear algebra package called `LINPACK`.

Description of LINPACK

This is a collection of Fortran subroutines which analyze and solve various linear equations and linear least-squares problems. The package solves linear systems where matrices are generally square, banded, symmetric indefinite, symmetric positive-definite, triangular or tridiagonal. In addition, the package computes the QR and singular value decompositions of rectangular matrices and applies them to linear least-squares problems. Single precision, double precision and complex versions of the code are included. The tape distributed contains the Fortran source for `LINPACK`, the Basic

Linear Algebra Subprograms (BLAS) needed by LINPACK, testing aids and program comments.

Chapter 6

Bistability

This chapter will provide an illustration of the behavior of steady state solutions to the chemical model that was defined in Chapter 5. Also, this chapter discusses the mathematical structure which is associated with the phenomenon of bistability. This discussion provides an explanation of how phase transitions, hysteresis, and cusp catastrophes are related to bistable phenomena.

Certain sets of initial conditions result in steady state solutions which, when plotted over a region of the parameter space, will exhibit discontinuous behavior. When the same calculation is performed in the parameter space but in a different direction we sometimes get a region where the solutions are unique and other times we get two different solutions. When we get two solutions we say the solutions are bistable. The topological structure which is associated with bistability is the catastrophe. Catastrophe theory provides a qualitative method for the interpretation of phase transitions and the hysteresis phenomenon. In this investigation the cusp catastrophe plays an important role in obtaining a qualitative explanation of the bistable phenomenon.

Fractional Ionization

Steady state solutions obtained by solving the chemical model are expressed as a vector \mathbf{X} . The dimension of the vector is the number of species in the chemical network and each component of \mathbf{X} corresponds to the fractional abundance of each species. Typically, chemical models involve modeling molecular clouds which contain between 100 and 400 species. A graphical representation which displays such a large number of species would not be practical. Fortunately, there is a suitable graphical representation of the solution.

Electrons account for a large percentage of the negative charge in the dark interstellar clouds. While other negative ions such H^- and C^- exist, they are several orders of magnitude less in abundance compared with the number of electrons. It is therefore convenient to characterize the chemistry of the cloud in terms of the electron abundance. The relative abundance of electrons is called the fractional ionization.

Mathematically, the **fractional ionization** is defined to be:

$$X_e = \frac{n_e}{n}. \quad (6.1)$$

Where n_e is the number density of electrons. And n is the number of hydrogen nuclei is defined by the following relation:

$$n = 2n_{H_2} + n_H. \quad (6.2)$$

The fractional abundance for all other species is defined to be:

$$X_m = \frac{n_m}{n}, \quad (6.3)$$

where n_m is the number density of the species and n the number density of the hydrogen nuclei.

Phase Transitions

Plots of the fractional abundance of steady state solutions to the chemical model sometimes produce curves which are discontinuous. As an example of this discontinuity consider Figure 4, a plot of the fractional abundance of H_2O which is expressed as $\frac{n_{H_2O}}{n}$ versus number density. Figure 4 shows a discontinuity at $n = 1500 \text{ cm}^{-3}$.

The left hand side of the graph is a convex function which is monotonically increasing, while the right side of the discontinuity is an approximately linear curve with a small decreasing slope. Analysis of this graph suggests that the chemistry which is producing the H_2O is different on different sides of the discontinuity.

A plot of the fractional ionization also shows a discontinuity at $n = 1500 \text{ cm}^{-3}$ (see Figure 5). The discontinuity will be defined as the **phase transition** in the chemistry which is expressed in the fractional ionization curve. The phase transition divides the regions of ionization into a high and low region. Note the region on the left side of the phase transition is the region of high ionization, while the region to the right represents the low ionization.

Physically, the phase transition corresponds to the point where the number of free electrons in the cloud increases or decreases substantially. Charge conservation implies that in the high ionization state there are more positive ions, while in the low ionization state there are less positive ions. This is one mechanism which influences

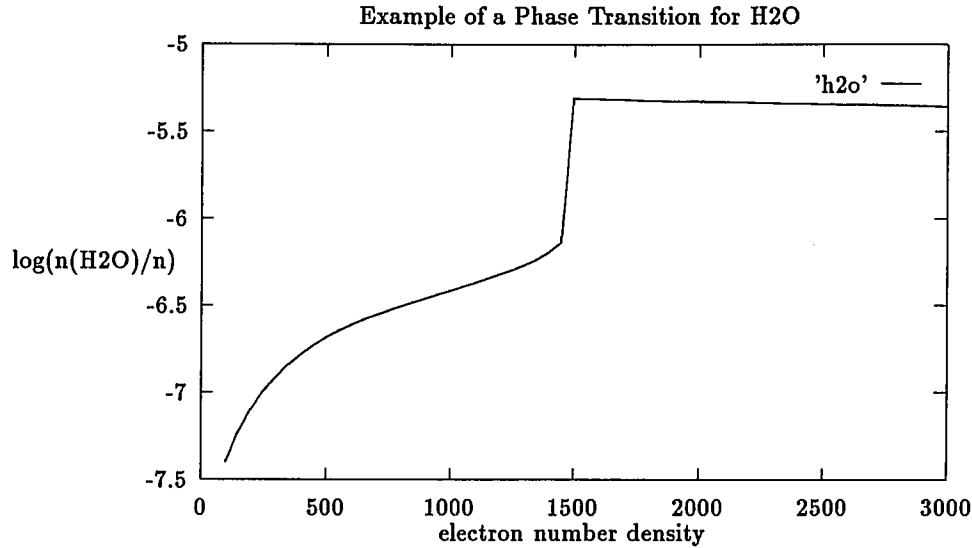


Figure 4: Phase Transition for H_2O Molecule

the chemistry of the molecular cloud. An analysis of the chemistry difference will be performed in chapter 7.

Procedure to Find a Bistable Region

Bistable regions are found by a three step process. An example will be given for an initial conditions given in Table 6 and a Temperature= 10 K. Steady state solutions will be obtained for the number density which varies from $100 - 3000 \text{ cm}^{-3}$ in increments of 50.

Step 1: The procedure will begin by computing a steady state solution for the system of equations with $X_{initial}$ which will correspond to the abundances given in Table 6. The number density will vary from $n= 100 \text{ cm}^{-3}$ to 3000 cm^{-3} . The solution for the first iteration X_1 will be used as the initial condition for the second steady

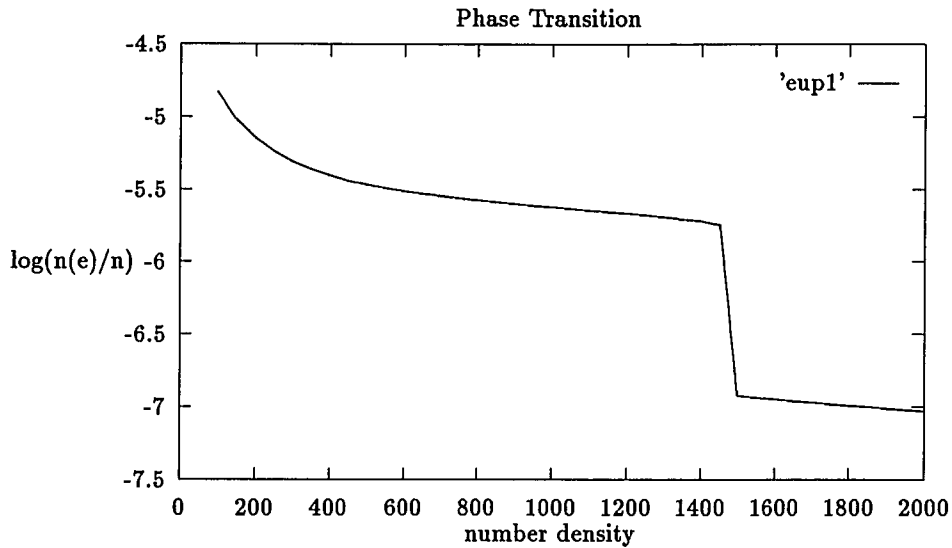


Figure 5: This Graph illustrates the phase transition

state solution. This process will be carried out 59 times for this example and a graph will be constructed which is represented in Fig 6. The fractional ionization X_{1e} will be plotted against n . Notice that at a number density of 1500 cm^{-3} illustrates that a phase transition has occurred.

Step 2: The second step will consist of doing the same thing that was done in step one, except that we are starting at a number density of 3000 cm^{-3} and decrementing by the number density in steps of 50 cm^{-3} . These results are then plotted in Figure 7. Observe that at a number density of 450 cm^{-3} a phase transition has occurred.

Step 3: The final step involves plotting the superimposed results obtained in steps 1 and 2 and comparing the results. Given 2 points (n, X_{ei}) (n, X_{ej}) where X_{ei}

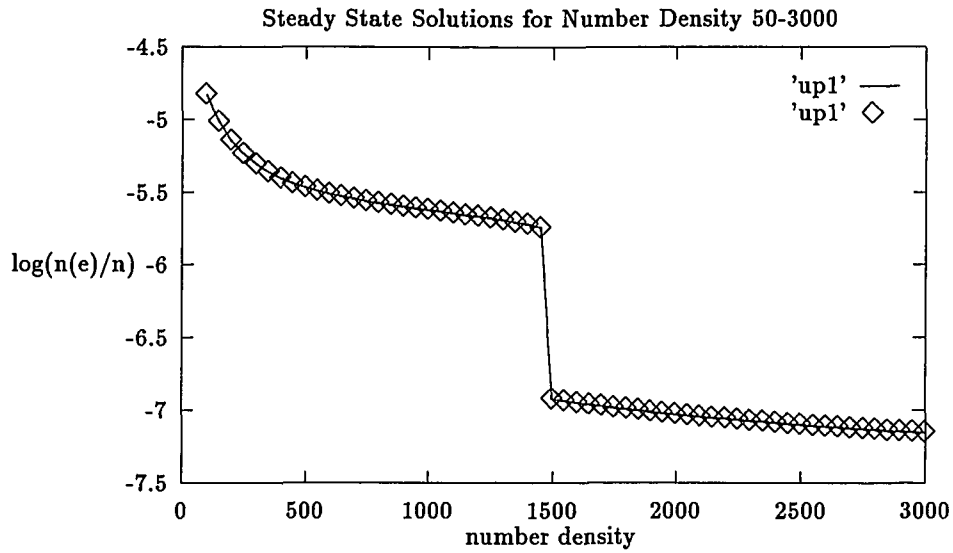


Figure 6: The phase transition for $50\text{-}3000 \text{ cm}^{-3}$ The diamonds represent the computed data points.

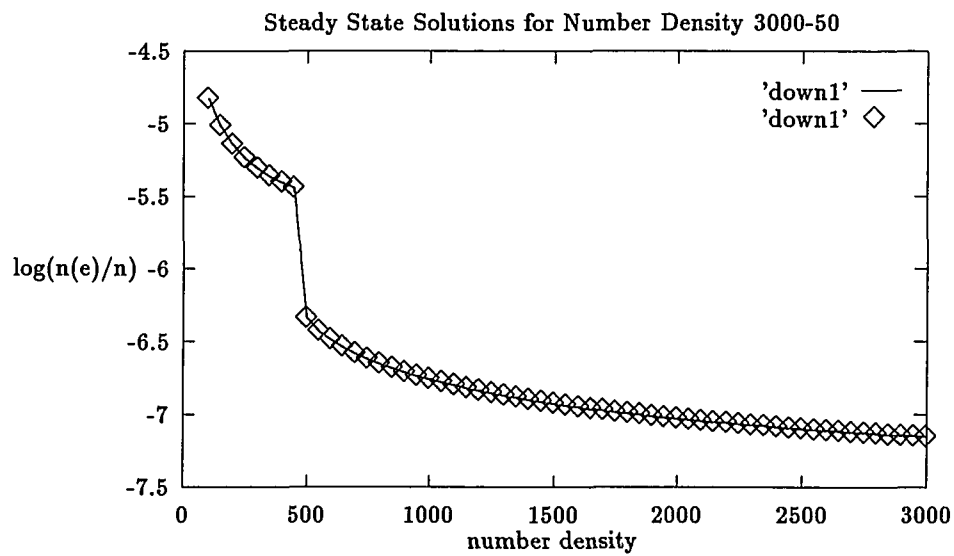


Figure 7: The phase transition $3000\text{-}50 \text{ cm}^{-3}$ The diamonds represent the computed data points.

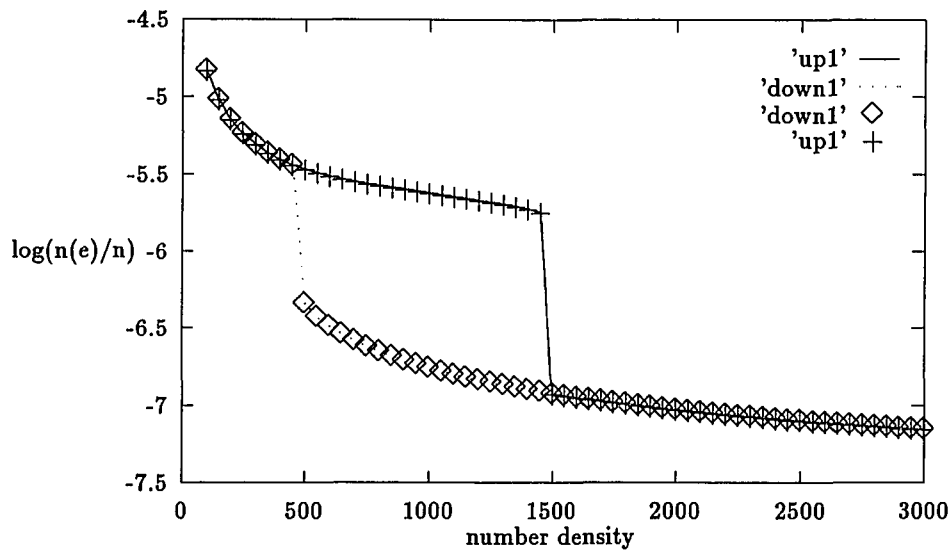


Figure 8: Superposition Figs. 6 and 7 Note the Bistable Region *The lines and dotted lines refer to the fits of the computed data points. The computed data points are represented by diaomnds and crosses.*

and X_{ej} are the fractional ionizations from a steady state solution, if

$$X_{ei} \neq X_{ej} \quad (6.4)$$

then a **Bistable Solution** exists. If the graphs of steady state solutions have a a region where two different solutions exist for the same density, this region is called a **Bistable Region**. Notice that for a number density of 450 cm^{-3} to 1500 cm^{-3} a bistable region exist. The loop in Figure 8 is called a hysteresis loop. The physical significance of this will be discussed later in this chapter.

The Bistability Diagram

The bistable region is represented schematically in Figure 9. Understanding Figure 9 is important because all of the bistable steady state solutions computed for the

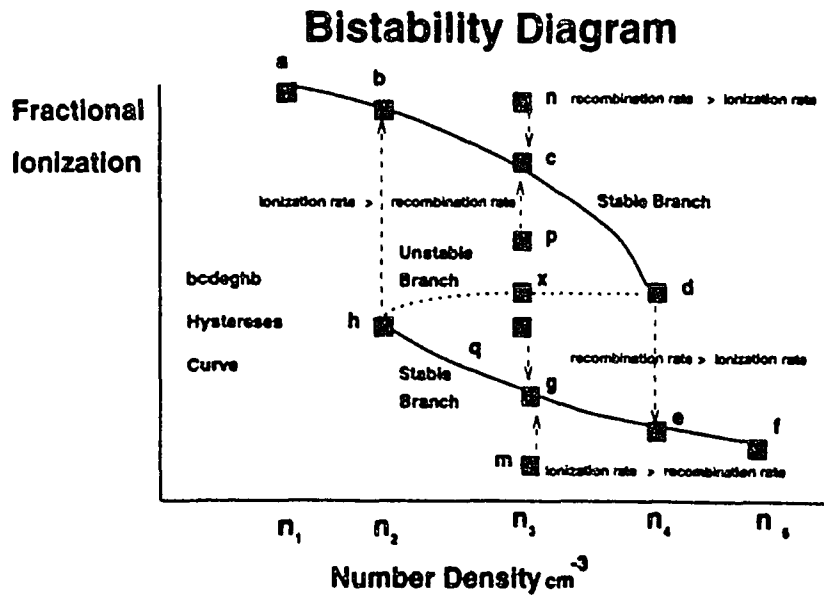


Figure 9: Points in the Bistable Region. Segments $abcd$ $hgef$ are stable solutions. The dotted line dxh is an unstable solution.

chemical model are topologically equivalent to Figure 9.

The prominent features of Figure 9 are the segments $abcd$ and $hgef$. These curves represent steady state solutions to the chemical model. The dotted line dxh represents a set of solutions which are in unstable equilibrium. If a point falls on any of these three curves the recombination rate is equal to the ionization rate. Notice that if the system is on curves $abcd$ or $hgef$, then a small perturbation from these curves will result in the system returning to the curves. This occurs because they are sets of solutions in stable equilibrium. However, if the system is on the unstable curve dxh , a perturbation will cause the system to diverge from dxh and approach the stable curves.

The remaining points not on these three curves are not in steady state equilibrium. Points n, p, q and m represent the non-equilibrium condition. Thus, the

recombination and ionization rates will not be equal. It is instructive to examine these points individually.

If the system is a point n , then the recombination rate will be higher than the ionization rate because to achieve equilibrium it must move to the lower fractional ionization region. If the system is at points p and q , it will tend to move away from the unstable curve dxh . Thus, point p will have to have an ionization rate larger than the recombination rate and will approach curve $abcd$, while point q will have to have a recombination rate higher than the ionization rate and will approach curve $hgef$. If the system is at point m , then in order for equilibrium to be achieved the ionization rate must be larger than the recombination rate, because it must approach curve $hgef$.

The phase transitions are represented by paths de and hb . It is important to point out that these paths may be traversed in only one direction. This behavior is the property that allows for the bistable phenomenon to occur. If the number density is monotonically increased from the initial point (n_1, a) , it will continue in the high ionization state until it reaches (n_4, d) . At (n_4, d) a phase transition will occur and it will move to the lower ionization state which is represented by (n_4, e) . If the number density continues to increase the system will remain in the low ionization state. However if the the number density is monotonically decreased, it will remain in the low ionization state until it reaches point (n_2, h) . By continuously decreasing the number density the system will return to the high ionization phase. When it reaches the high ionization phase, it is possible to increase the number density and

the system will continue to move around the curve **bcdeghb**.

The Belousov-Zhabotinski (B-Z) type reaction consist of chemical system which undergos self-sustained oscillations which can be periodic or chaotic (Thompson 1982). The loop **bcdeghb** is known as a hysteresis loop. If a cycle happens to occur, then a Belousov-Zhabotinski type reaction is possible (Thompson 1982). Note that the direction that the loop can only be transversed in a clockwise direction. From a theoretical prospective, this is important because it will allow one to determine the history of the system once the hysteresis curve has been calculated. The clouds number density is related to the clouds volume by the expression: $n = \frac{k}{V}$ where k is the total number of particles in the cloud.

Thus, if the system is at point g there are only two possible paths that would allow the system to reach g, namely **feg** and **abcdeg**. It seems unlikely that a mechanism exists that allows the volume of the cloud to contract then suddenly expand. It would require a large change in the kinetic energy of the system i.e (a large amount of work would have to be performed). There are no physical processes that could provide the energy to do this work in a quiescent cloud. This implies that the cloud would not traverse path **abcdeg**. Thus, if the system is at point g, we must conclude the cloud is undergoing some type of expansion.

If there were some mechanism which would supply the energy to allow this path to be taken, it would be theoretically possible to observe a B-Z type reaction. If the B-Z reaction were observed then observers would in principal be able to detect variations in chemical abundances over astronomical time scales.

A more practical procedure would be to search for signatures of each ionization phase. The high C abundance ($N_{CI} = 0.1N_{CO}$) has been in several sources: the core of the Orion Molecular, (Phillips and Higgins 1981) (Jaffe, Harris, Silber, Genzel, and Betz 1985) M17,W51,W3 (Zmuidzinas Betz and Goldhaber 1986) and S140 (Keene, Blake, Phillips ,Huggins and Beichman 1985). This is particularly tantalizing since high C abundances are found in the high ionization phase.

The Cusp Catastrophe

It is interesting to note that bistability can be expressed in terms of a new paradigm, which is called catastrophe theory. Paradigms that enhance qualitative interpretation of steady state solutions are useful because sometimes they provide insight into physical process. The Cusp Catastrophe can be used as a new paradigm to understand bistable phenomenon. A bistability is generated when a cross section is taken from a cusp catastrophe. This section provides a graphical explanation of the cusp catastrophe.

Consider the surface which is represented in Figure 10. Each point on the surface of the graph represents a steady state solution in which the system is in equilibrium. Note the graph has a pleat. The pleat can be interpreted as the set of inaccessible points while point on the surface which are above and below the pleat may be interpreted as bimodal set stable points. Catastrophe theory denotes parameters as control variables. However, for this study the phrase control variable will be synonymous with parameter.

The cusp catastrophe occurs when the system in question has 2 different control

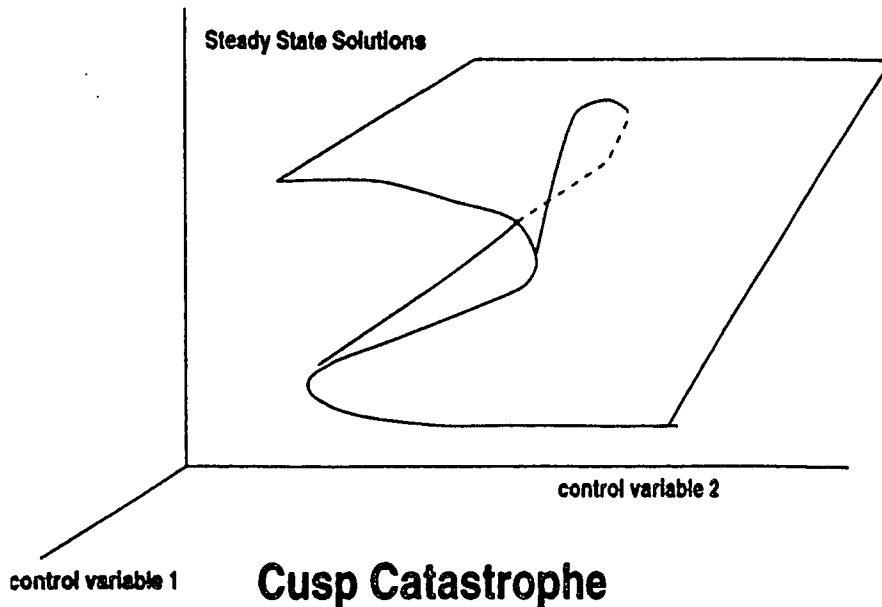


Figure 10: Graph of a Cusp Catastrophe: *Notice the pleat represents a region that is not accessible.*

factors. Its graph is a three dimensional surface with a pleat. A graph of a cusp catastrophe is given in Figure 10. Every point on the surface and not on the pleat is a point in steady state equilibrium. Further inspection of Figure 10 illustrates that there are certain combinations of control factors which allow two possible states. The behavior of the system under these conditions is referred to as bimodality.

Figure 11 is similar to Figure 10 but it has labels. As the surface is traversed from c to a to b to e it is possible to follow this path in any direction. This is denoted by the existence of double arrows. However, while it is possible to traverse the graph from c to d to e to f, it is not possible to traverse the surface from c to f to e to d. Notice the change from c to a to b to e is a smooth change and will occur slowly. A

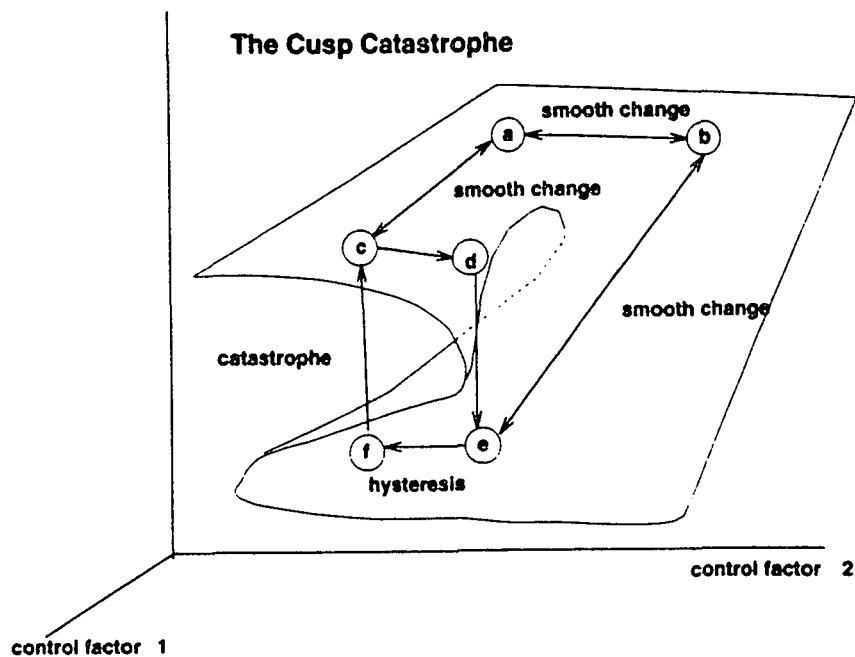


Figure 11: Traversing the Cusp Catastrophe: *There are two possible paths to point e. Path cabe involves a smooth change while path cde involves a discontinuous change. A cross section through cdef is a bistable region.*

catastrophe will occur when the surface is traversed from d to e or from f to c.

Summary

The following summary of chapter 6 is presented. The fractional ionization has been defined to characterize the steady state solutions associated with the chemical model of the molecular cloud. Phase transitions have been identified as a discontinuity of the steady state solution set which shows where a phase transition occurs. It has also been shown that sensitivity to the initial conditions will cause the existence of a bistable region. The bistable region is a cross sectional cut of the topological surface known as a cusp catastrophe. It was speculated that the bistable curve has a hysteresis region

which might support a B-Z type reaction.

Chapter 7

Phase Transitions in Molecular Clouds

This chapter will explain the general characteristics of chemical phase transitions in the molecular cloud and the effect of the phase transition on the chemistry of the cloud. The chemistry of the molecular cloud is characterized by the fractional ionization. Steady state solutions of the chemical model sometimes exhibit discontinuous behavior. As was explained in chapter 6, the discontinuity that appears in the fractional ionization curve separates the two chemical phases. The two phases of chemistry associated with the molecular or dark interstellar clouds are designated as the **high ionization phase (HIP)** or the **low ionization phase (LIP)**. This chapter will explain the chemical process that allows a phase transition to occur between HIP and the LIP. We will then explain how various species behave in the HIP and LIP. All solutions discussed in this chapter will be considered at steady state.

The slope of the fractional ionization

The steady state behavior of the fractional ionization is crucial for understanding phase transitions. An empirical description of this behavior is given by plotting the logarithm of the fractional ionization versus number density. When the logarithm of

the fractional ionization is plotted as a function of the number density the slope is always negative in regions where the function is piecewise continuous. This behavior can be modeled as

$$\log X_e = \log A - \beta \log(n) \quad (7.1)$$

or by transposing to an algebraic form:

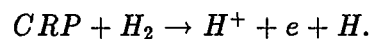
$$X_e = \frac{A}{n^\beta} \quad (7.2)$$

where β is a positive constant, A is a constant and n is the number density. Chapter 9 presents some methods for estimating β for special cases, but in general all that can be ionization has an inverse relationship to n , the number density.

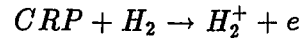
The General Chemistry of the LIP and the HIP

The ratio of H_2 with the second most abundant species in the cloud CO has been measured to be 8000 to 1 (Wootten et. al. 1982). The large abundance of hydrogen implies that hydrogen in some ionic or molecular form will contribute significantly to the molecular cloud chemistry. A large portion of the chemistry of the LIP and the HIP can be understood by understanding the ionization and recombinations of H^+ and H_3^+ .

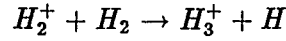
Solutions to the chemical model indicate that the dominant mechanism for the productions of H^+ is a one step process:



While, the production of H_3^+ is a two step process.

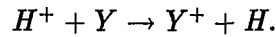


The H_2^+ is quick to react with the molecular hydrogen to produce H_3^+

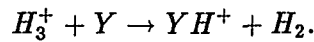


For both the HIP and LIP the rate of H^+ , H_3^+ and electron production is constant. Thus, the difference in the abundances of H^+ , H_3^+ and electrons can be attributed to the recombination of H^+ and the destruction of H_3^+ .

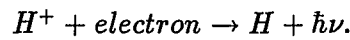
It has been established by Le Bourlot (1993) that the HIP is dominated by the charge transfer reaction of H^+ . This is reflected in the fact that the charge transfer reaction:



dominates the proton transfer reaction:



The H_3^+ will react with electrons in both the HIP and the LIP. H^+ will not react with a significant number of electrons. The reason for this is that H^+ reacts with electrons via radiative association:



The radiative association rate coefficient is $3.5 \times 10^{-12} \text{ cm}^3 \text{ s}^{-1}$, while the rate coefficient for dissociative recombination of H_3^+ is $5.23 \times 10^{-7} \text{ cm}^3 \text{ s}^{-1}$. Thus, H_3^+ will react with electrons at a rate equal to 5 orders of magnitude faster than H^+ . The

charge transfer rate coefficient of H^+ is between 1.0×10^{-9} and $9.00 \times 10^{-9} \text{ cm}^3 \text{ s}^{-1}$. Therefore, the H^+ ion will react via charge transfer. Since there is a relatively large abundance of H^+ , the charge transfer process is dominant at HIP.

Examination of the UMIST Ratefile (Farquhar and Millar 1993) shows that a very large proportion of the reactions with the H^+ ion are charge transfer reactions. This is convenient because it allows us to write a model for the steady state abundance of the H^+ ion based on the charge transfer. Note, that the radiative recombination is a slow process and its effect will be negligible.

The sum of the creation and recombination terms may be expressed as:

$$\frac{d[H^+]}{dt} = \zeta[H_2]f_{H^+} - \sum_i [H^+][Y_i] \quad (7.3)$$

where f_{H^+} corresponds to the amount of H_2 that is converted to H^+ in the cosmic-ray ionization process of H_2 . The steady state condition implies:

$$\frac{d[H^+]}{dt} = 0. \quad (7.4)$$

Substituting (7.2) and rewriting yields:

$$\zeta[H_2]f_{H^+} = \sum_i [H^+][Y_i]. \quad (7.5)$$

Converting to the fractional ionization produces:

$$\zeta f_{H^+} X_{H_2} = n X_{H^+} \sum_i X_{Y_i}. \quad (7.6)$$

Solving for the fractional abundance of H^+ yields:

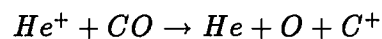
$$X_{H^+} = \frac{\zeta X_{H_2} f_{H^+}}{n \sum_i X_{Y_i}}. \quad (7.7)$$

The fact that the fractional abundance is a function of $\frac{1}{n}$ and the fractional ionization is a function of the $\frac{1}{n^\beta}$ provides a clue as to why the phase change occurs. Notice when the number density increases the abundance of H^+ and the electrons decrease. Since there are fewer electrons, to react with H_3^+ , there will be more H_3^+ available to undergo proton transfer.

The extra H_3^+ ions will begin to react with the CO and the O to form HCO^+ and OH^+ . The OH^+ will react with molecular hydrogen to produce H_2^+O . The H_2^+O will react quickly with H_2 to produce H_3^+O .

The creation of H_3^+O has two important effects. First, the H_3^+O can undergo dissociative recombination to produce H_2O and OH . This reaction will compete with the H_3^+ for electrons. This has the effect of freeing up H_3^+ to undergo proton transfer with other species. The second effect involves the OH . It can now react with atomic oxygen to produce molecular oxygen which can react with the atomic ions such as S^+ , H^+ , and C^+ . This has a dramatic impact on the ratio of H_3^+ to H^+ as is illustrated in Figure 12. This process is a result of the system moving from the HIP to the LIP. In addition to this process, the HCO^+ will also compete with electrons. Thus, as the phase transition point is reached, the H_3^+ will begin to increase in abundance. This is illustrated by the high resolution graph.

Carbon ions are responsible for the ionization of the sulphur, silicon, phosphorous and the metals. The C^+ will charge exchange with these species. The C^+ is produced by



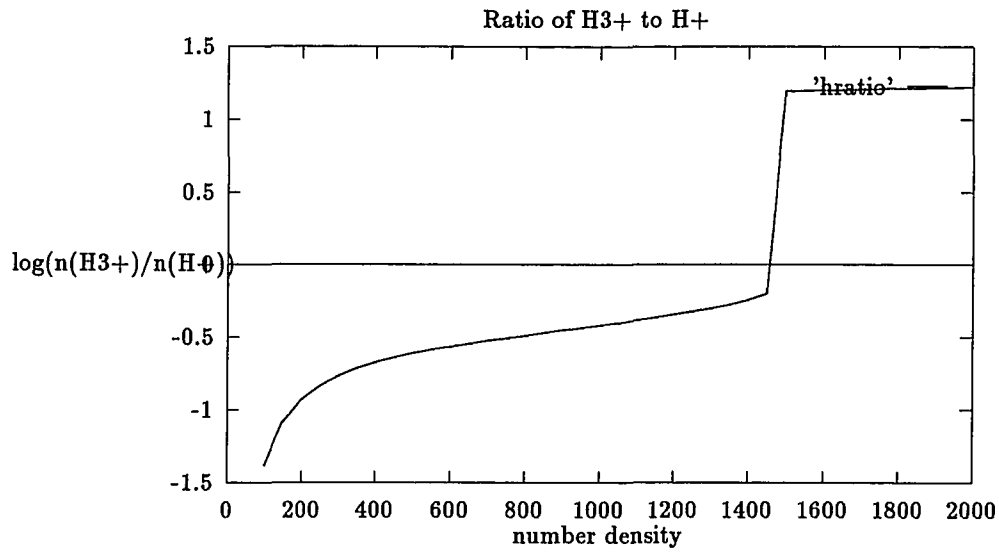


Figure 12: The ratio H_3^+ to H^+ Note different functional forms for HIP and LIP.

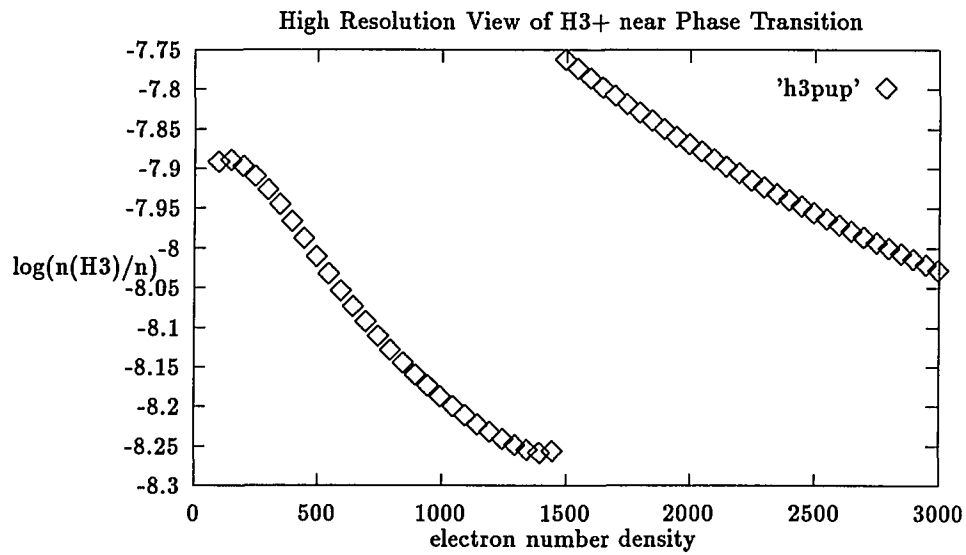


Figure 13: H_3^+ Phase Transition from HIP to LIP Note this is a high resolution graph

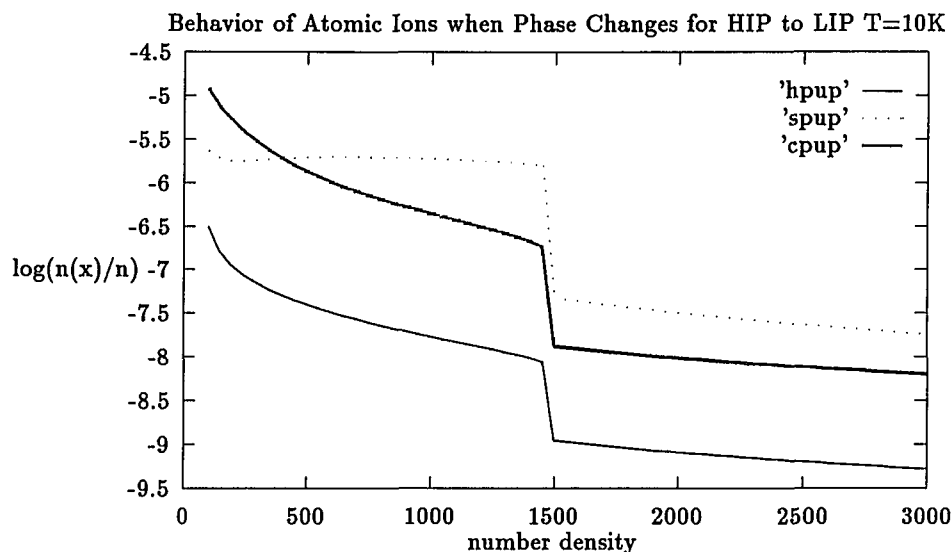


Figure 14: Major atomic ions C^+ , H^+ , S^+ for HIP and LIP (hpup= H^+ , spup= S^+ and cpup= C^+)

When the system is in the HIP sulphur, silicon, phosphorous and the metals are all ionized. However when the system moves from HIP to LIP, the number of monatomic ions such as H^+ , C^+ and S^+ decrease. This is illustrated in Figure 14.

The metals, on the other hand, remain ionized. This effect can be attributed to the fact that metal will recombine though the radiative recombination process:



where M is either Na , Mg or Fe . The radiative recombination rate coefficient is of the order of $10^{-12} \text{ cm}^3 \text{ s}^{-1}$, which is relatively slow. The metallic ions therefore tend to remain in ionic form as the system undergoes phase transition. In the LIP more metals will be ionized because the molecular ions will charge transfer with the metals.

One characteristic difference between the HIP and the LIP is the types of ions

that are dominant in each state. Figure 14 illustrate some of the atomic ions in both phases. As would be expected, they decrease in abundance as the system moves to the LIP. Figure 15 illustrates some of the difference in molecular ions. The molecular ions increase in abundance as the system moves form HIP to LIP. The molecular ions recombine via charge transfer to produce molecules, this is illustrated in Figure 16.

We will conclude this discussion by pointing to an interesting fact. When we enhance the abundance of metals, carbon, sulphur or silicon to an abnormally high level, it is possible to maintain the system in a HIP. This can be attributed to charge conservation. Since the initial abundance is enhanced, a large fraction of the species become ionized. Charge conservation dictates that the negative charge must be in the form of electrons. The additional electrons are available to undergo dissociative recombination with the H_3^+ . This decreases the number of H_3^+ ions and allows the H^+ to dominate the chemistry allowing the system to maintain itself in the HIP.

Mathematical Conditions for the HIP and LIP

Tables 7 and 8 illustrate that when the cloud is in a HIP the dominant mechanism for the removal of electrons is the dissociative recombination reaction with H_3^+ and the electrons. By inspection of Tables 6 and 7, we note that when the system is in the LIP the dominate mechanism for electron removal is electrons undergoing dissociative recombination with HCO^+ and H_3O^+ . The dominate mechanism for the removal of H_3^+ is its reactions with CO and O .

These facts motivate the construction of a mathematical model of the which places

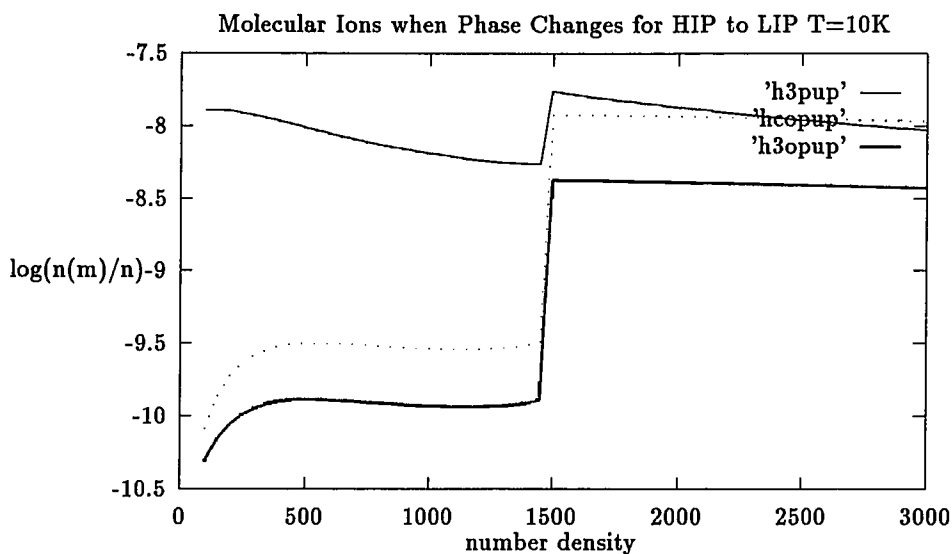


Figure 15: Behavior of Molecular Ions in LIP and HIP. This figure illustrates the behavior of molecular ions H_3^+ , HCO^+ and H_3O^+ . The abundance increases after the phase transition to LIP.

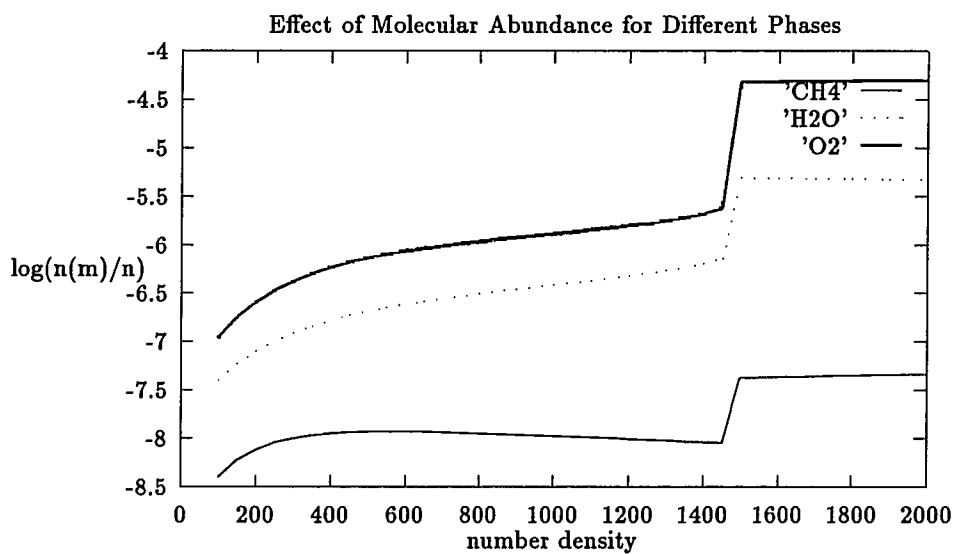


Figure 16: Behavior of Molecules in HIP and LIP. This figure illustrates the behavior of molecules CH_4 , H_2O and O_2 . The abundance increases after the phase transition to LIP.

HIP	
Reaction	H_3^+ Rate
$H_2^+ + H_2 \rightarrow H_3^+ + H$	$1.18 \times 10^{-17} \text{sec}^{-1}$
$H_3^+ + O \rightarrow OH^+ + H_2$	$1.31 \times 10^{-18} \text{sec}^{-1}$
$H_3^+ + CO \rightarrow CO^+ + H_2$	$1.93 \times 10^{-18} \text{sec}^{-1}$
$H_3^+ + e \rightarrow 3H$	$4.30 \times 10^{-18} \text{sec}^{-18}$
$H_3^+ + e \rightarrow H_2 + H$	$4.30 \times 10^{-18} \text{sec}^{-18}$
LIP	
Reaction	H_3^+ Rate
$H_2^+ + H_2 \rightarrow H_3^+ + H$	$1.18 \times 10^{-17} \text{sec}^{-1}$
$H_3^+ + e \rightarrow 3H$	$9.48 \times 10^{-19} \text{sec}^{-1}$
$H_3^+ + e \rightarrow H_2 + H$	$9.49 \times 10^{-19} \text{sec}^{-1}$
$H_3^+ + O \rightarrow OH^+ + H_2$	$2.14 \times 10^{-18} \text{sec}^{-1}$
$H_3^+ + CO \rightarrow HCO^+ + H_2$	$6.31 \times 10^{-18} \text{sec}^{-1}$

Table 7: Rates for creation and destruction of H_3^+ in HIP and LIP

HIP	
Reactions	Electron Rate
$H_2 + CRP \rightarrow H_2^+ + e$	$1.2 \times 10^{-17} \text{sec}^{-1}$
$H_3O^+ + e \rightarrow H_2O + H$	$5.09 \times 10^{-19} \text{sec}^{-1}$
$H_3O^+ + e \rightarrow OH + H$	$1.18 \times 10^{-18} \text{sec}^{-1}$
$HCO^+ + e \rightarrow H + CO$	$2.75 \times 10^{-18} \text{sec}^{-1}$
$H_3^+ + e \rightarrow 3H$	$4.3 \times 10^{-18} \text{sec}^{-1}$
$H_3^+ + e \rightarrow H_2 + H$	$4.3 \times 10^{-18} \text{sec}^{-1}$
LIP	
Reactions	Electron Rate
$H_2^+ + H \rightarrow H_3^+ + H$	$1.18 \times 10^{-17} \text{sec}^{-1}$
$H_3^+ + e \rightarrow 3H$	$9.48 \times 10^{-19} \text{sec}^{-1}$
$H_3^+ + e \rightarrow H_2 + H$	$9.48 \times 10^{-19} \text{sec}^{-1}$
$H_3O^+ + e \rightarrow H_2O + H$	$1.421 \times 10^{-18} \text{sec}^{-1}$
$H_3O^+ + e \rightarrow OH + H$	$2.65 \times 10^{-18} \text{sec}^{-1}$
$HCO^+ + e \rightarrow H + CO$	$6.95 \times 10^{-18} \text{sec}^{-1}$

Table 8: Rates for recombination and ionization of electrons in HIP and LIP

bounds on the abundances of CO , O , HCO^+ , and H_3O^+ for the HIP and the LIP.

We begin by writing expressions for the rates of the electron and H_3^+ as follows:

$$\frac{d[H_3^+]_+}{dt} = k_{H_2^+}[H_2][H_2^+] \quad (7.8)$$

for the rate of formation of H_3^+ and we can also write

$$\frac{d[e]_+}{dt} = \zeta[H_2] \quad (7.9)$$

to represent the formation of electrons.

The destruction of the H_3^+ ions and electrons is described by the following relations.

$$\frac{d[H_3^+]_-}{dt} = 2k_e[H_3^+][e] + k_1[H_3^+][CO] + k_2[H_3^+][O] + \epsilon_{H_3^+} \quad (7.10)$$

$$\frac{d[e]_-}{dt} = 2k_e[H_3^+][e] + k_3[HCO^+] + k_4[H_3O^+][e] + \epsilon_e \quad (7.11)$$

Combining equations 7.8, 7.9, 7.10 and 7.11 we obtain an expression for the which approximates the rate of formation and recombination for H_3^+ ions and electrons.

The terms ϵ_e and $\epsilon_{H_3^+}$ represent the other recombination processes associated with the following equations:

$$\frac{d[H_3^+]}{dt} = k_{H_2^+}[H_2][H_2^+] - 2k_e[H_3^+][e] - k_1[H_3^+][CO] - k_2[H_3^+][O] - \epsilon_{H_3^+}. \quad (7.12)$$

and

$$\frac{d[e]}{dt} = k_{H_2^+}[H_2][H_2^+] - 2k_e[H_3^+][e] - k_3[HCO^+] - k_4[H_3O^+][e] - \epsilon_e \quad (7.13)$$

As previously stated, when the system is in the high ionization state the models indicate that dissociative recombination of the H_3^+ ion is the dominant mechanism

for the destruction of H_3^+ and electrons. Because the production of H_3^+ and electrons is virtually constant, we consider only those terms which destroy H_3^+ and electrons.

When the system is in the HIP the following inequalities were observed to hold.

$$2k_e[H_3^+][e] > k_1[H_3^+][CO] + k_2[H_3^+][O] \quad (7.14)$$

and

$$2k_e[H_3^+][e] > k_3[HCO^+][e] + k_4[H_3O^+][e] \quad (7.15)$$

for the HIP.

H_3^+ appears on both sides of the first inequality so it cancels, while electrons appear on both sides of the second so they cancel. If we divide by the number density we obtain:

$$2k_e X_e > k_1 X_{CO} + k_2 X_O. \quad (7.16)$$

and

$$2k_e X_{H_3^+} > k_3 X_{HCO^+} + k_4 X_{H_3O^+} \quad (7.17)$$

We can now divide both sides by $2k_e$ to obtain:

$$X_e > \frac{k_1 X_{CO} + k_2 X_O}{2k_e} \quad (7.18)$$

and

$$X_{H_3^+} > \frac{k_3 X_{HCO^+} + k_4 X_{H_3O^+}}{2k_e} \quad (7.19)$$

For the LIP, the rate of electron destruction is dominated by the dissociative recombination of electrons with HCO^+ and H_3O^+ . Mathematically, it means that we can reverse the signs in the above inequalities to obtain conditions for the LIP:

$$2k_e[H_3^+][e] < k_1[H_3^+][CO] + k_2[H_3^+][O] \quad (7.20)$$

The rate at which H_3^+ ion are removed is dominated by the protonation of atomic oxygen and carbon monoxide:

$$2k_e[H_3^+][e] < k_3[HCO^+][e] + k_4[H_3O^+][e] \quad (7.21)$$

Now we can divide both sides of the inequality by the number density and $2k_e$ to yield.

$$X_e < \frac{k_1X_{CO} + k_2X_O}{2k_e} \quad (7.22)$$

$$X_{H_3^+} < \frac{k_3X_{HCO^+} + k_4X_{H_3O^+}}{2k_e} \quad (7.23)$$

Expressions 7.18 and 7.23 are useful because they allow us to predict what initial abundances will produce an HIP or a LIP. An example will be presented in the next section.

Amount of Metals Needed to Maintain HIP in TMC1

For example if we want to know how much initial metallic abundance we need to remain in the HIP we can use expression 7.18

$$X_e > \frac{k_1X_{CO} + k_2X_O}{2k_e} \quad (7.24)$$

and the Oppenheimer approximation for the fractional ionization (see Chapter 9 for a discussion and derivation):

$$n_e^3 = \frac{\zeta\beta n n_M}{\alpha_r \alpha} \quad (7.25)$$

We must rewrite expression 7.25 in terms of the fractional ionization. This requires that both sides be divided by the number density cubed.

$$X_{n_e} = \left(\frac{\zeta\beta X_M}{n\alpha_r \alpha} \right)^{\frac{1}{3}} \quad (7.26)$$

Substitution (7.26) into (7.24) yields:

$$\left(\frac{\zeta\beta X_M}{n\alpha_r \alpha} \right)^{\frac{1}{3}} > \frac{k_1 X_{CO} + k_2 X_O}{2k_e}. \quad (7.27)$$

Several constants in these equations are known $\zeta = 1.25 \times 10^{-17} \text{sec}^{-1}$, $\beta = 10^{-9} \text{cm}^3 \text{sec}^{-1}$, $\alpha = 10^{-6} \text{cm}^3 \text{sec}^{-1}$, $\alpha_r = 10^{-11} \text{cm}^3 \text{sec}^{-1}$, $k_1 = 1.7 \times 10^{-9} \text{cm}^3 \text{sec}^{-1}$, $k_O = 8.0 \times 10^{-10} \text{cm}^3 \text{sec}^{-1}$, and $2k_e = 2.75 \times 10^{-7} \text{cm}^3 \text{sec}^{-1}$

We may now substitute the constants into expression (7.13.20), noting that the term involving the oxygen can be ignored because we cube both sides of the inequality.

$$\frac{X_M}{n} > X_{CO}^3 \times 1.8 \times 10^2 \quad (7.28)$$

For the TMC the measured value of the relative abundance of CO is 8.00×10^{-5} . If this value is substituted into the inequality we can write:

$$X_M > 9.2 \times 10^{-11} \times n \quad (7.29)$$

For a number density of $n = 10^4$, then fractional abundance of metals must be greater than 9.2×10^{-7} to maintain the HIP. This value has been confirmed by the chemical model.

Addition of Electron Rich Sources

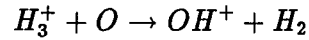
Consider the expression below:

$$X_e > \frac{k_1 X_{CO} + k_2 X_O}{2k_e}. \quad (7.30)$$

Notice that if the dissociative recombination constant is increased, then number of electrons necessary to maintain the HIP will decrease. Also, notice that by depletion of the atomic oxygen and the carbon monoxide, the number of electrons necessary to maintain the HIP is lower. If we have an element such as sulphur, which provides electrons to maintain the HIP it will take less sulphur to maintain the HIP, in a depleted region. This is in agreement with Le Bourlot et. al. (1993) model which used ultra-low depletions.

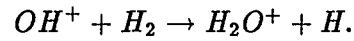
Hydrogen Oxygen Chemistry

The chemistry of hydrogen and oxygen undergoes a dramatic change when the system goes from HIP to LIP. There are two important species that are the end products of this process: H_2O and OH . An examination of Table 9 illustrates this process. The most interesting feature of this table is the dramatic increase in the abundance of water by a factor of 30. There is also a 7 fold increase the OH abundance. The reason for this increase is due to the increased rate of OH^+ production via dissociative recombination in the low ionization phase. The reaction:

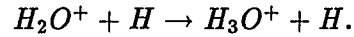


is 2.8 times faster in the low ionization phase than in the high ionization phase. This is the initial step in the process which creates H_3O^+ .

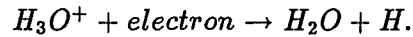
The OH^+ ion reacts with H_2 to produce H_2O^+



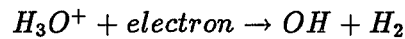
The H_2O^+ ion reacts with H_2 to produce H_3O^+ :



The H_3O^+ can now through dissociative recombination form H_2O or OH :

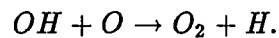


We note that the next reaction is responsible for the production of the OH radical.



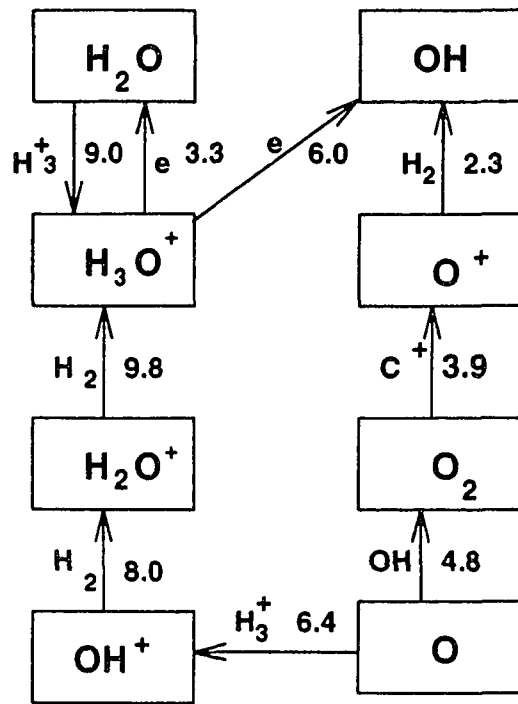
In the low ionization state this reaction is 3.63 times faster than the high ionization state.

The enhanced rate of this reaction is the reason that more atomic oxygen is converted into molecular oxygen:



Figures 17 and 18 illustrate the hydrogen oxygen chemistry for these reactions in the LIP and the HIP phase.

Hydrogen Oxygen Chemistry HIP



Multiply by $1.0 \times 10^{-19} \text{ sec}^{-1}$

Figure 17: HIP Reaction Networks for the Hydrogen Oxygen Chemistry

Hydrogen Oxygen Chemistry LIP

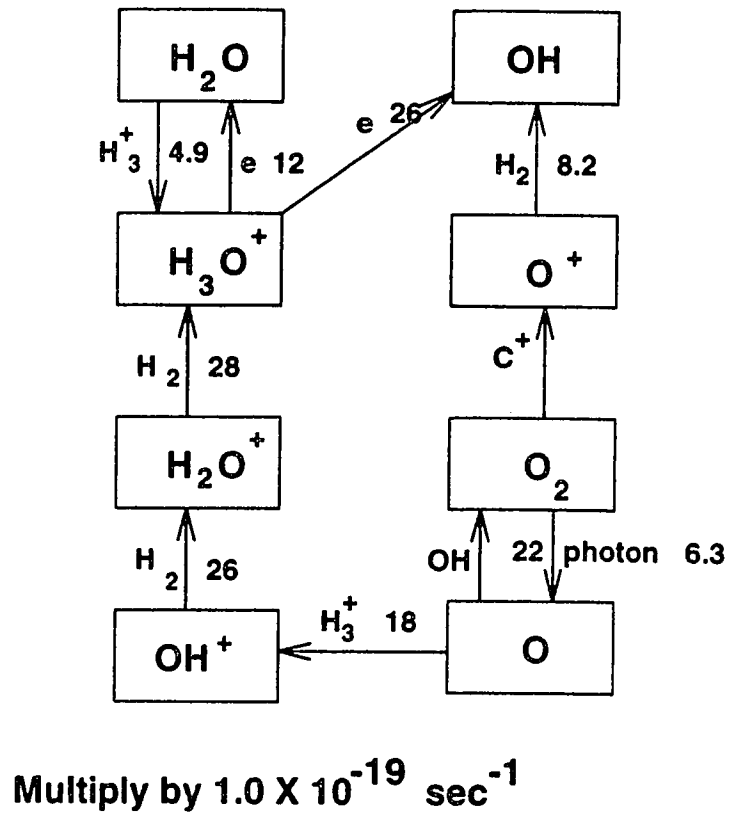


Figure 18: LIP Reaction Networks for the Hydrogen Oxygen Chemistry

Hydrogen Oxygen Abundance n=130		
Species	High Ionization	Low Ionization for
H_2O	1.64×10^{-07}	4.90×10^{-06}
O	2.40×10^{-04}	1.35×10^{-04}
H_2O^+	8.64×10^{-12}	2.63×10^{-11}
H_3O^+	2.51×10^{-10}	9.53×10^{-09}
OH	1.94×10^{-07}	1.54×10^{-06}
OH^+	6.85×10^{-12}	2.05×10^{-11}
H_2	9.95×10^{-01}	9.95×10^{-01}

Table 9: Hydrogen Oxygen Abundances at HIP and LIP *notice the increased abundance of molecules in the HIP.*

Carbon Oxygen Chemistry

The importance of oxygen and carbon to the chemistry of the dark interstellar cloud is based on their abundance and reactivity. Oxygen and carbon are, respectively, the third and fourth most abundant species in the cloud. Oxygen is highly reactive and will form oxides with most compounds, while carbon tends to form CO , triatomics, and molecules which have relatively long chains. Therefore, any substantial change in either of these species will significantly effect the chemistry of the dark interstellar cloud.

Table 9 lists some steady state solutions for some of the carbon species at the high and low ionization phases.

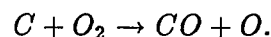
An analysis of Table 10 illustrates four important facts about the oxygen carbon chemistry as system moves form the HIP to the LIP. First, the amount of carbon C decreases by a factor of 120. Second, the amount of molecular oxygen O_2 increases by a factor of 56. Third, the amount of carbon monoxide CO increases by a factor of

Carbon and Oxygen n=130		
Species	High Ionization	Low Ionization
C	2.55×10^{-05}	2.11×10^{-07}
CO	1.10×10^{-04}	1.44×10^{-04}
O	2.40×10^{-04}	1.35×10^{-04}
O_2	5.72×10^{-07}	3.24×10^{-05}
C^+	4.77×10^{-06}	2.29×10^{-07}
CO^+	1.00×10^{-12}	1.82×10^{-12}
O^+	1.06×10^{-12}	3.71×10^{-12}

Table 10: Oxygen and Carbon Species At High and Low Ionization

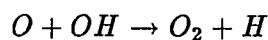
0.236. And fourth, the amount of atomic oxygen O decreases by a factor of 0.4375.

An explanation of these results can be found by examining the process which is destroying the atomic carbon C . We note in the low ionization phase the dominant process for the destruction of carbon involves the reaction with molecular oxygen O_2 :



Thus the increase in abundance of O_2 is responsible for the destruction of carbon.

The next question is how is the molecular O_2 oxygen created? In the HIP there is less O_2 available to react with the atomic carbon. This is because O_2 is produced by the reaction in both the high and the low ionization phases by reacting with the OH radical.



Figures 19 and 20 illustrate the reaction networks for this process.

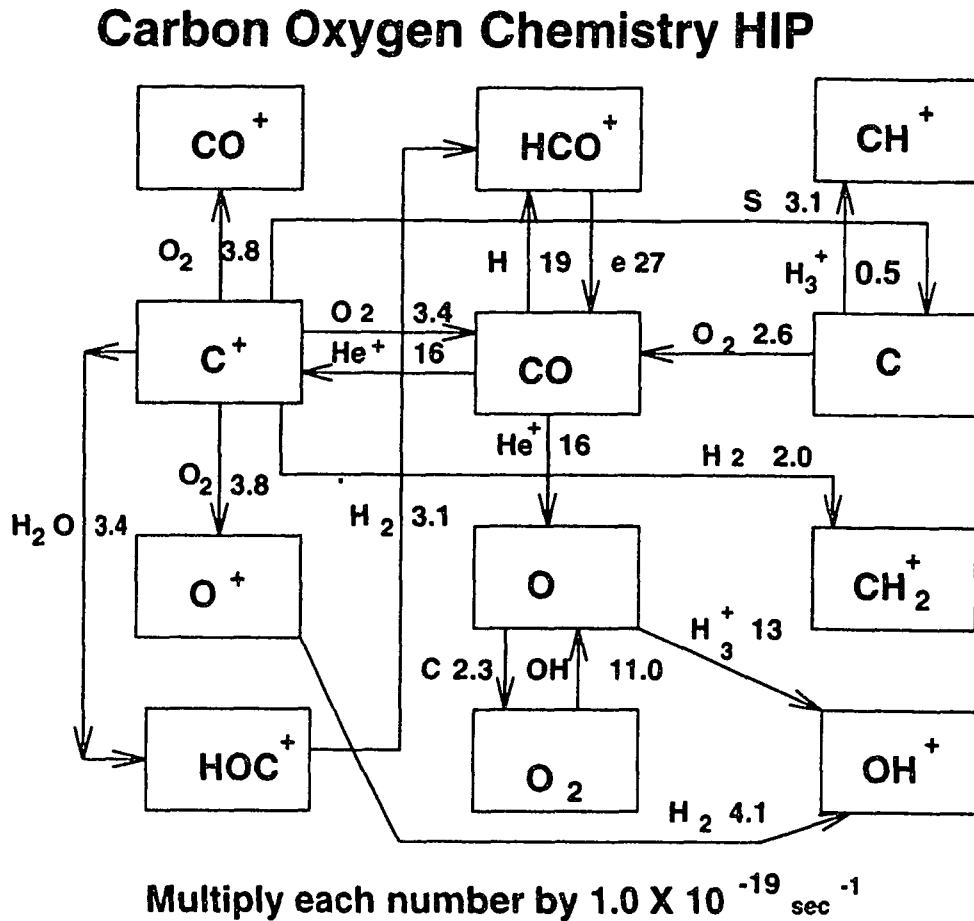


Figure 19: HIP Reaction Networks for the Carbon Oxygen Chemistry

Carbon Oxygen Chemistry LIP

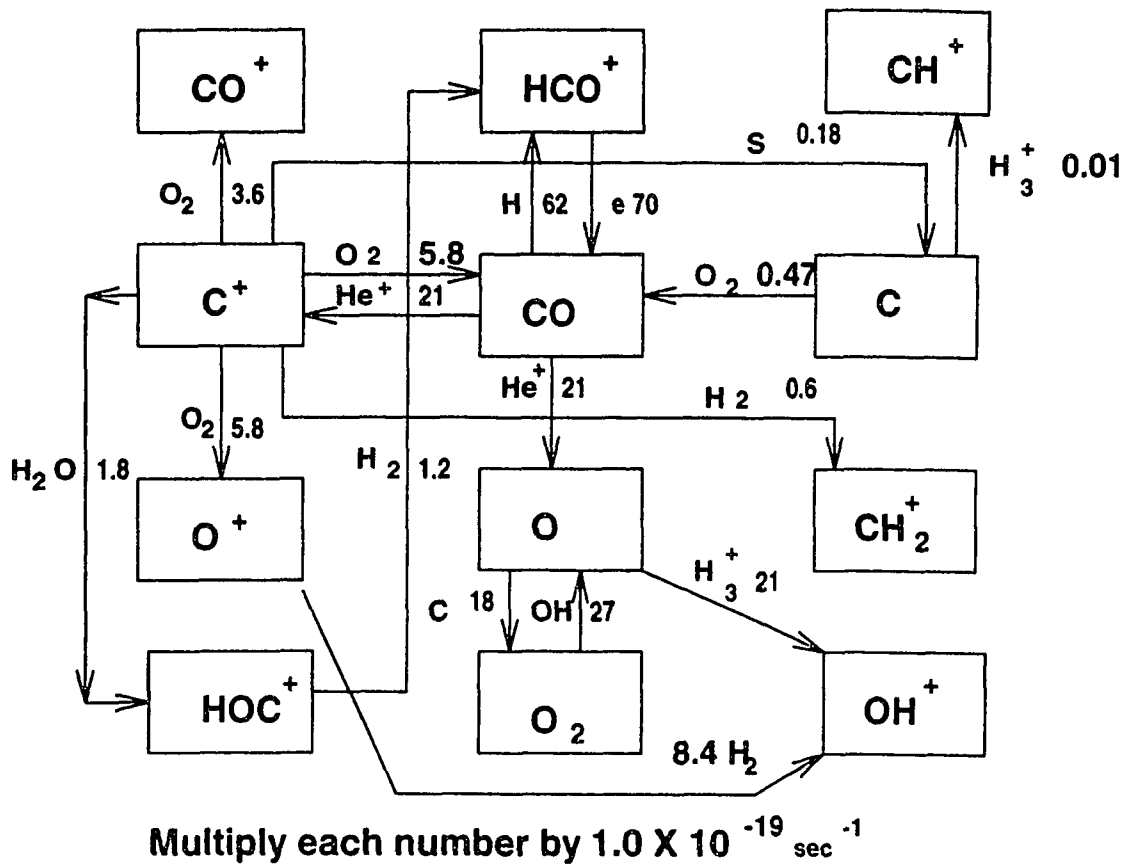
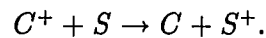


Figure 20: LIP Reaction Networks for the Carbon Oxygen Chemistry

Sulphur Chemistry

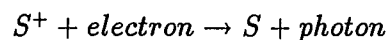
Sulphur can have a great impact on the chemistry of a dark molecular cloud. This is because sulphur can form sulphur ions, S^+ , by undergoing charge transfer with several different species while it is in the HIP. When the system is in the HIP a large proportion of the sulphur is ionized, by charge transferring with C^+



Refer to Table 11 to see the actual abundances in numerical form.

Sulphur is the dominant ion for charge transfer with Mg , Na , Si and it is competitive with the carbon ion for the ionization of Fe . Therefore, if the initial abundances of the sulphur are enhanced, the cloud will tend to remain in the HIP. Charge conservation dictates that there must exist an equal number of negative charges which will be in the form of electrons for the gas phase process. The large abundance of electrons will react through dissociative recombination with H_3^+ to decrease the number of H_3^+ . This will allow the charge transfer chemistry induced by the H^+ to remain dominant.

By inspecting Figure 21 the reader notices that as the system moves toward phase transition the abundance of S begins increasing. This effect can be attributed to the increasing abundance of molecular oxygen. The increased fractional abundance of oxygen will react with the C^+ ion. When S recombines it is less likely to react with C^+ . Some of the sulphur will recombine by radiative recombination.



Sulphur Chemistry n=1450		
Species	High Ionization	Low Ionization
S	7.96×10^{-7}	5.40×10^{-7}
SO	2.36×10^{-7}	1.73×10^{-6}
SO_2	6.69×10^{-10}	4.28×10^{-7}
S^+	1.56×10^{-6}	5.02×10^{-8}

Table 11: Sulphur Chemistry at LIP and HIP *Sulphur will provide a large number of ions in the HIP. However, when the system undergoes a transition into the LIP most of the S is in the form of the oxide SO.*

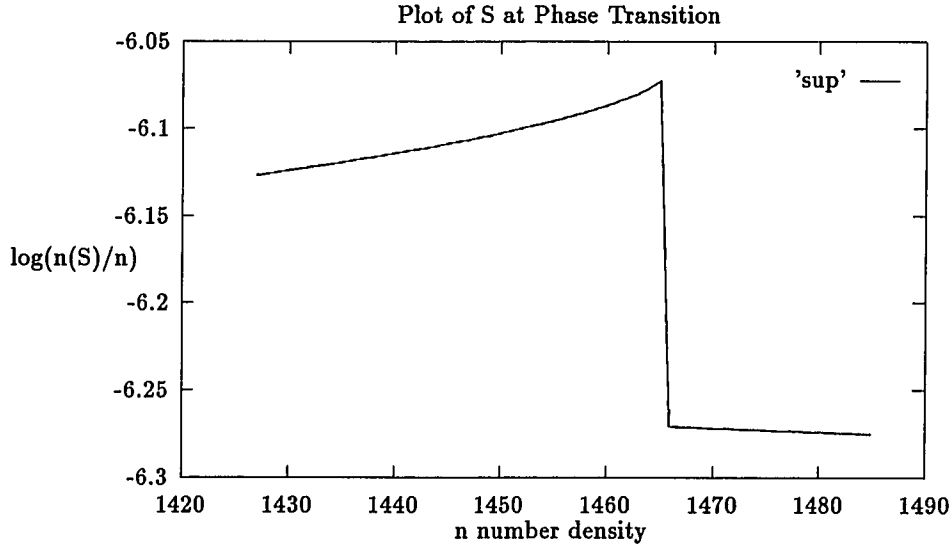


Figure 21: Behavior of Sulphur near the Phase Transition Note that $S=(\text{sup})$ up means we increment from low to high number density

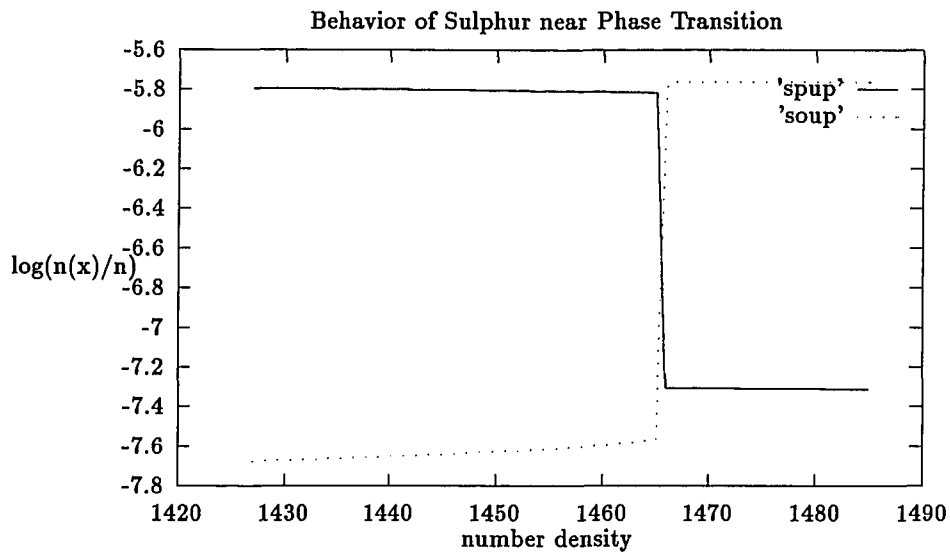


Figure 22: Behavior of S^+ (spup) and SO(soup) near the Phase Transition

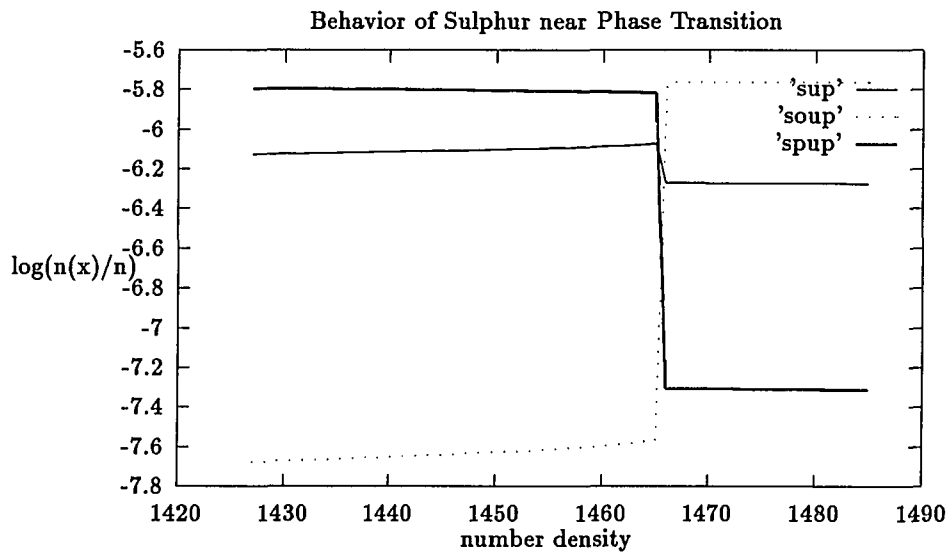
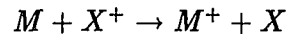


Figure 23: Behavior of S, S^+ , and SO near the Phase Transition

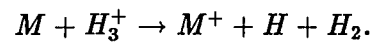
This reaction accounts for the increase in sulphur that is exhibited in Figure 21.

Metals

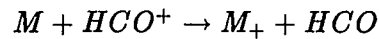
The metals in the molecular cloud are iron, magnesium and sodium. For the purpose of this discussion the metals, *Na*, *Mg* and *Fe* will be referred to as *M*. Metals once ionized tend to maintain their positive charge in both the low and high ionization phase. Metals are ionized by the charge transfer process



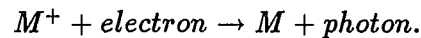
In the HIP, X^+ will correspond to a monatomic ion such as C^+ or S^+ . In the LIP, the metals are ionized by a dissociative recombination with H_3^+ or a charge transfer with a molecular ion such as HCO^+ :



and



The reason that metallic ions tend not to recombine is that metallic ions recombine with electrons through the process of radiative recombination.



The typical radiative recombination process is a slow process, the rate coefficient is of the order of $10^{-12} \text{ cm}^3 \text{ s}^{-1}$. The charge transfer process has a rate coefficient of

Na, Fe, and Mg n=1450		
Species	High Ionization	Low Ionization
Fe	4.0×10^{-10}	1.9×10^{-10}
Fe^+	5.5×10^{-9}	5.8×10^{-9}
Na	2.98×10^{-10}	1.9×10^{-10}
Na^+	3.7×10^{-9}	3.8×10^{-9}
Mg	7.4×10^{-10}	4.9×10^{-10}
Mg^+	5.25×10^{-9}	5.5×10^{-9}

Figure 12: Metals at High and Low Ionization *This table illustrates the behavior of metals. Once ionized, metals tend to remain ionized. This is because radiative recombination is a slow process. There is not an appreciable change in the ionic abundance in the HIP and the LIP. Most of the positive charge will be deposited on the metallic ions via the charge transfer process.*

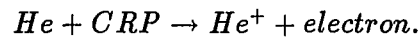
the order of $10^{-9} \text{ cm}^3\text{s}^{-1}$ and the molecule-ion process has a rate coefficient of the order $10^{-7} \text{ cm}^3\text{s}^{-1}$. This results in a large fraction of the positive charge of the cloud being in the form of metallic ions for both the LIP and the HIP. . Table 11 list the metals and their ions for both the HIP and LIP. Notices that as the system changes from the HIP to the LIP the fractional abundance of the ions increase.

When in the LIP metals receive their charge by reacting with molecular ions such as HCO^+ , H_3^+ and C^+ . Mg and Na will react with HCO^+ , while Fe will react with H_3^+ . The C^+ is about one order of magnitude less in reactivity. The propensity of metals to maintain charge will effect the fractional ionization. Enhancement of the initial metallic abundance will result with an increase in positive ions. Charge conservation dictates the these excess charges must balance. Because the electrons are the major carrier of negative charge, they must increase in number. This has the effect of destroying H_3^+ ions which allows the H^+ to remain dominant.

He⁺ and C⁺

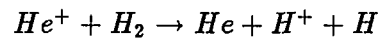
He⁺ and *C⁺* are important ions because they control the transfer of positive charge among the more abundant species. *He⁺* is important for the decomposition of *CO*. *C⁺* is important because it can charge transfer with a variety of species. *C⁺* can charge transfer with sulphur, silicon, phosphorus and metals. It is the dominant reactions with molecular oxygen and can react with molecular hydrogen to create *CH₂⁺*.

Ionic helium is produced at a constant rate by the cosmic ray ionization of helium:



He⁺ reacts primarily with *CO*, because the rate coefficient with molecular hydrogen is very small.

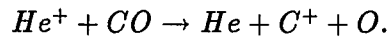
The rate coefficient for the reaction:



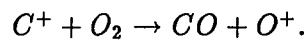
is given by

$$k_{He^++H} = 3.7 \times 10^{-14} cm^3 s^{-1}.$$

Because the rate coefficient is so low, *He⁺* does not react that rapidly with *H₂*. The *He⁺* provides a pathway for atomic carbon to be ionized. The rates of formation of *He⁺* is virtually the same for the HIP and the LIP. The amount of *He⁺* available to interact with primarily *CO* is dependent on the rate *He⁺* is destroyed. In both phases the reaction with *CO* is the primary destruction path:



As mentioned above, ionic helium will decompose carbon monoxide which will produce the C^+ . The C^+ will participate in several different processes. For both ionization phases the C^+ ion will be the dominant reactant with molecular oxygen.



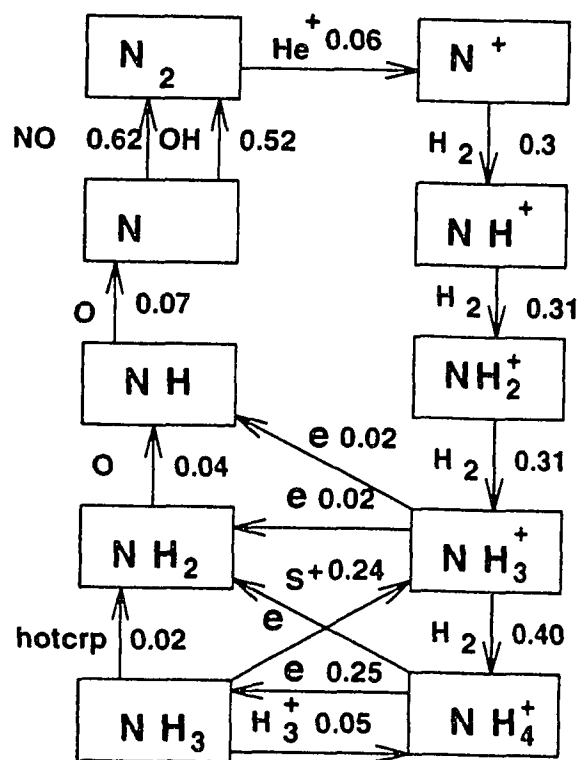
Notice that this is the primary reaction for the production of CO .

The C^+ is the primary ion for the charge transfer with sulphur, silicon, phosphorous and the metals. The C^+ will also react with molecular hydrogen to produce CH_2^+ . Because the helium abundance and the CO abundance are large and almost constant, the production of C^+ is almost constant. Thus the steady state C^+ abundance is dependent on the amount of O_2 available. This implies that when molecular oxygen increases in abundance the C^+ will decrease in abundance. The converse of this statement is also true: as the O_2 decreases, the C^+ will increase.

Nitrogen

The abundance of nitrogen has little effect on the ionization phase of the molecular cloud. This can be attributed to the fact that nitrogen is slow to react with most species. Atomic nitrogen reacts through the neutral-neutral processes which has rate coefficients of the order of $10^{-11} \text{ cm}^3 \text{ s}^{-1}$. Nitrogen molecules will be formed as the system moves to the LIP. However, the proton transfer reaction with H_3^+ is endothermic (Burt et.al. 1970). Figures 24 and 25 illustrate the chemistry of NH in the LIP and HIP.

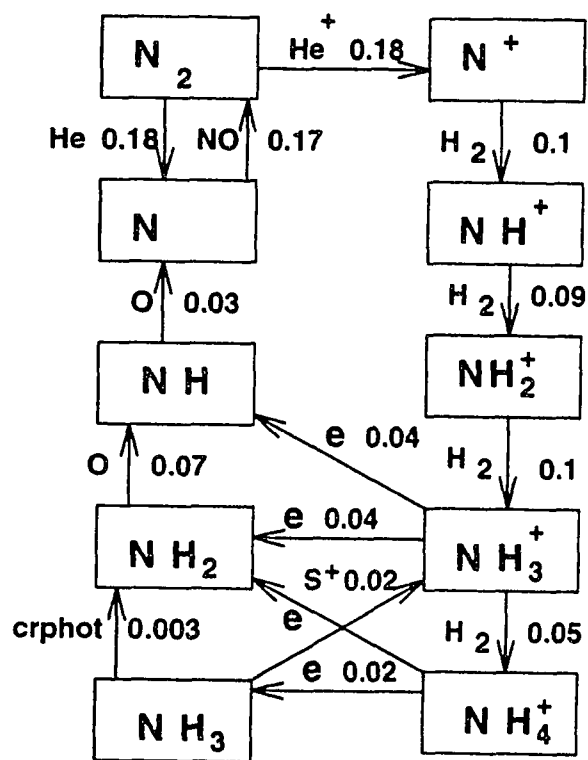
NH Chemistry LIP



multiply each number by $1.0 \times 10^{-19} \text{ sec}^{-1}$

Figure: 24 LIP Reaction Networks for the Nitrogen Hydrogen Chemistry

NH Chemistry HIP



multiply each number by $1.0 \times 10^{-19} \text{ sec}^{-1}$

Figure 25: HIP Reaction Networks for the Nitrogen Hydrogen Chemistry

Carbon and Oxygen n=1450		
Species	High Ionization	Low Ionization
<i>Si</i>	1.99×10^{-10}	8.60×10^{-11}
<i>SiO</i>	2.68×10^{-9}	5.7×10^{-9}
<i>Si⁺</i>	3.09×10^{-9}	6.4×10^{-11}
<i>Mg</i>	7.4×10^{-10}	4.9×10^{-10}
<i>Mg⁺</i>	5.25×10^{-9}	5.5×10^{-9}

Table 13: Silicon and Magnesium at High and Low Ionization

Silicon Chemistry

The behavior of Si is similar to that of Sulfur. We note that when the system is in the HIP the Si will exist in an ionic form and will participate in charge transfer. Silicon is ionized by charge transferring with the sulphur ion. However, when in the LIP, silicon will be in oxide form.

It is instructive to compare Si with Mg. Table 13 illustrates that magnesium and silicon behave differently. In the HIP *Mg* and *Si* are both ionized, however in the LIP, *Mg* is ionized, while the *Si* is in the form of oxides. Once the magnesium positive ion is formed it does not recombine at a high rate. Hence most of the metal becomes positively charged. Silicon will produce a large number of positive atomic ions in the HIP state however, in the LIP Silicon will recombine to form *SiO* and *SiO₂*.

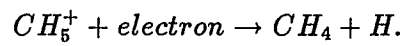
Hydrocarbon Chemistry

One of the remarkable properties of dark molecular clouds is their ability to shield molecules from ultraviolet photons thus allowing a favorable environment for molecular growth. The purpose of this section is to examine the behavior of the hydrocarbon

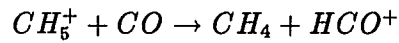
chemistry under the HIP and LIP ionization regimes. We will examine short chain and long chain hydrocarbons. Methane will be selected to represent the short chained hydrocarbon, while C_4H will represent the long chain chemistry. Figures 26 and 27 show how the chemical networks as the ionization state changes.

The methane molecule participates in a variety of different chemical reactions. Hence, it is useful to examine how it is formed in the LIP and the HIP.

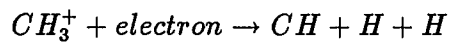
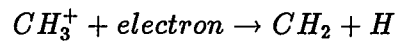
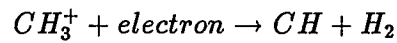
Formation of the methane molecule depends on the abundance of CH_5^+ . The following two reactions illustrate this dependence:



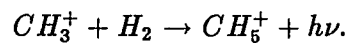
or



The abundance of CH_5^+ is dependent on the abundance of CH_3^+ . When the system is in the HIP, the CH_3^+ destruction is dominated by the dissociative recombination.



When the system is in LIP the dominate reaction for destruction of CH_3^+ is the radiative association with the hydrogen molecule:



Because this reaction results in more CH_5^+ in the LIP, there will be more methane in the LIP.

The formation of the large carbon chain C_4H is initiated by reactions of C^+ with C_2H_2 . This reaction is representative because C_4H is an intermediate in the formation of longer chain molecules. We have alluded to the fact that the LIP supports more complex molecules. This is also the case for most long chained hydrocarbons . The following sequence show how C_4H can be formed.

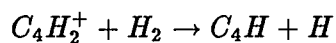
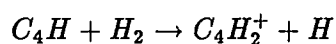
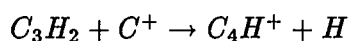
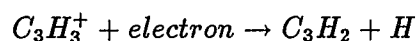
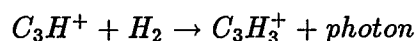
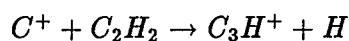
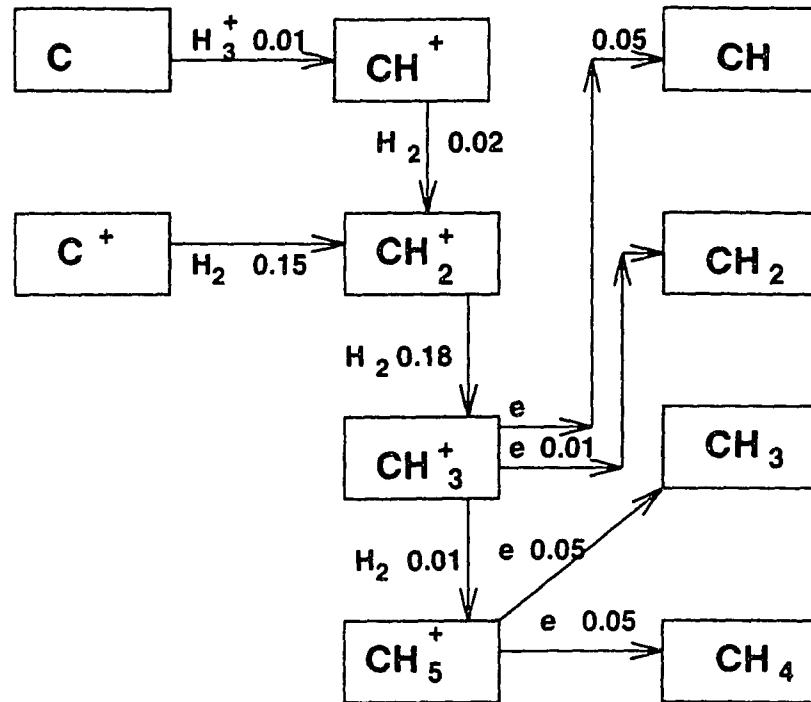


Table 14 illustrates the abundances for the HIP and LIP. Figures Figure 26 and 27 show the chemistry of hydrocarbons in the HIP and LIP.

Summary

When the system is in the HIP the chemistry is dominated by the charge transfer process, with H^+ . For the LIP, the chemistry is dominated by the proton transfer

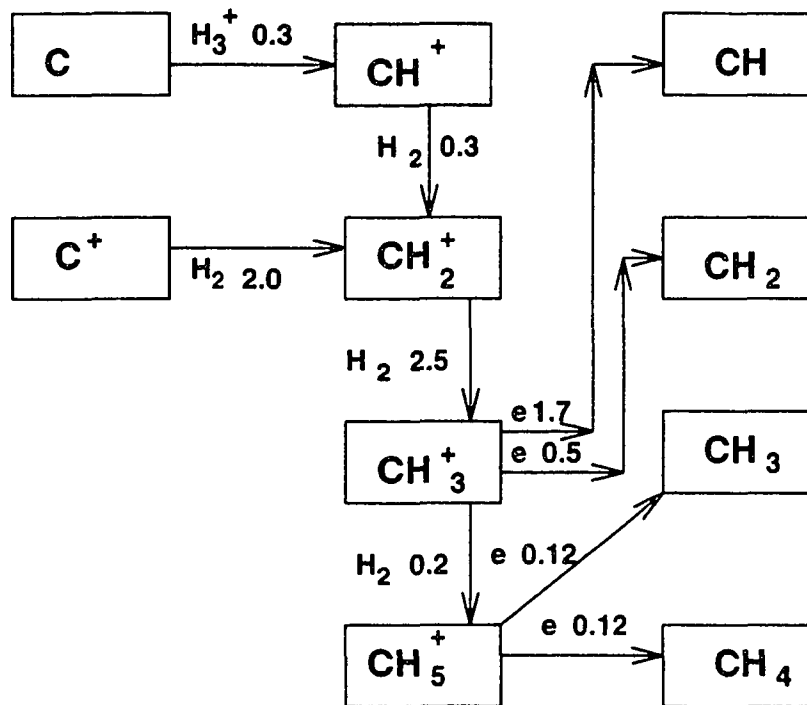
Hydrogen Carbon Chemistry LIP



Multiply by $1.0 \times 10^{-19} \text{ sec}^{-1}$

Figure 26: LIP Reaction Networks for the Hydrocarbon Chemistry

Hydrogen Carbon Chemistry HIP



Multiply by $1.0 \times 10^{-19} \text{ sec}^{-1}$

Figure 27: HIP Reaction Networks for the Hydrocarbon Chemistry

Species	High Ionization	Low Ionization
C_4H	1.22×10^{-10}	3.4×10^{-10}
$C_3H_3^+$	9.94×10^{-13}	3.88×10^{-12}
C_2H_2	1.5×10^{-9}	6.8×10^{-9}
C^+	1.8×10^{-7}	1.37×10^{-8}

Figure 14: Abundances of Selected Hydrocarbons n=1450

process. The proton transfer process has H_3^+ as the dominant ion. The HIP tends to have a large abundance of atomic ions while, the LIP tends to have a large abundance of molecules. We note that there is an increase in the number of oxides as we move from HIP to LIP. Species such as sulphur will provide a source of electrons which will cause the system to remain in the HIP. The sensitivity of the system to electron rich species such as sulphur is crucial for obtaining a bistable solution as the number density increases.

The metals will provide a site for the positive charges to form. Once formed, these species will remain in ionic form. Species such as Si and P can also be a source of electrons which can drive the system into the HIP. However, these species tend to form oxides in the LIP.

Chapter 8

Bistability and Parameter Variation

Charge transfer reactions are dominated by the H^+ , ion while proton transfer reactions are dominated by the H_3^+ ion. The competition between these two processes determines whether the system is in the LIP or the HIP. This chapter to explains how initial abundances, cosmic ionization rate, dissociative recombination rate coefficients, temperature, number density and large molecules in the form of polycyclic aromatic hydrocarbons (PAH) affect the bistable region.

The Bistable Region

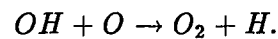
Bistability means there are two steady state solutions at particular number density (n), temperature (T) and cosmic ray ionization rate (ζ) to a system of differential equations. The solutions to the differential equations are dependent on the initial conditions. If a point in parameter space is defined as (n, T, ζ) and there exists a bistable solution vector in the HIP called \mathbf{X}_1 for point $(n - \epsilon, T, \zeta)$ and a bistable solution vector in the LIP called \mathbf{X}_1 the point $(n + \epsilon, T, \zeta)$ for some ϵ greater than zero. The solutions for initial conditions defined by a steady state conditions computed at $(n - \epsilon, T, \zeta)$ and steady state conditions computed at $(n + \epsilon, T, \zeta)$ will be different (See Chapter 7).

Elemental Abundances

The purpose of this section is to briefly review the effects of elemental depletions and enhancements in the bistable region. Variation of oxygen or carbon have a significant effect on the bistability. Nitrogen will have very little effects on the bistable region. Metals accumulate charge and and increase the fractional ionization. Sulfur and silicon will provide a source of electrons which will tend to drive the system into the HIP for high values of n . In the LIP sulfur and silicon exist as oxides. Changing the abundances of chlorine and phosphorous by factors of $\frac{1}{2}$ and 2 do not have any effect on the bistable region.

Effects of Oxygen on the Bistable Region

Molecular oxygen has the effect of reducing the number of atomic ions. Molecular oxygen is formed by the process:



This reaction implies that the abundance of molecular oxygen is positively correlated to the abundance of atomic oxygen. Molecular oxygen has the effect of destroying ions hence, if we increase the abundance of atomic oxygen there will be a decrease in the abundance of atomic ions and the fractional ionization will decrease. Notice that Figure 28 illustrates a shrinking the bistable region as the abundance of O increases .

The effect of the depletion of oxygen is illustrated in Figure 29. These calculations indicate that when the abundance of oxygen is depleted the system will tend to stay in the HIP for large values of n .

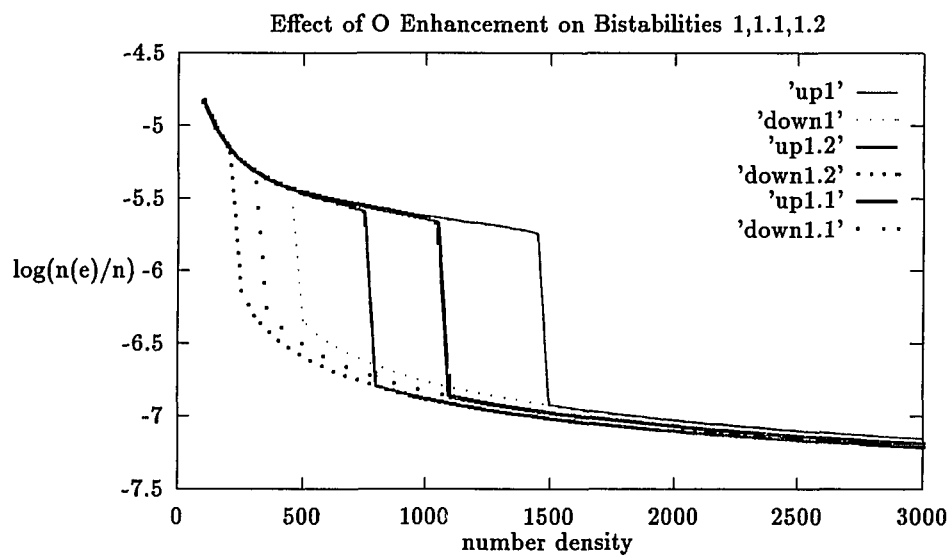


Figure 28: As the Oxygen abundance is enhanced the Bistable Region Disappears. *Up* means that we increment initial conditions starting from a low number density to a high number density. *Down* means that we decrement initial conditions starting from a high number density to a low number density. The number following the word *up* or *down* is a multiple of the original cosmic abundance as was defined in Table 5 chapter 5.

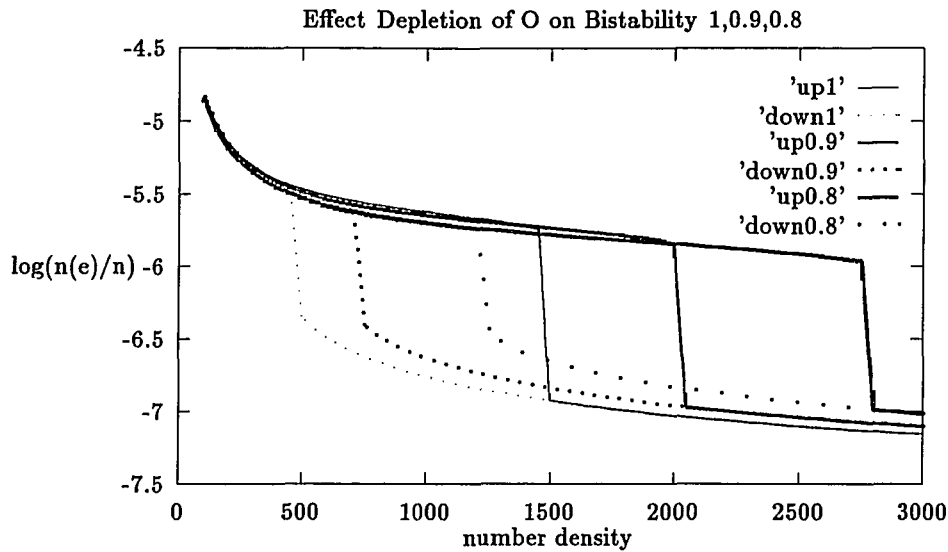


Figure 29: As the Oxygen abundance is depleted the Bistable Region Increases (see Figure 28 for an explanation of the symbols).

Effects of Carbon on a Bistable Region

This section considers the effects of carbon abundance on the bistable region. When there is an enhancement of the initial carbon abundance the steady state solutions will have a large number of C^+ ions present in the HIP. Charge conservation dictates there must be more available electrons to react with the H_3^+ . Hence the number of H_3^+ will be reduced and the ion chemistry will tend to be dominated by the H^+ (see Figure 30).

At ultra-high enhancement, the excess carbon will react with the remaining oxygen to create CO . Because the carbon has been enhanced there will be excess carbon atoms hence, the excess carbon will remain ionized as C^+ and the system will remain in the HIP for large values of n .

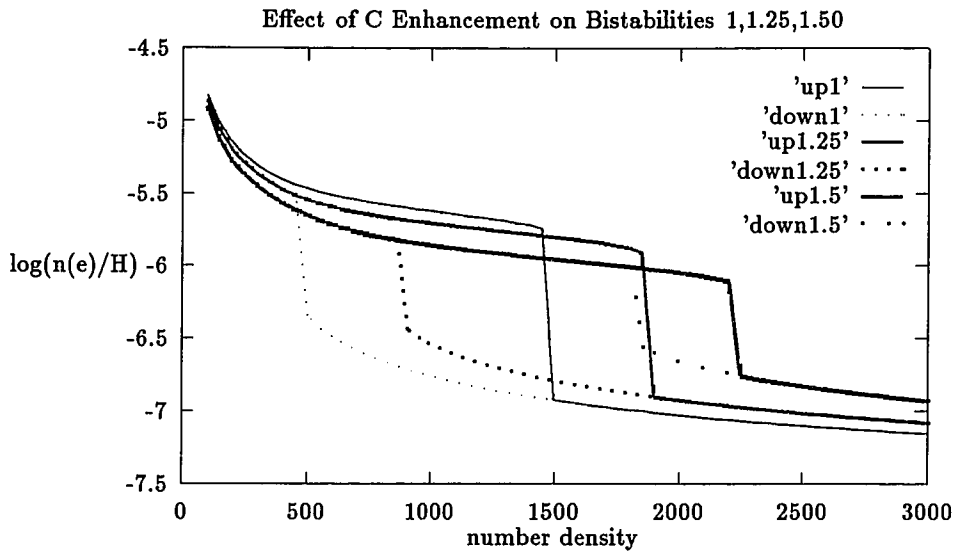


Figure 30: C is Enhanced the Bistable Region Disappears (see Figure 28 for an explanation of the symbols)

Depletion of carbon has the opposite effect of enhancement. As the system moves toward the steady state solution a large proportion of the carbon will react with the oxygen to form CO. This leads to fewer C^+ ions. Hence, the system will only be in the HIP for low values of n (see Figure 31).

Nitrogen

Inspection of Figure 32 indicates that enhancement or depletion of the nitrogen has little effect on the bistable region. By increasing the abundance of the nitrogen two fold there is a marginal shift of the bistable region to the higher density region. When the system is depleted by a factor of 0.5 there is no distinct shift in the bistable region.

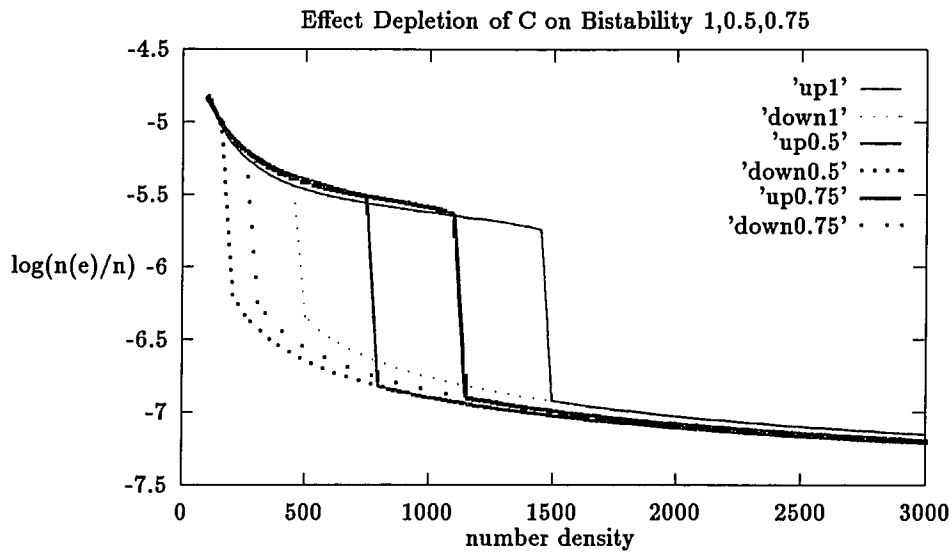


Figure 31: C is Depleted the Bistable Region Disappears (see Figure 28 for an explanation of the symbols)

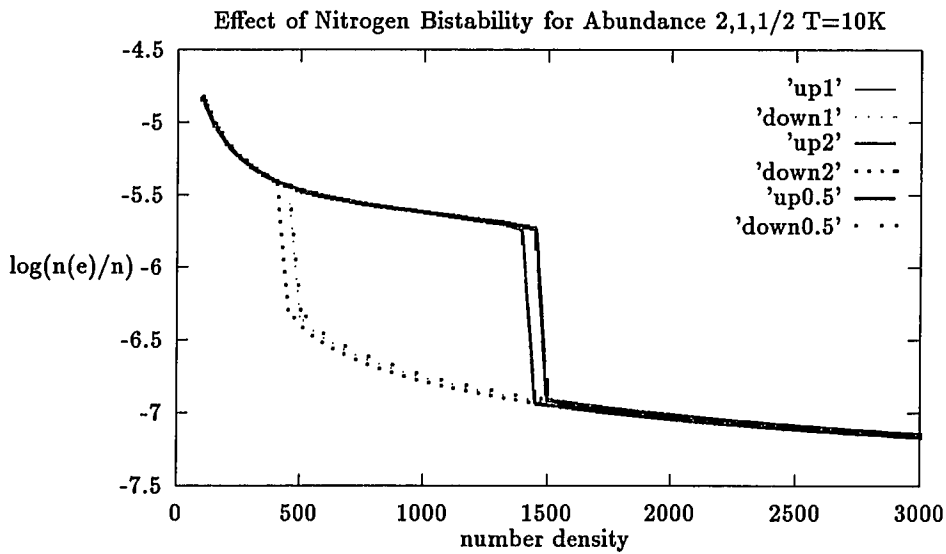


Figure 32: Affect of Nitrogen on Bistability for abundances 1.0 0.5 and 2 (see Figure 28 for an explanation of the symbols)

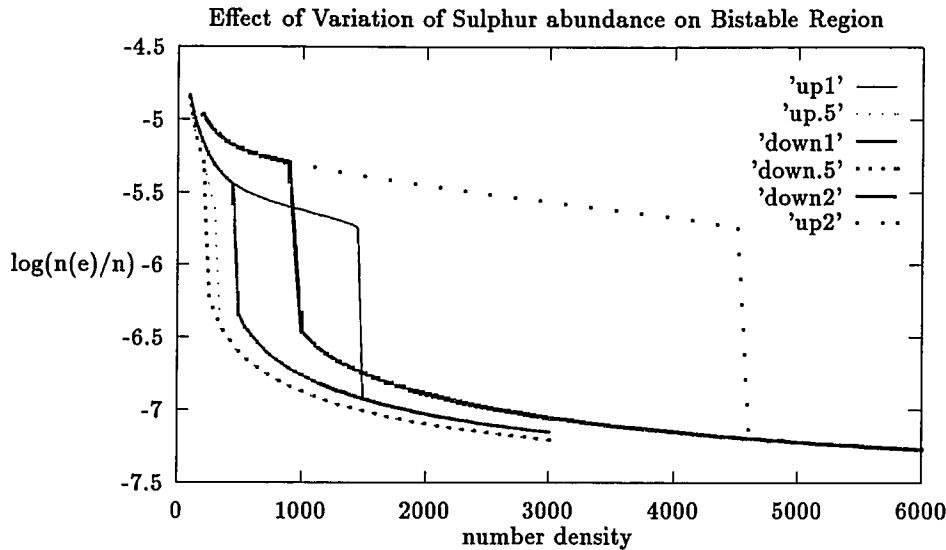


Figure 33: Effect of Sulphur on the Bistable Region *This figure shows that as the amount of sulfur is doubled, the bistable region shifts to the higher number density region and increases in width. If the abundance of sulphur is decreased the bistable region shifts to the lower number density region and shrinks (see Figure 28 for an explanation of the symbols)*

Effects of Sulfur

Sulphur will charge transfer with C^+ . As the number of sulphur ions increase the fractional ionization will increase because of charge conservation. Thus the enhancement of sulphur will allow the system to remain in the HIP for higher values of n . If the sulphur abundance is depleted the system will only be in the HIP for low values of n (see Figure 33).

There is an extreme cases where sulphur is not required to maintain the HIP. When the system is solved using only hydrogen, helium, carbon, oxygen and nitrogen, the bistable region exist for a number density between 80 cm^{-3} and 150 cm^{-3} . Thus, it is possible to have a bistable region without sulphur (See Figure 34).

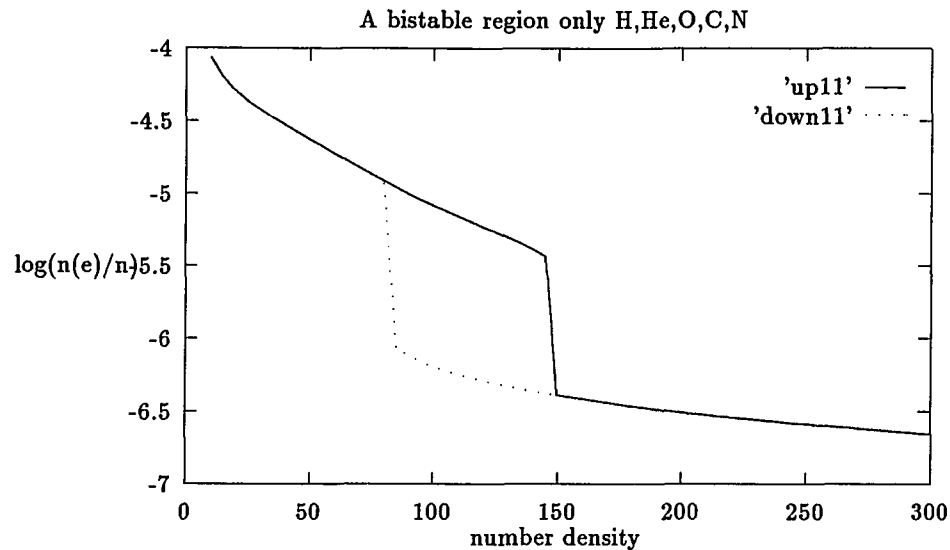


Figure 34: The Bistable Region with only H He C N O present

Effect of Metals

Enhancement of the metal abundance will increase the number of metallic ions. As stated in chapter 7, once these ions are formed, they will tend to remain in ionic form because they recombine via radiative recombination. As the enhancement increases, the total fractional ionization will increase and the system will maintain itself in the HIP for large values of n . Depletion of metals does not imply that the system will not exhibit bistable behavior. If a source of electrons is such as sulphur given in the initial conditions, then bistable behavior will be exhibited in the ultra-high depletion regions (Bourlot 1993). Inspection of Figure 35 shows that as magnesium is enhanced by a factor of 100 the bistable region exist for large values of n . For other metals Fe and Na, this phenomenon is also observed (see Figure 36, Figure 37 and Figure 38).

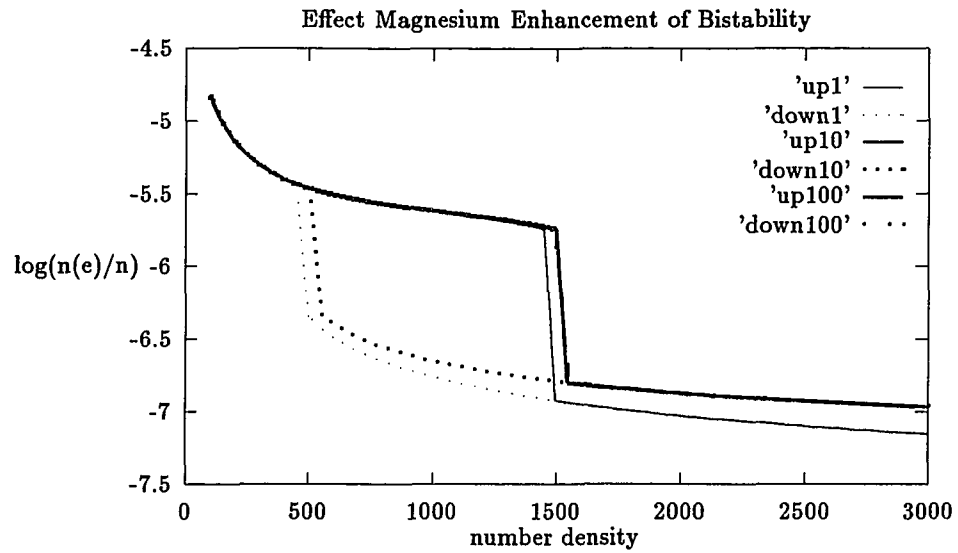


Figure 35: As Mg Abundance is increased the hysteresis shifts to high number density (see Figure 28 for an explanation of the symbols)

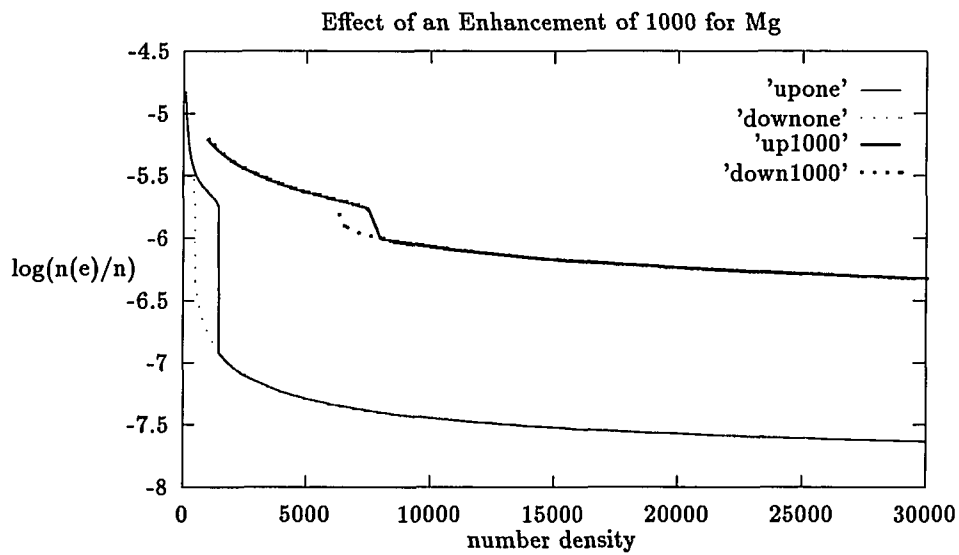


Figure 36: An Example of Extreme Mg Enhancement (see Figure 28 for an explanation of the symbols)

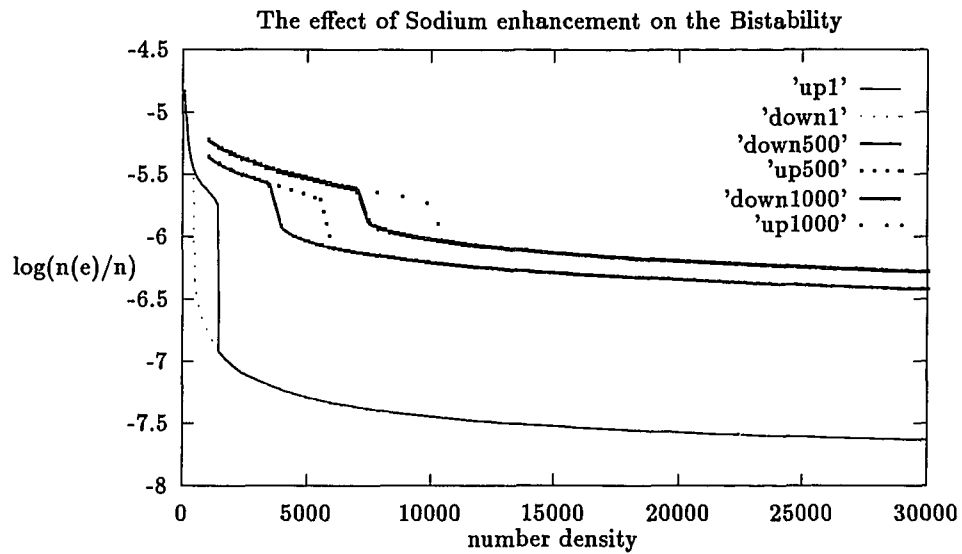


Figure 37: Hysteresis Loop Shrinks Metallic Abundance Increases (see Figure 28 for an explanation of the symbols)

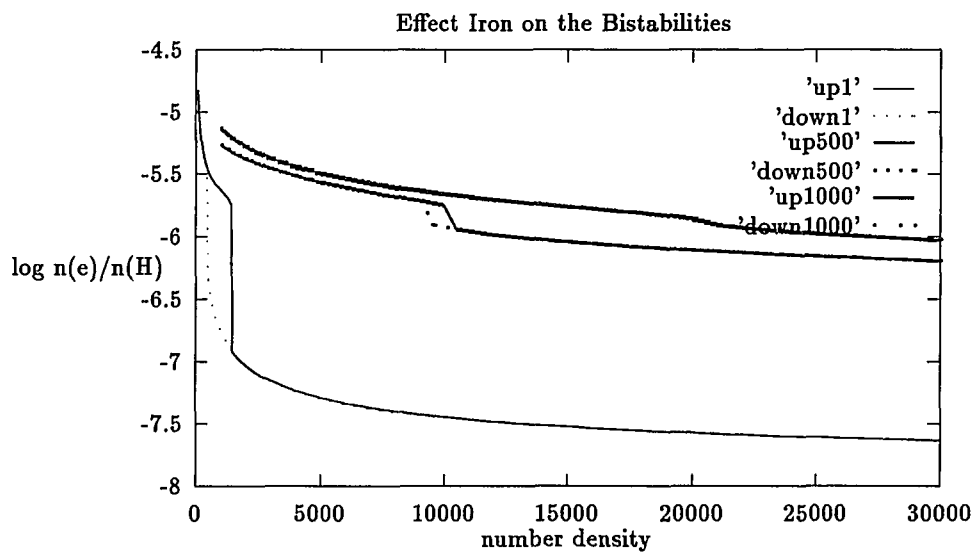


Figure 38: In this example the loop is small indicating the HII will dominate. (see Figure 28 for an explanation of the symbols)

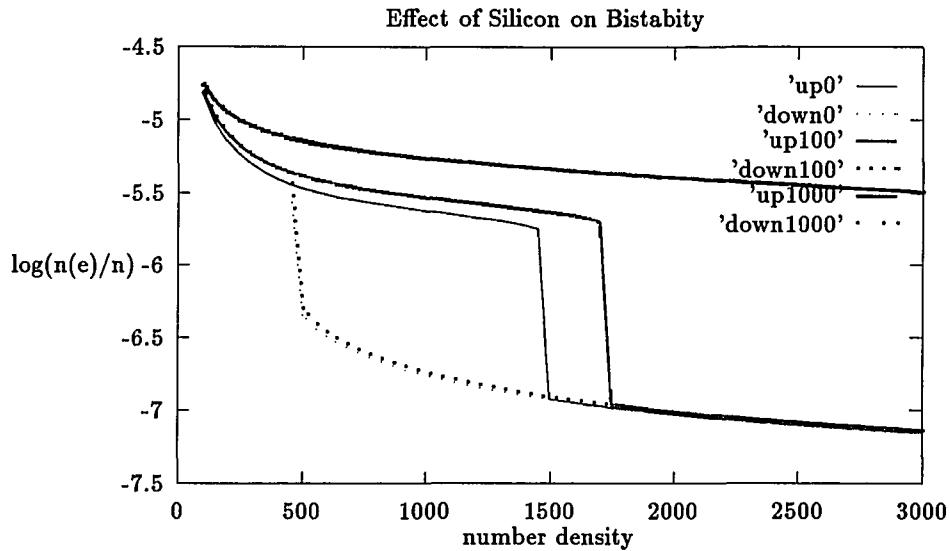


Figure 39: Silicon will behave like a metal for large enhancements when the system is in the HIP. (see Figure 28 for an explanation of the symbols)

Silicon

The behavior of silicon in the HIP is similar to metals because Si charge transfer with C^+ and S^+ . The enhancement of the initial abundance of Si will tend to maintain the HIP for large values of n . When the abundance of silicon increased to 1000 times the initial abundance the system will move into the HIP phase for large values of n (see Figure 39).

Effects of Cosmic Ray Ionization

Molecular synthesis in interstellar clouds is driven by ion-neutral reactions. The principle initiating step is the ionization of molecular hydrogen. The cosmic ray ionization rate determines the rate of H_3^+ production. These proton transfer reactions with H_3^+

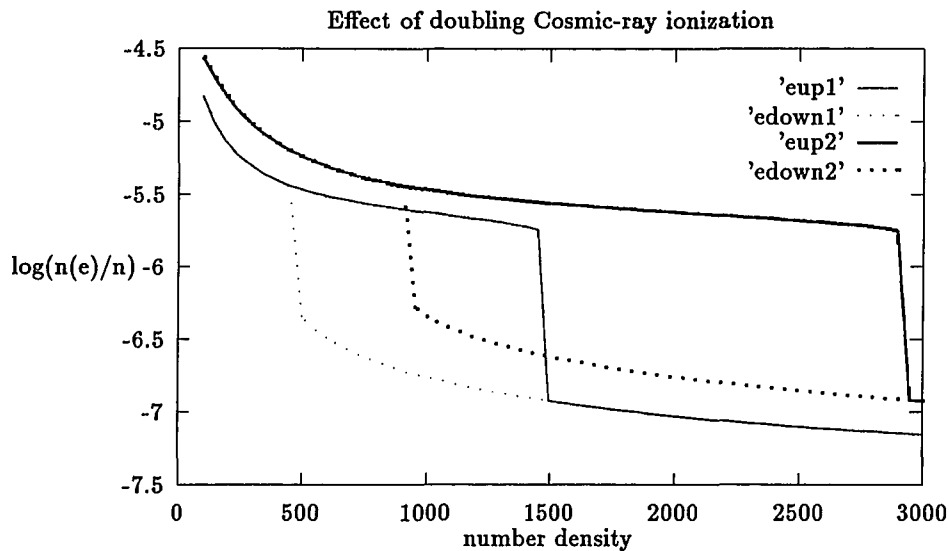


Figure 40: Effect of doubling the ionization rate. (see Figure 28 for an explanation of the symbols)

are the initial reactions in the ion-molecule networks (Lepp 1992). Ion-neutral reactions at cloud temperatures tend to be exothermic. Dark clouds models which utilize the cosmic ray ionization process to drive the chemistry adopt an ionization rate of the order of 10^{-17} ionization per second per hydrogen nucleon. This rate is consistent with observation of species (Farquhar, Millar and Herbst 1994). Thus as the ionization rate is increased by factor of 2, 5 and 10 the bistable regions exist for larger values of number density (see Figure 40 and 41).

There is some evidence which suggests that the cosmic ray ionization rate may be variable (Skibo and Ramaty 1993). Thus bistability might be used as a probe for detecting cosmic ray ionization.

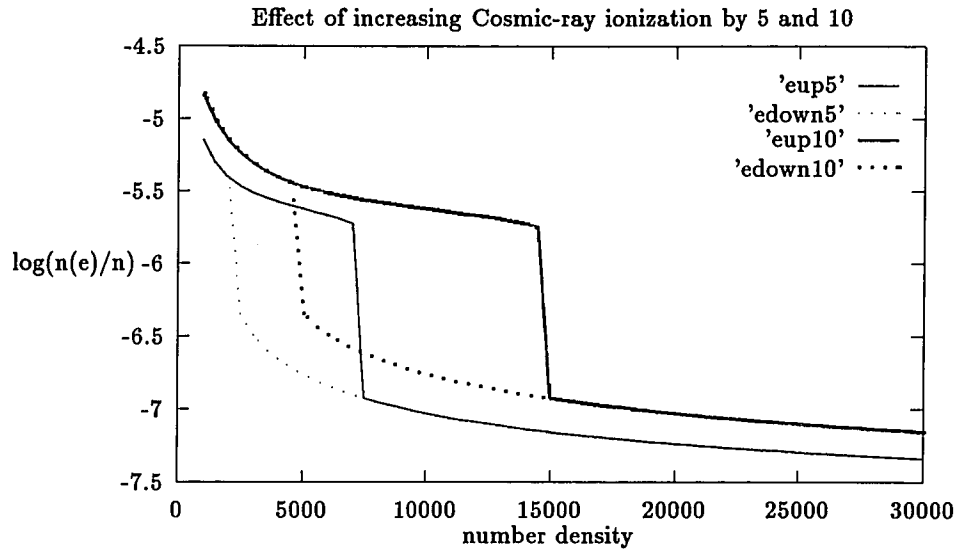


Figure 41: Effect of increasing the Cosmic Ray Ionization Rate by factors of 5 and 10.(see Figure 28 for an explanation of the symbols)

Effects of Dissociative Recombination

In the HIP the fractional ionization is observed to occur when the condition

$$X_e > \frac{k_1 X_{CO} + k_2 X_O}{2k_e} \quad (8.1)$$

is satisfied. As the dissociative recombination coefficient increases, the left hand side of the equation will get smaller. Thus, as k_e increases, the system will remain in the HIP for large values of n .

The dissociative recombination reaction rate is important because it determines the dissociative recombination rate of H_3^+ . During the last ten years the value for this rate constant has been subject to much debate. It is generally agreed that the rate is given by the general form.

Dissociative Recombination Rate Coefficient	Investigator
$1.5 \times 10^{-7} \text{ cm}^3 \text{ s}^{-1}$	Canosa(1992)
$2.9 \times 10^{-9} \text{ cm}^3 \text{ s}^{-1}$	Herbst and Leung(1989)
$1.1 \times 10^{-11} \text{ cm}^3 \text{ s}^{-1}$	Adams and Smith(1988)
$1.2 \times 10^{-8} \text{ cm}^3 \text{ s}^{-1}$	Smith and Spanel(1993)
$1.15 \times 10^{-7} \text{ cm}^3 \text{ s}^{-1}$	Sundstrom(1994)

Table 15: Dissociative Recombination Rates and Investigators

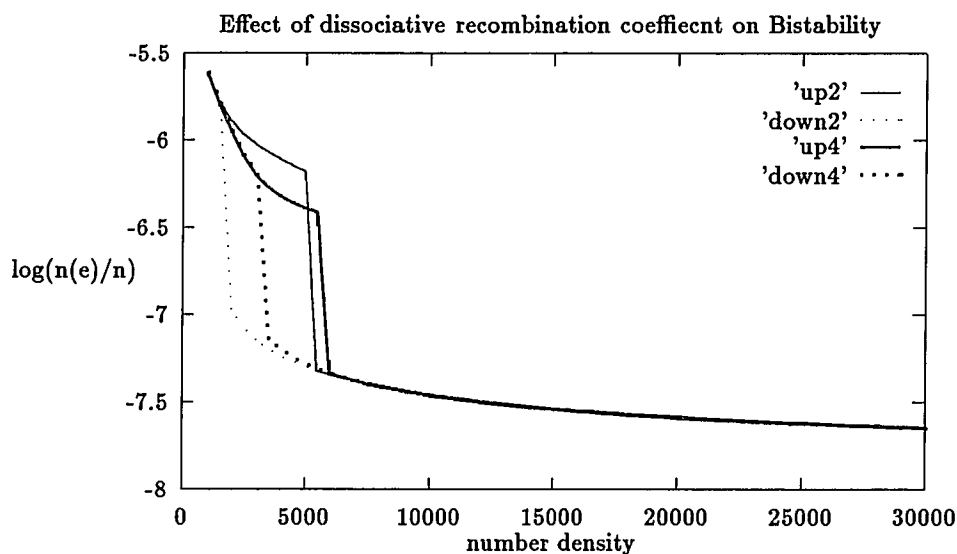


Figure 42 Increasing the Dissociative Recombination Rate by factor of 2 and 4. (see Figure 28 for an explanation of the symbols)

$$\kappa_e(H_3^+) = \alpha \sqrt{\frac{300}{T}} \quad (8.2)$$

However, there is still much debate as to what is the correct value for α . Table 15 lists some of the dissociative recombination for H_3^+ rates and the principal investigators. Notice the wide variation of the various rates.

For this study $\alpha = 5.5 \times 10^{-8} \text{ cm}^3 \text{ s}^{-1}$. As α is increased the dissociative recom-

bination rate increases and the fractional abundance of H_3^+ decreases. Thus as α is increased the system will stay in the HIP for larger values of n . This investigation looked at the effects by increasing α by a factor of 2 and a factor of 4 exist of large values of n . Notice in Figure 42 that as the rate coefficient k_e is increased by a factor of 2 and 4 the bistable region increases.

Variation of Temperature and Density

The rate coefficient for the dissociative recombination is a function of the temperature:

$$\kappa_e(H_3^+) = \alpha \sqrt{\frac{300}{T}}. \quad (8.3)$$

When the temperature is increased, κ_e will get smaller. This implies that fewer H_3^+ ions will be destroyed per unit time. This will lead to an excess of H_3^+ ions and the proton transfer process will be dominant. Thus, as the temperature is increased the system will be in the LIP.

When the number density is increased this will decrease the number of electrons. As the number of electrons decrease, there will be more H_3^+ available to participate in proton transfer. Consequently, the system will move to the LIP. This can be observed in Fig. 43. Observe that as the number density and the temperature increase the system will be in the LIP for large values of n and temperature.

Effects of Large Molecules

Observational data from infrared emission bands at 3.3, 6.2, 7.7, 8.6 and 11.3 μm have been observed in a large number of astrophysical objects such as galactic forma-

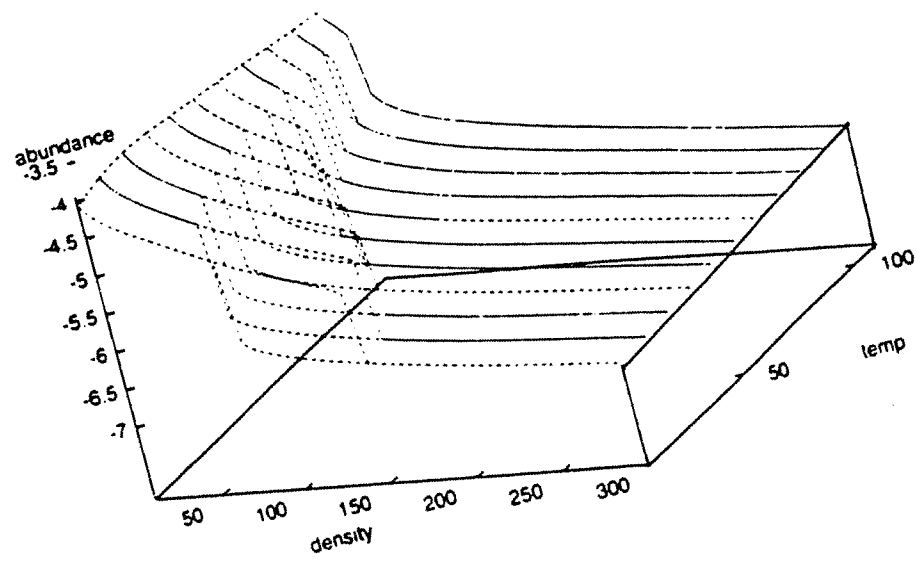


Figure 43: Surface plot of Temperature and Number Density An interesting feature of this plot is that is similar to the graph of the cusp catastrophe (See Chapter 6).

tion, planetary nebulae and reflection nebulae (Dwek et.al. 1980). These IR bands have been associated with functional groups that are attached to aromatic hydrocarbons (Duley and Williams 1981). These observations prompted Leger and Puget (1984) to suggest the hypothesis that large molecules called polycyclic aromatic hydrocarbons (PAH) that are causing infrared emissions. If there are large molecules, it is reasonable to expect them to participate in the molecular cloud chemistry. Omont (1986) calculated the rates for a variety of reactions which involved large molecules in the form of 50 atom PAH's . Lepp and Dalgarno (1988) used Omont's rate coefficients to construct a chemical model of a dark molecular cloud which included the PAH's. This section will examine the effects of the PAH's on the bistability. The rate coefficients that were calculated by Omont (1986) will be incorporated into the chemical model.

The UMIST Ratefile was modified to include the PAH data. The inclusion of the large molecules in the form of PAH's in the gas phase chemistry requires a set of rate coefficients which account for the reactions of the other species with the PAH's. There are two categories of reaction: those involving electrons with large molecules and those involving positive ions with large molecules.

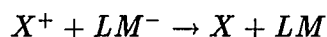
Electrons interact with the positive large molecular ions through the process



The rate coefficient for this reaction is $5.7 \times 10^{-6} \text{ cm}^3\text{s}^{-1}$. Electrons can also react with the LM to create a negative large molecular ion.



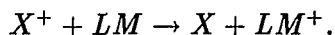
The rate coefficient for this reaction is $7.7 \times 10^{-7} \text{ cm}^3 \text{ s}^{-1}$. The symbol X^+ will be used to represent a generic positive ion. There are two process for which a positive ion will react:



The rate coefficient for this reaction given by

$$1 \times 10^{-6} T^{-\frac{1}{2}} \text{ cm}^3 \text{ s}^{-1}.$$

The charge transfer reaction is given by



The rate coefficient for this reaction is $4.0 \times 10^{-9} \text{ cm}^3 \text{ s}^{-1}$ and

Calculation of the effect of large molecules required the modification of the UMIST Ratefile and the species list. The modification of the species list is accomplished by adding the species identifiers. The modification of the reaction set is more involved because four types of reactions which involve the large molecules must be added.

Two of the four reactions are easy to append because they involve the electrons. The addition of reactions containing electrons is simple because there are only two reactions. These reactions may be typed, in or a small piece of fortran code can be written to add them to a supplementary reaction set.

Addition of the positive ions is more involved because the list of species names must be searched twice. The first search determines if a species is a positive ion. If

it is, the computer must then determine whether it transfers a charge to a neutral PAH. If the reaction is in the reaction list, then the reaction of the positive ion and the neutral PAH is written to a supplementary reaction file. Next the positive ion is allowed to react with a negative PAH. If the product is in the reaction set then this reaction is added to the supplementary reaction set. After these operations the supplementary reaction set is appended to the UMIST Ratefile. The modified UMIST Ratefile contains 3969 reactions and 392 species.

Addition of the large molecules to the UMIST Ratefile leads to the disappearance of the bistable region when the fractional abundance increase above 10^{-8} . Physically, this is meaningful because the values of n_{LM} greater than 10^{-8} correspond to measured values. Inspection of Figure 45 illustrates the existence of the bistable region for ultra-low values of n_{LM} bistability. Thus, for the UMIST Ratefile (Farquhar and Millar 1993) the addition of PAH damps out the bistable region for PAH abundances greater than 10^{-7} .

Figure 44 illustrates the disappearance of the Bistability as the fractional abundance of the large molecules approach 10^{-7} .

Summary

The bistable regions are affected by the certain elemental abundances. Enhancements of oxygen will decrease the bistable region while an increase in carbon allows the bistable region to exist for large number densities. Enhancement of sulfur will allow the system exist in the HIP as number density increases. Enhancement of metals

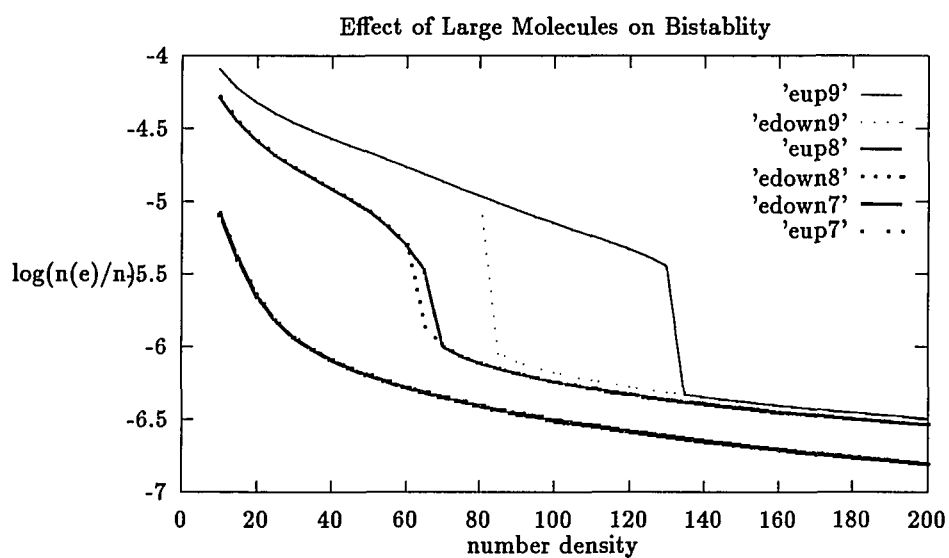


Figure 44: Disappearance of Bistability as n_{LM} increases. Note *up* means that we increment from low to high number density and *edown* means that we decrement from high to low number density. The 7, 8 and 9 refer to initial abundance of LM i.e. 7 means LM initial abundance 10^{-7} , 8 means LM initial abundance 10^{-8} and 9 means LM initial abundance 10^{-9} .

allow the bistable region to exist for large number densities. By increasing the cosmic ray ionization rate or the dissociative recombination coefficient The bistable region will exist for large number density. The addition of large molecules will inhibit the bistable region.

Chapter 9

Approximation of the Fractional Ionization

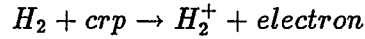
Charge transfer reactions of atomic and molecular ions with neutral metal atoms can significantly increase the amount of fractional ionization in a cold dense molecular cloud. This chapter will develop three analytical models which are useful when studying the ionization of the cloud. The first model will consider the effects of no metals on the cloud. The second model will be similar to the Oppenheimer (1974) model of fractional ionization. The third model of fractional ionization will include a correction when cosmic ray induced photons are included in the model.

No metals

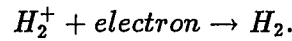
The model with no metals is interesting because it is simple and in some cases predictive. Most models of dark clouds assume that the elements of the cloud have been depleted by a certain amount. It is not uncommon for a model to assume that metals have been depleted by a factor of 100 to 1000. When this assumption is made the results from this section give a very accurate estimation of the fractional ionization.

This model assumes that the system consists of only H_2 . The H_2 bombarded by cosmic rays has an ionization rate ζ . When a cosmic ray interacts with the H_2 an

electron and a H_2^+ are formed. (This assumption is not that unrealistic when one considers that H_2 accounts for most of the clouds mass.)



As mentioned above, the rate of this process is given by ζ . Since the only molecule in the dark cloud is H_2 , the number of ions must be equal to the number of H_2^+ ions created. The rate at which ions are created is given by the expression ζn_{H_2} . The process that controls recombination is given by the reaction



The rate of recombination is $kn_{H_2^+}n_e$. The sum of the recombination rate and the ionization rate is equal to the rate of change of H_2 . This can be written as

$$\frac{dn_{H_2}}{dt} = -\zeta n_{H_2} + kn_{H_2^+}n_e. \quad (9.1)$$

When the rate of ionization is equal to the rate of recombination a steady state is obtained. This can be expressed as

$$\frac{dn_{H_2}}{dt} = 0. \quad (9.2)$$

Substituting this result into 9.1 yields:

$$0 = -\zeta n_{H_2} + kn_{H_2^+}n_e. \quad (9.3)$$

This may be solved to yield:

$$\zeta n_{H_2} = kn_{H_2^+}n_e. \quad (9.4)$$

Charge conservation implies that

$$n_{H_2^+} = n_e. \quad (9.5)$$

is true. Substituting equation 9.5 into equation 9.4 yields

$$n_e^2 = \zeta n_{H_2} \quad (9.6)$$

Divide by n^2 where

$$n = 2n_{H_2} + n_H \quad (9.7)$$

to obtain the abundance:

$$\frac{n_e^2}{n^2} = \frac{\zeta n_{H_2}}{kn^2} \quad (9.8)$$

and

$$X_e^2 = \frac{\zeta X_{H_2}}{kn}. \quad (9.9)$$

Taking the square roots of both sides and letting the fractional abundance of molecular hydrogen be 1 yields:

$$X_e = \sqrt{\frac{\zeta}{kn}}. \quad (9.10)$$

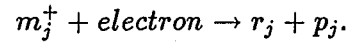
Oppenheimer's Fractional Ionization Equation

The previous section derived an approximation formula for the fractional ionization for a cloud containing no metals. This section examines the behavior of the fractional ionization when there are metals in the cloud.

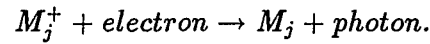
Electrons are removed from the cloud via two processes dissociative recombination and radiative recombination. Let m_j^+ define a molecule, let α_j be the dissociative

recombination rate coefficients, α_{ir} be the radiative recombination rate coefficients and let M_j^+ be the number of metal ions.

The general expression for the dissociative recombination is



where $r_j + p_j$ are products. Electrons can also be removed from the clouds via radiative recombination with a metal M. For radiative recombination we have the reaction



The rate which the metal ions M_j^+ are neutralized is given by the term $\alpha_{ri} n_{M_i^+} n_e$.

Let DR=dissociative recombination and let RR=radiative recombination.

$$DR = \sum_j \alpha_j n_{m_j^+} n_e \quad (9.11)$$

for the sum of all terms which contribute to dissociative recombination and

$$RR = \sum_i \alpha_{ir} M_i n_e. \quad (9.12)$$

for the sum of all terms which contribute to radiative recombination.

The rate at which electrons are created is given by ζn hence,

$$\frac{dn_e}{dt} = \zeta n - DR - RR \quad (9.13)$$

or

$$\frac{dn_e}{dt} = \zeta n - \sum_j \alpha_j n_{m_j^+} n_e - \sum_i \alpha_{ri} n_{M_i^+} n_e. \quad (9.14)$$

The steady state condition is given when:

$$\frac{dn_e}{dt} = 0 \quad (9.15)$$

$$\zeta n - \sum_j \alpha_j n_{m_j^+} n_e - \sum_i \alpha_{ri} n_{M_i^+} n_e = 0 \quad (9.16)$$

Rearranging (9.16) produces

$$\zeta n = \sum_j \alpha_j n_{m_j^+} n_e + \sum_i \alpha_{ri} n_{M_i^+} n_e. \quad (9.17)$$

Now, n_e may be factored from (9.3.9) to yield:

$$\zeta n = n_e \left(\sum_j \alpha_j n_{m_j^+} + \sum_i \alpha_{ri} n_{M_i^+} \right). \quad (9.18)$$

Solving for n_e and rearranging yields

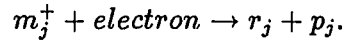
$$n_e = \frac{\zeta n}{\sum_j \alpha_j n_{m_j^+} + \sum_i \alpha_{ir} n_{M_j^+}} \quad (9.19)$$

Molecular ions are formed at a rate

$$\gamma_j \zeta n \quad (9.20)$$

where γ_i is a fractionalization factor that indicates how large molecular ions are formed from the ionization of H_2^+ .

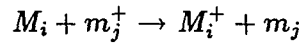
The molecular ion m_j^+ is neutralized by the process of dissociative recombination



The rate of dissociative recombination for this process is given by the expression:

$$\alpha_j n_{m_j^+} n_e. \quad (9.21)$$

The molecular ions are also neutralized by the process of charge transfer:



hence, the rate of destruction per molecular ion is:

$$\beta_{ij} n_{M_i} n_{m_j^+} \quad (9.22)$$

where β_{ij} is the rate coefficient for charge transfer. If the sum is taken over expression (9.3.14) for the entire network the following expression

$$\sum_i \beta_{ij} n_{M_i} n_{m_j^+} \quad (9.23)$$

gives the total rate of neutralization by charge transfer.

Adding (9.20) and subtracting expressions (9.21) and (9.23) allows the rate equation for the ionic molecules to be constructed.

Thus the rate of change for all charged ions is given by:

$$\frac{dn(m_j^+)}{dt} = \gamma_j \zeta n - \alpha_j n(m_j^+) n_e - \sum_i \beta_{ji} n_{M_i^+} n_{m_j^+}. \quad (9.24)$$

When the ionization rates are equal to the recombination rates the steady state is reached. Mathematically, this is expressed as:

$$\frac{dn_{m_j^+}}{dt} = 0. \quad (9.25)$$

Substituting (9.25) into (9.24) yields:

$$\gamma_j \zeta n - \alpha_j n(m_j^+) n_e - \sum_i \beta_{ji} n_{M_j^+} n_{m_j^+} = 0 \quad (9.26)$$

$$\gamma_j \zeta n = \alpha_j n_{m_j^+} n_e + \sum_i \beta_{ji} n_{M_j^+} n_{m_j^+} \quad (9.27)$$

The manipulations and solution of the equation is made tractable by making the following definitions and approximations. Define

$$n_{m^+} = \sum_i n_{m_j^+} \quad (9.28)$$

and

$$n_M = \sum_i n_{M_i} \quad (9.29)$$

The central idea in the Oppenheimer approximation is to assume all of the rate coefficients are equal for a particular process. One can approximate that the dissociative recombination rate coefficients are all equal

$$\alpha_j = \alpha. \quad (9.30)$$

The Radiative Association can be approximated as:

$$\alpha_{ir} = \alpha_r. \quad (9.31)$$

And the charge transfer rate coefficient represented as:

$$\beta_{ij} = \beta. \quad (9.32)$$

Substituting (9.29), (9.30), (9.31) and (9.32) into (9.27) yields

$$\gamma_j \zeta n = \alpha n_{m_j^+} n_e + \beta n_M n_{m_j^+} \quad (9.33)$$

Factoring out $n_{m_j^+}$ yields:

$$\gamma_j \zeta n = (\alpha n_e + \beta n_M) n_{m_j^+}. \quad (9.34)$$

Summing over all species will force the fractionalization factor γ to one

$$\sum_j \gamma_j \zeta n = (\alpha n_e + \beta n_M) \sum_j n_{m_j^+} \quad (9.35)$$

$$\zeta n = (\alpha n_e + \beta n_M) \sum_j n_{m_j^+}. \quad (9.36)$$

$$n_{m_j^+} = \frac{\gamma \zeta n}{\alpha n_e + \beta n_M} \quad (9.37)$$

The sum of the negative charge is approximately equal to the number of electrons, while the positive charges reside on the metals and the positive ions. This allows the conservation of charge to be used to create the following equation.

By conservation of charge

$$n_e = \sum_i n_{M_i^+} + \sum_j n_{m_j^+} \quad (9.38)$$

rearranging(9.38) yields

$$\sum_i n_{M_i^+} = n_e - \sum_j n_{m_j^+} \quad (9.39)$$

If the following definition is introduced:

$$\sum_j n_{M_j^+} = n_{M^+} \quad (9.40)$$

and (9.28) is substituted into (9.39) the charge conservation may be written as:

$$n_{M^+} = n_e - n_{m^+} \quad (9.41)$$

$$n_e = \frac{\zeta n}{\alpha n_{m^+} + \alpha_r n_{M^+}} \quad (9.42)$$

$$n_e = \frac{\zeta n}{\alpha n_{m^+} + \alpha_r (n_e - n_{m^+})} \quad (9.43)$$

$$\alpha n_e n_{m^+} + \alpha_r n_e^2 - \alpha_r n_e n_{m^+} = \zeta n \quad (9.44)$$

Grouping common terms

$$(\alpha - \alpha_r) n_e \alpha_r n_e^2 = \zeta n. \quad (9.45)$$

Substituting equation (9.37) into (9.45) yields

$$\frac{n_e(\alpha - \alpha_r)\zeta n}{(\alpha n_e + \beta n_M)} + \alpha_r n_e^2 = \zeta n. \quad (9.46)$$

Multiplying both sides of equation (9.41) by $(\alpha n_e + \beta n_M)$ yields

$$(\alpha - \alpha_r) n_e \zeta n + \alpha \alpha_r n_e^3 \alpha_r \beta n_M n_e^2 = \alpha n_e \zeta n + \beta n_M n \zeta. \quad (9.47)$$

Now cancel out common terms

$$-\alpha_r n_e \zeta n + \alpha \alpha_r n_e^3 \alpha_r \beta n_M n_e^2 = \beta n_M n \zeta. \quad (9.48)$$

Rearranging this equation, then divide by $\alpha \alpha_r$. This yields a cubic equation for the fractional ionization:

$$n_e^3 + \frac{\beta n_M n_e^2}{\alpha} - \frac{\zeta n n_e}{\alpha} - \frac{\beta \zeta n n_M}{\alpha_r \alpha} = 0. \quad (9.49)$$

Since

$$0 < \alpha_r \alpha \ll 1$$

the second and the third terms are small for conditions close to interstellar .

Hence, we can write

$$n_e^3 - \frac{\zeta \beta n n_M}{\alpha_r \alpha} \approx 0 \quad (9.50)$$

and solve for n_e

$$n_e \approx \sqrt[3]{\frac{\beta \zeta n n_M}{\alpha_r \alpha}} \quad (9.51)$$

The Effect of Cosmic Ray Induced Photons

Cosmic ray particles with energies between 10 Mev and 100 Mev ionize molecular hydrogen in the interior of the clouds and produce secondary electrons with an average energy of 30 eV (Cravens and Dalgarno 1978). The electrons lose their energy by exciting, dissociating and ionizing H_2 . The electrons which excite the molecular hydrogen are responsible for the generation of ultraviolet photons. These electrons excite the Lyman band (90-170 nm) and Werner bands (90-130 nm) of H_2 . When the H_2 de-excites ultraviolet photons are radiated. The model derived in this section includes the a correction term that arise due to the Prasad Tarafdar Process. Increasing the number of ultraviolet photons causes there to be an additional amount

of charge. Thus, it is necessary to add another term to the rate equation of fractional ionization.

$$\frac{dn_e}{dt} \text{ Prasad-Tarafdar} = \sum_k \frac{p_k \zeta n_k}{(1 - \omega)} \quad (9.52)$$

This term must be added to the rate equation described by (9.3.6) to account for the number of electrons added to the cloud by the cosmic ray induced photons.

$$\frac{dn_e}{dt} = \zeta n + \sum_k \frac{p_k \zeta n_k}{(1 - \omega)} - \sum_j \alpha_j n_{m_j^+} n_e - \sum_i \alpha_{ir} n_{M_i^+} n_e \quad (9.53)$$

When the system reaches steady state equilibrium, then the rate is set equal to zero.

$$\frac{dn_e}{dt} = 0. \quad (9.54)$$

The equation can now be rearranged into the following form:

$$\zeta n + \sum_k \frac{p_k \zeta n_k}{(1 - \omega)} = \sum_j \alpha_j n_{m_j^+} n_e + \sum_i \alpha_{ir} n_{M_i^+} n_e \quad (9.55)$$

It is possible to simplify these equations by assuming the rate constant dissociative recombination of electrons with molecule, associative recombination and charge transfer are equal. This assumption is valid give the order of these coefficients are of equal magnitude. Hence, assume as was done in the previous section that:

$$\alpha_j = \alpha, \quad (9.56)$$

$$\alpha_{ri} = \alpha_r, \quad (9.57)$$

and

$$\beta_i = \beta. \quad (9.58)$$

It is convenient to let

$$C\zeta = \sum_k \frac{p_k \zeta n_k}{(1 - \omega)} \quad (9.59)$$

Notice in this case the α s and the β s are independent of the the subscripts i and j.

Thus it is possible to substitute (9.56), (9.57) and (9.58) into (9.55) to obtain.

$$\zeta n + C\zeta = \alpha \sum_j n_{m_j^+} n_e + \alpha_r \sum_i n_{M_i^+} n_e. \quad (9.60)$$

Substituting (9.28) and (9.29) into (9.60) yields

$$\zeta n + C\zeta = \alpha n_{m^+} n_e + \alpha_r n_{M^+} n_e \quad (9.61)$$

$$n_e = \frac{n\zeta + C\zeta}{\alpha \sum n_{m_j^+} + \alpha_r \sum n_{M_i^+}}. \quad (9.62)$$

The rate for all positive charged molecular ions is similar to equation (9.3.16). When the term for the cosmic ray induced ionization added formulated as follows we obtain the following expression

$$\frac{dn(m_j^+)}{dt} = \gamma_j \zeta n - \alpha_j n(m_j^+) n_e + \sum_k \frac{\gamma_j p_k \zeta n_k}{(1 - \omega)} - \sum_i \beta_i n_{M_i} n_{m_j^+}. \quad (9.63)$$

The steady state condition occur when the ionization rates are equal to the recombination rates.

$$\frac{dn_{m_j^+}}{dt} = 0. \quad (9.64)$$

Substitute (9.64) into (9.63) to yield:

$$\gamma_j \zeta n - \alpha n (m_j^+) n_e + \sum_k \frac{p_k \zeta \gamma_j n_k}{(1-\omega)} - \beta \sum_i n_{M_i} n_{m_j^+} = 0. \quad (9.65)$$

Rearranging (9.65) gives

$$\gamma_j \zeta n + \sum_k \frac{p_k \zeta \gamma_j n_k}{(1-\omega)} = \alpha n_{m_j^+} n_e + \beta n_M n_{m_j^+} \quad (9.66)$$

and

$$\alpha n_{m_j^+} n_e + \beta n_M n_{m_j^+} = \gamma_j \zeta n + \sum_k \frac{p_k \zeta \gamma_j n_k}{(1-\omega)}. \quad (9.67)$$

Now factor out $n_{m_j^+}$ and solve for $n_{m_j^+}$:

$$n_{m_j^+} = \frac{\gamma_j \zeta n + \frac{\sum_k p_k \zeta \gamma_j n_k}{(1-\omega)}}{\alpha n_e + \beta n_M}. \quad (9.68)$$

Now sum over j

$$\sum_j n_{m_j^+} = \frac{\sum_j \gamma_j \zeta n + \frac{\sum_k p_k \zeta \gamma_j n_k}{(1-\omega)}}{\alpha n_e + \beta n_M}. \quad (9.69)$$

Note that the we sum over the gammas and use the fact the $\sum_i \gamma_i = 1$. This gives a solution for the total number of molecular ions.

$$n_{m^+} = \frac{\zeta n + \frac{\sum_k p_k \zeta \gamma_j n_k}{(1-\omega)}}{\alpha n_e + \beta n_M}. \quad (9.70)$$

Now substitute (9.59) into (9.76)

$$n_{m^+} = \frac{\zeta n + C \zeta}{\alpha n_e + \beta n_M}. \quad (9.71)$$

This is the expression for the steady state abundance of n_{m^+} . This will be used to obtain a value for the fractional ionization, but it is necessary to rewrite (9.62)

$$n_{M^+} = n_e - n_{m^+}. \quad (9.72)$$

Substitute (9.28) and (9.38) into (9.62) to obtain another expression for the fractional ionization.

$$n_e = \frac{n\zeta + C\zeta}{\alpha n_{m^+} + \alpha_r n_{M^+}}. \quad (9.73)$$

Multiply both sides by $\alpha n_{m^+} + \alpha_r n_{M^+}$

$$n_e \alpha n_{m^+} + n_e \alpha_r n_{M^+} = n\zeta + C\zeta \quad (9.74)$$

Now substitute the charge conservation equation (9.4.20) for n_{M^+}

$$n_e \alpha n_{m^+} + n_e \alpha_r (n_e - n_{m^+}) = n\zeta + C\zeta. \quad (9.75)$$

Now rearrange (9.75) to obtain

$$(\alpha - \alpha_r) n_e n_{m^+} + \alpha n_e^2 = n\zeta + C\zeta. \quad (9.76)$$

Next substitute (9.71) for n_{m^+} .

$$(\alpha - \alpha_r) \frac{\zeta n + C\zeta}{\alpha n_e + \beta n_M} n_e + \alpha n_e^2 = n\zeta + C\zeta. \quad (9.77)$$

Multiply both sides of (9.4.25) by $\alpha n_e + \beta n_M$ to produce the following equation.

$$(\alpha - \alpha_r)(\zeta n + C\zeta) + (\alpha n_e + \beta n_M) \alpha_r n_e^2 = (\zeta n + C\zeta)(\alpha n_e + \beta n_M) \quad (9.78)$$

We may rearrange this equation to obtain:

$$\alpha \alpha_r n_e^3 + \alpha_r \beta n_M n_e^2 = (\zeta n + C\zeta)(\alpha n_e + n_M \beta + \alpha_r - \alpha). \quad (9.79)$$

Now divide both sides of (9.79) by $\alpha\alpha_r$.

$$n_e^3 + \frac{n_e^2 n_M}{\alpha\beta} = (\zeta n + C\zeta) \left(\frac{n_e}{\alpha_r} + \frac{\beta n_M}{\alpha\alpha_r} + \frac{1}{\alpha} - \frac{1}{\alpha_r} \right) \quad (9.80)$$

and rearrange to yield:

$$n_e^3 + \frac{n_e^2 n_M}{\alpha\beta} - (\zeta n + C\zeta) \left(\frac{n_e}{\alpha_r} + \frac{\beta n_M}{\alpha\alpha_r} + \frac{1}{\alpha} - \frac{1}{\alpha_r} \right) = 0. \quad (9.81)$$

Expand (9.81) and this will give the equation

$$n_e^3 + \frac{n_e^2 n_M}{\alpha\beta} - (\zeta n + C\zeta) \left(\frac{n_e}{\alpha_r} \right) - (\zeta n + C\zeta) \left(\frac{\beta n_M}{\alpha\alpha_r} \right) - (\zeta n + C\zeta) \left(\frac{1}{\alpha} \right) + (\zeta n + C\zeta) \left(\frac{1}{\alpha_r} \right) = 0. \quad (9.82)$$

Note that the second, fourth and fifth terms are small. This is due to the fact that $\alpha \approx 10^{-9}$ $\alpha_r \approx 10^{-11}$ are small. The quotient $\frac{1}{\alpha\alpha_r}$ is therefore of the order 10^{-20}

$$n_e^3 + \frac{n_e^2 n_M}{\alpha\beta} - (\zeta n + C\zeta) \left(\frac{\beta n_M}{\alpha\alpha_r} \right) = 0. \quad (9.83)$$

rearrange this and take the cube root of both sides

$$n_e \approx \sqrt[3]{\frac{\beta\zeta n n(M)(1+C)}{\alpha_r \alpha}} \quad (9.84)$$

Substitute (9.59) into (9.84) to yield an expression for the fractional ionization due to cosmic ray induced photoionization.

$$n_e \approx \sqrt[3]{\frac{\beta\zeta n n(M) \left(1 + \sum_k \frac{p_k n_k}{(1-\omega)}\right)}{\alpha_r \alpha}} \quad (9.85)$$

This is the correction to the Oppenheimer model which includes the cosmic ray induced ionization. We may now convert equation (9.85) into the fractional ionizations

and fractional abundances.

$$X_e \approx \sqrt[3]{\frac{\beta \zeta X_M (1 + \sum_k \frac{p_k n X_k}{(1-\omega)})}{\alpha_r \alpha n}} \quad (9.86)$$

The species with the largest value of $p_k n X_k$ is carbon monoxide. The efficiency is equal to 5 (Farquhar and Miller 1993) while the relative abundance of CO is 10^{-4} . The UMIST Ratefile incorporates 60 reactions which contain the cosmic-ray induced photons so the summation is over 60 terms . For a number density of 10^3 , a metal relative abundance of 10^{-6} $\beta = 10^{-9}$, $\alpha = 10^{-7}$ and $\alpha_r = 10^{-11}$ Equation (9.4.34) yields a result of 5.5×10^{-6} . The model calculates the result to be 9.0×10^{-7} .

Summary

This chapter has presented 3 approximations for the fractional ionization. The non-metal model will yield reasonable results when the metallic depletion is low. Also, this model would be applicable for regions of space that where populated by Type II stars. The Oppenheimer model would be useful in regions where there might be metallic enhancements. In regions where the cosmic ray induced ionization was large the model derived in this chapter would be expected to be useful.

Chapter 10

A Parameter Study

The mathematical structure of the chemical model described in Chapter 5 suggests that the chemical composition of a molecular cloud should vary as the temperature and density vary. Observations of molecular clouds verify this assumption. This chapter investigates how the variation of temperature and number density systematically affect the solutions of the gas phase model. We will also compare observed abundances in the L134, TMC1 (Taurus Molecular Cloud), The Orion Ridge and Sgr B2 (Sagittarius B2) with abundances computed from the chemical model.

Selection of a Parameter Set

The selection of a realistic parametric grid is based on observations of giant molecular and dark molecular clouds (see Table 2). Values of temperature and density were selected to bound the values listed in Table 2. The grid was constructed by taking the Cartesian product of the temperatures 10 K, 25 K, 50 K, 100 K, 200 K and 1000 K and the densities 10^2 cm^{-3} , 10^4 cm^{-3} , 10^6 cm^{-3} and 10^8 cm^{-3} . The chemical model was integrated over this parametric domain to obtain solutions.

T(K) vs. $n(\text{cm}^{-3})$	10^2	10^4	10^6	10^8
10	H	CO	CO	CO
25	H	CO	CO	CO
50	H	CO	CO	CO
100	H	CO	CO	CO
200	H	CO	CO	CO
1000	H	H_2O	H_2O	H_2O

Table 16: Third Most Abundant Species

Results on Grid Boundary

Molecular hydrogen and helium are the most abundant species in the cloud. Generally, when calculations are done for most dark cloud models we find that CO is the third most abundant species. However, for certain temperatures and number densities this is not true. Inspection of Table 15 indicates that when the number density is 100 cm^{-3} the third most dominant species is H . Also notice that when $T=1000\text{K}$ and n is greater than 100 the third most abundant species is H_2O .

Effects of low number densities on the abundance

The large abundance of atomic hydrogen, for small values of n , can be explained by approximating the rate equation of molecular hydrogen. Molecular hydrogen is ionized by cosmic-rays, the abundance of H_2 decreases as:

$$\frac{dn_{H_2}}{dt} = -\zeta n_{H_2}, \quad (10.1)$$

where, $\zeta = 1.2 \times 10^{-17} \text{ sec}^{-1}$.

Molecular hydrogen is created by the surface reaction on grains. The rate for this process is:

$$\frac{dn_{H_2}}{dt} = 2k_g n_H n \quad (10.2)$$

where k_g is the rate coefficient ($k_g = 9.5 \times 10^{-18} \text{cm}^3 \text{sec}^{-1}$).

Combining both the ionization rate and production rate gives the rate equation for molecular hydrogen.

$$\frac{dn_{H_2}}{dt} = 2k_g n_H n - \zeta n_{H_2} \quad (10.3)$$

The number density is defined to be:

$$n = 2n_H + 2n_{H_2}. \quad (10.4)$$

When the abundance of molecular hydrogen is much greater than atomic hydrogen we can assume $2n_{H_2} = n$. This implies we can rewrite the differential equation as

$$\frac{dn_{H_2}}{dt} = 4k_g n_H n_{H_2} - \zeta n_{H_2}. \quad (10.5)$$

At equilibrium

$$\frac{dn_{H_2}}{dt} = 0. \quad (10.6)$$

Now substitute 10.6 into 10.5 and rearrange:

$$4k_g n_H n_{H_2} = \zeta n_{H_2}, \quad (10.7)$$

note n_{H_2} cancelis and division by the number of hydrogen nuclei yields:

$$X_H = \frac{\zeta}{4nk_g}. \quad (10.8)$$

Thus, the fractional abundance of n_H is inversely proportional to the number density.

We can determine the upper bound for n by letting

$$X_H > X_O. \quad (10.9)$$

We may substitute (10.8) into the inequality. X_H . We can now write:

$$\frac{\zeta}{nk_g} > X_O, \quad (10.10)$$

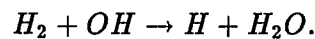
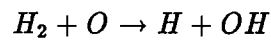
and solve for n .

$$\frac{\zeta}{X_O k_g} > n. \quad (10.11)$$

Thus when n is less than 400.0 cm^{-3} the atomic hydrogen will be the third most abundant species. This result is obtained by substituting $7.3 \times 10^{-4} \text{ cm}^{-3}$ (the elemental abundance of oxygen) into the inequality for the relative abundance of hydrogen and solving for n .

Effects of temperatures above 300 K

Inspection of Table 16 shows that for temperature of 1000 K and a number density greater than 100 cm^{-3} the third most abundant species is H_2O . Increasing the temperature leads to an increase in the rate coefficient for the reactions.



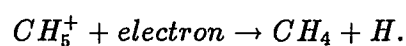
This makes H_2O a good probe cloud temperature.

Analysis of Variance of the Grid

This section considers the case where carbon monoxide is the third most abundant species at steady state. An additive analysis of variance model is used on each species to determine which species are sensitive to number density, temperature and/or both. The logarithms of various species were computed and an analysis of variance was used to detect differences in magnitude. Two null hypothesis were tested, H_{o_1} : (the temperature had no effect on abundance) and, H_{o_2} : (number density had no effect on abundance). Rejection levels were set so the probably of making a type one error (the probably of rejecting the null hypothesis when it is true) was 0.001.

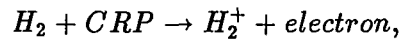
The results from the analysis of variance suggest that the abundance of electrons is dependent on the number density and the temperature. The fact that electrons are dependent on the number density was established analytically in chapter 9. Electron abundance is positively correlated with temperature because virtually all electrons recombine via dissociative recombination. The dissociative recombination rate coefficient is inversely proportional to the square root of the temperature. Thus, an increase in temperature will decrease the recombination rate.

The analysis of variance points out that methane was only dependent on the variation of the temperature. The data suggests that as temperature increases the abundance of methane decreases. This is because the major pathway of methane production is dissociative recombination.

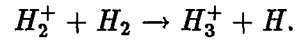


Because electrons recombine at a slower rate as temperature is increased, the production of methane will decrease with increasing temperature.

The analysis of variance model shows a significance inverse dependence of the ion H_3^+ with the number density. This can be explained by approximating the rate equation for the abundance of H_2^+ . H_2^+ is created by the reaction:



and destroyed by the reaction:



Therefore, the rate equation for H_2^+ is:

$$\frac{dn_{H_2^+}}{dt} = -\zeta n_{H_2} + kn_{H_2}n_{H_2^+}. \quad (10.12)$$

The steady state condition is expressed as:

$$\frac{dn_{H_2}}{dt} = 0. \quad (10.13)$$

Substituting (10.13) into (10.12) and rearranging the result yields:

$$\zeta n_{H_2} = kn_{H_2}n_{H_2^+}, \quad (10.14)$$

now divide by n_{H_2} to obtain:

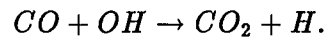
$$kn_{H_2^+} = \zeta. \quad (10.15)$$

We may now divide by the number density n and solve for the relative abundance of H_2^+ :

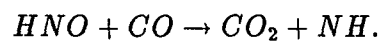
$$X_{H_2^+} = \frac{\zeta}{kn} \quad (10.16)$$

Since virtually all of the H_2^+ reacts with H_2 to produce H_3^+ , we would expect the fractional abundance of H_3^+ to decrease as the number density increases.

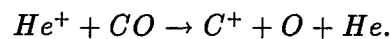
The amount of molecular carbon dioxide CO_2 increases as a function of temperature. When the temperature reaches 100 K the carbon dioxide has abundance on the order of carbon monoxide. This is because the dominant reaction responsible for the creation of CO_2 is:



This is in contrast to the dominant reaction at 10K which is given below:



When the temperature has increased to 100K the reaction with OH is 100 times faster than the reaction involving HNO. These reactions imply that the effect of increasing the abundance of CO_2 will decrease the abundance of CO . Because CO reacts with He^+ via the reaction:



OH as a Probe of Density

Analysis of variance indicates that OH is negatively correlated with density. This indicates that OH would be an acceptable probe for the density. Table 17 illustrates how OH varies over the grid.

T(K) vs. n(cm^{-3})	10^2	10^4	10^6	10^8
10	1.4(-7)	4.4(-8)	4.9(-10)	5.3(-12)
25	1.6(-7)	4.6(-8)	5.2(-10)	5.6(-12)
50	2.2(-6)	4.6(-8)	5.1(-10)	5.3(-12)
100	1.8(-6)	3.1(-8)	3.8(-10)	3.5(-12)
200	1.3(-6)	1.9(-8)	2.1(-10)	5.7(-12)
1000	1.8(-7)	1.3(-9)	1.3(-11)	1.1(-13)

Table 17: This table represents the OH abundances for the grid. *OH decreases as the density increases. The analysis of variance model indicates this trend is significant.* $a(-b) = a \times 10^{-b}$

Comparison of Model with Observations

The observations have been taken from the L134, Taurus Molecular Cloud (TMC1), The Orion Complex and Sagittarius B2 (Sgr B2). It is important to distinguish between the structure of these 4 clouds. The TMC1 and L134 are a quiescent clouds while the The Orion Complex and Sagittarius B2 are active in the sense that they are heated by external sources.

One important measure of the activity of these clouds is the ratio of hydrogen cyanide to that of hydrogen iso-cyanide. This ratio was calculated for the grid and is presented in Table 18.

Observations of TMC1 indicate that this ratio should be approximately unity. However, when regions of the Orion Complex are measured we find a variation in this ratio (Goldsmith et. al. 1981). The variations in the $\frac{HCN}{HNC}$ isomer abundance ratio is correlated with temperature (Irvine 1990). Our gas phase model does not account for high ratios observed in the Orion Hot Core ($\frac{HCN}{HNC} = 200$) or the Orion Extended Ridge ($\frac{HCN}{HNC} = 10$). This is because we model a quiescent cloud. To improve our

T vs. n	10^2	10^4	10^6	10^8
10	2.31	0.552	1.44	2.01
25	1.50	0.402	1.08	2.70
50	0.338	0.355	0.908	2.87
100	0.347	0.362	0.760	2.62
200	0.634	0.868	1.05	2.35
1000	2.90	1.16	1.03	1.00

Table 18: The HCN to HNC Ratio $\frac{HCN}{HNC}$ These results are in agreement with observation for TMC1 and L134 (Goldsmith et. al. 1981)

results it would be necessary to include time dependent effects such as molecules coming off grains.

Taurus Molecular Cloud TMC1

This section will compare the gas phase chemical model with observations of the Taurus Molecular Cloud TMC. TMC is a cloud that does not have any measurable internal sources of energy. Thus we would expect it to be similar to the model of the chemical network that we have constructed. Table 19 list the calculated values verses the observations.

The ratio of carbon to carbon monoxide $\frac{C}{CO}$ is 10^{-5} for the chemical model used in this investigation. The observed values yield a $\frac{C}{CO}$ ratio of 0.1. Inspection Table 19 indicates that most of the carbon is in the form of CO. This fact would account for many of the other species which contain carbon atoms to be in disagreement with observation. The model closely agrees with observations of CO , CS , SO , HCO^+ , SO_2 , NH_3 , C_2H and CH_3CHO .

Species	Calculated	Observed
<i>CO</i>	1.4×10^{-4}	8.0×10^{-5}
<i>C₂H</i>	3.53×10^{-8}	$5 - 10 \times 10^{-8}$
<i>OH</i>	4.4×10^{-8}	3×10^{-7}
<i>CN</i>	9.1×10^{-10}	3×10^{-8}
<i>HCN</i>	3.3×10^{-9}	2×10^{-8}
<i>HNC</i>	6.0×10^{-9}	3×10^{-8}
<i>C₃O</i>	9.9×10^{-12}	2×10^{-10}
<i>C₃N</i>	2.1×10^{-11}	2×10^{-10}
<i>NH₃</i>	6.95×10^{-8}	1×10^{-8}
<i>CH₃OH</i>	1.59×10^{-10}	2×10^{-9}
<i>H₂CO</i>	6.4×10^{-9}	2×10^{-8}
<i>CS</i>	7.4×10^{-9}	1×10^{-8}
<i>OCS</i>	1.5×10^{-11}	2×10^{-9}
<i>SO</i>	1.9×10^{-8}	5×10^{-9}
<i>SO₂</i>	1.6×10^{-8}	1×10^{-8}
<i>HCO⁺</i>	7.7×10^{-9}	2×10^{-9}
<i>CH₃CHO</i>	1.3×10^{-10}	6×10^{-10}
<i>HC₃N</i>	2.8×10^{-10}	6.0×10^{-9}
<i>HC₅N</i>	1.8×10^{-12}	3.0×10^{-9}
<i>HC₇N</i>	1.4×10^{-14}	1.0×10^{-9}
<i>HC₉N</i>	1.0×10^{-16}	3.0×10^{-10}
<i>SiO</i>	5.9×10^{-9}	5×10^{-12}
<i>C₄H</i>	8.9×10^{-10}	$< 2 \times 10^{-8}$

Table 19: Comparison of calculated to observed values for TMC1. The calculations were done for number density = 10^4 and temperature = 10 K. (Observations are adopted from Irvine et. al. 1987)

Species	Calculated	Observed
<i>CO</i>	1.4×10^{-4}	8.0×10^{-5}
<i>C</i>	1.29×10^{-9}	1.0×10^{-6}
<i>CH</i>	1.3×10^{-11}	1.0×10^{-8}
<i>OH</i>	4.4×10^{-8}	8×10^{-8}
<i>CN</i>	9.1×10^{-10}	3×10^{-9}
<i>CS</i>	7.4×10^{-9}	1×10^{-9}
<i>C₂H</i>	8.9×10^{-10}	$< 1 \times 10^{-7}$
<i>C₄H</i>	8.9×10^{-10}	$< 1 \times 10^{-9}$
<i>C₃H₂</i>	2.3×10^{-10}	4×10^{-9}
<i>HCN</i>	3.3×10^{-9}	2×10^{-9}
<i>HNC</i>	6.0×10^{-9}	6×10^{-9}
<i>NH₃</i>	6.95×10^{-8}	2×10^{-7}
<i>CH₃OH</i>	1.59×10^{-10}	4×10^{-9}
<i>H₂CO</i>	6.4×10^{-9}	2×10^{-8}
<i>HCO⁺</i>	7.7×10^{-9}	2×10^{-9}
<i>HC₃N</i>	2.8×10^{-10}	2.0×10^{-10}
<i>HC₅N</i>	1.8×10^{-12}	9.0×10^{-11}
<i>HC₇N</i>	1.4×10^{-14}	$< 2.0 \times 10^{-11}$
<i>CH₃CHO</i>	1.3×10^{-10}	6×10^{-10}
<i>SO</i>	1.9×10^{-8}	2×10^{-8}
<i>SO₂</i>	1.6×10^{-8}	4×10^{-9}

Table 20: Comparison of calculated to observed values for L134. The calculations were done for number density = 10^4 and temperature = 10 K. (Observations are adopted from Irvine et. al. 1987)

L134

The gas phase model is in excellent agreement with observations. Diatomic molecules such as *CO*, *OH*, *CN*, *SO* and *CS*. The model also is in close agreement with for large molecules such as *HCN*, *HNC*, *HC₃N*, *HCO⁺* and *CH₃OH*.

Orion Ridge and Sgr B2

the Orion Ridge and Sgr B2 are example of giant molecular clouds. The Orion Ridge consist of gas and dust with newly formed massive stars which are detectable in the

Species	T=50 n=10 ⁴	Observed
<i>CO</i>	1.4×10^{-4}	8.0×10^{-5}
<i>CH₄</i>	3.2×10^{-8}	8×10^{-7}
<i>C</i>	1.0×10^{-9}	1×10^{-5}
<i>C₂H</i>	4.6×10^{-10}	1×10^{-8}
<i>CN</i>	1.5×10^{-10}	5×10^{-9}
<i>HCN</i>	1.1×10^{-9}	2×10^{-8}
<i>HNC</i>	3.2×10^{-9}	4×10^{-10}
<i>C₃O</i>	9×10^{-14}	3×10^{-11}
<i>NH₃</i>	9×10^{-8}	2×10^{-7}
<i>CH₃OH</i>	4.7×10^{-11}	4×10^{-8}
<i>C₂H₅OH</i>	1.1×10^{-16}	4×10^{-8}
<i>H₂CO</i>	1.6×10^{-9}	$3 - 30 \times 10^{-8}$
<i>CS</i>	4.6×10^{-9}	4×10^{-9}
<i>HCS⁺</i>	1.8×10^{-11}	2×10^{-10}
<i>SO</i>	2.6×10^{-8}	2.0×10^{-9}
<i>HCO⁺</i>	7.7×10^{-9}	2×10^{-9}
<i>CH₃CHO</i>	1.8×10^{-12}	2×10^{-10}
<i>HCl</i>	2.0×10^{-9}	1×10^{-8}
<i>SiO</i>	1.0×10^{-9}	5×10^{-9}
<i>SiS</i>	6.0×10^{-9}	$\times 10^{-12}$

Table 21: Comparison of calculated to observed values for the Orion Ridge. The calculations were done for number density = 10^4 and temperature = 50 K. (Observations are adopted from Irvine et. al. 1987)

infrared (Friberg and Hjalmarsen 1990). The Orion ridge and Sgr B2 are rare in the sense that they have been surveyed. Most GMC have not been measured. Tables 17 and 18 compare computed abundances to the observational values. It should be noted that the calculations have been based on a quiescent dark cloud model.

Values from the grid study which approximated the Orion ridge and Sgr B2 were selected as the computed values. It should be noted that the giant clouds consist of several regions which possess different physical properties.

Species	Calculated $T = 100$ $n = 5.0 \times 10^5$	Observed
C_2H	3.0×10^{-15}	$> 5 \times 10^{-9}$
CN	4.2×10^{-13}	2×10^{-8}
HCN	1.4×10^{-10}	2×10^{-8}
HNC	1.9×10^{-10}	3×10^{-9}
C_3O	1.6×10^{-16}	2×10^{-10}
C_3N	9.3×10^{-17}	$< 2 \times 10^{-10}$
NH_3	2.4×10^{-8}	$1 - 10 \times 10^{-8}$
CH_3OH	4.6×10^{-12}	2×10^{-7}
H_2CO	1.4×10^{-10}	$2 - 10 \times 10^{-8}$
CS	7.7×10^{-12}	1×10^{-8}
HCS^+	3.3×10^{-14}	2×10^{-10}
OCS	1.0×10^{-12}	2×10^{-8}
SO	1.7×10^{-8}	1×10^{-9}
SO_2	2.21×10^{-8}	2×10^{-8}
SiS	1.1×10^{-19}	$0.3 - 2 \times 10^{-10}$
C_2H_5OH	8.0×10^{-18}	3×10^{-9}
HCO^+	7.7×10^{-9}	2×10^{-9}
CH_3CHO	5.0×10^{-14}	1×10^{-10}

Table 22: Comparison of calculated to observed values for the Sgr-B Complex. The calculations were done for number density = 10^6 and temperature = 100 K. (Observations are adopted from Irvine et. al. 1987).

Species	T=10	T=50	T=200
CO	8.6(5)	1.4(4)	1.3(4)
O	2.6(4)	1.2(4)	1.3(4)
C	4.5(5)	2.6(7)	2.3(7)
CH	1.4(7)	7.5(9)	7.0(9)
CH_4	7.3(9)	1.2(8)	4.6(9)
OH	1.4(7)	2.3(6)	1.3(6)
NH_3	7.5(11)	2.2(7)	2.3(7)
H_2O	9.1(8)	4.8(6)	4.4(6)
NO	7.1(9)	8.0(7)	9.3(7)
H_2CO	7.7(9)	3.9(9)	1.5(9)
O_2	2.8(7)	3.7(5)	2.7(5)
SO	1.4(12)	8.6(9)	7.0(9)
CN	6.0(8)	4.2(8)	2.9(8)
CS	2.5(8)	7.2(9)	8.3(10)
HCO^+	2.6(10)	1.3(11)	3.6(7)
SO_2	1.7(15)	1.0(9)	5.3(10)
e^-	8.4(6)	7.2(7)	9.8(7)
H_3^+	2.2(8)	2.0(7)	2.2(7)
H^+	4.2(7)	1.2(8)	3.2(8)
H	1.2(2)	1.2(2)	1.2(2)
CO_2	2.7(12)	4.8(7)	1.3(5)

Table 23: Parameter Study: T=10 K, T=50 K and T=200 K $n=10^2$ $a(b) = a \times 10^{-b}$

Representative results of the Parameter Study

Tables 23, 24 and 25 are representative of the parameter study over the grid.

Species	T=10	T=50	T=200
CO	1.4(4)	1.4(4)	1.3(4)
O	8.6(5)	8.3(5)	1.0(4)
C	1.2(9)	1.0(9)	1.3(9)
CH	1.3(11)	1.7(11)	1.6(11)
<i>CH</i> ₄	7.4(8)	3.2(8)	9.1(9)
OH	4.4(8)	4.6(8)	1.9(8)
<i>NH</i> ₃	6.7(8)	9.0(8)	5.3(8)
<i>H</i> ₂ O	3.3(6)	1.8(6)	1.1(6)
NO	1.6(8)	5.3(8)	4.5(8)
<i>H</i> ₂ CO	6.5(9)	1.6(9)	3.0(10)
O ₂	5.8(5)	6.0(5)	4.2(5)
SO	1.9(8)	2.6(8)	3.3(8)
CN	9.2(10)	1.5(10)	6.6(11)
CS	7.4(9)	4.5(9)	1.1(9)
<i>HCO</i> ⁺	7.7(9)	2.4(8)	5.5(8)
<i>SO</i> ₂	1.2(8)	8.0(9)	4.2(9)
e ⁻	3.2(8)	5.1(8)	8.5(8)
<i>H</i> ₃ ⁺	3.1(9)	3.2(9)	3.0(9)
<i>H</i> ⁺	1.6(10)	2.3(10)	2.2(10)
H	1.2(4)	1.1(4)	1.2(4)
<i>CO</i> ₂	6.4(8)	8.0(7)	1.6(5)

Table 24: Parameter Study: T=10 K, T=50 K and T=200 K $n=10^4$ $a(b) = a \times 10^{-b}$

Summary

The parameter study indicated that at low densities the abundance of atomic hydrogen would be the 3rd most dominant species. An analysis of variance suggested that there were trends that depended on the temperature and number density. An interesting trend was that of an increase in carbon dioxide as temperature increased. The model calculated abundances that closely agree with observed abundances in TMC1 and the L134. Tables 25, 24, and 25 are representative of the results computed in parameter study.

Species	T=10	T=50	T=200
CO	1.4(4)	1.4(4)	1.4(4)
O	8.0(5)	7.8(5)	9.0(5)
C	1.2(11)	9.3(12)	1.0(11)
CH	6.0(14)	8.1(14)	5.5(14)
CH ₄	7.7(8)	4.5(8)	2.7(8)
OH	4.9(10)	5.1(10)	3.3(10)
NH ₃	3.4(8)	3.2(8)	2.0(8)
H ₂ O	1.7(6)	7.3(7)	4.5(7)
NO	1.9(10)	6.4(10)	6.0(10)
H ₂ CO	1.8(9)	3.9(10)	1.4(10)
O ₂	6.2(5)	6.2(5)	5.5(5)
SO	1.2(9)	1.0(8)	1.7(8)
CN	1.7(11)	8.4(13)	4.2(13)
CS	3.6(10)	3.0(10)	7.7(12)
HCO ⁺	2.4(10)	1.0(10)	1.4(9)
SO ₂	3.8(8)	2.9(8)	2.2(8)
e ⁻	1.0(8)	1.6(8)	1.7(8)
H ₃ ⁺	3.3(11)	3.3(11)	3.3(11)
H ⁺	1.7(12)	2.3(12)	2.4(12)
H	1.2(6)	1.2(6)	1.2(6)
CO ₂	7.0(8)	8.2(7)	9.2(6)

Table 25: Parameter Study: T=10 K, T=50 K and T=200 K $n=10^6$ $a(b) = a \times 10^{-b}$

Chapter 11

Conclusions

The UMIST Rate file was used to construct a model of the gas phase chemistry of giant and dark molecular clouds. Steady state solutions were calculated for given temperature, number density, elemental abundance, cosmic-ray ionization rate and dissociative recombination rate for H_3^+ . Temperature and number density were allowed to vary systematically in order to map abundances of trace species. We have made predictions of water, molecular oxygen, carbon monoxide and atomic carbon computed by our gas phase which may be compared with observations by the Submillimeter Wave Astronomy Satellite (SWAS) which is scheduled to be launched by NASA in 1996.

Bistability

Over certain regions of parameter space, it was discovered that bistable solutions existed. Bistable solutions are important because when they are understood they may help us to comment on the history of a molecular cloud. The stable phase a cloud is in is determined by its initial conditions. The bistable solutions are also of interest because of their relation to chaotic phenomena. This study is the first to

discuss bistable phenomenon for a gas phase model for realistic depleted elemental abundances.

Bistability was examined for variations in: chemical abundance, cosmic ray ionization rate, temperature, number density, dissociative recombination rate of H_3^+ , and large molecules. Enhancement of the abundances of carbon, sulphur, silicon, and metals allowed the bistable region to exist in for higher values of number density. Enhancement of the oxygen abundance has the opposite effect. Changing the abundance of nitrogen, phosphorous and chlorine has no substantial affect on the bistability. The inclusion of large molecules in the gas phase model damps out bistable behavior. The bistable region will exist at higher number densities when the cosmic ray ionization is increased.

Chemistry as a Probe of Physical Conditions

The parameter study showed that the chemistry varied greatly over the density and the temperature. Hydrogen was the third most abundant species for number densities less than 400 cm^{-3} . H_2O is the third most abundant species for temperatures above 300 K. For intermediate temperatures, carbon monoxide was the third most abundant species.

The water molecule could potentially be used as a probe of the temperature of the gas. At high temperatures much of the oxygen is in water. The atomic to molecular hydrogen ratio is a possible diagnostic of density. As was shown in chapter 10 the ratio varies with density with atomic hydrogen more abundant at lower densities.

The parameter study showed the abundance of OH decreases as the density increases. This may provide a probe for determining the number density of the cloud.

Molecular oxygen may provide a probe for determining the ionization phase of a region. A measurement of the relative abundance of O_2 that is small would be consistent with region being in the HIP. The SWAS satellite will measure the abundance of molecular oxygen.

The Model of Interstellar Clouds

The gas phase model abundances compared well with those observed in the L134 and The Taurus Molecular Cloud. The ratio of hydrogen cyanide and hydrogen isocyanide for both the The Taurus Molecular Cloud and the L134 was near unity which corresponds to observations.

The chemical model predicts the abundance of several important diatomic molecules within a factor of 2 for L134. The model also is in reasonable agreement with observations taken from TMC1.

Overall we conclude that the model is a useful tool for understanding interstellar clouds. It makes predictions of abundances which may be observed. It also helps us to infer the physical conditions in these clouds. The discovery of bistable solutions in interstellar cloud models is an exciting time in astrophysics. We do not yet have a full understanding of the implications of this discovery, but that understanding will likely also lead to a greater understanding of molecular clouds.

References

- Adams, N. G. and Smith, D. 1988, in *Rate Coefficients in Astrochemistry*.
- Allamandola, L. J. Tielens, A. G. M. and Barker, J. R. 1985, *Ap. J. (letters)* **290**, L25.
- Bates, D. R. and Spitzer, L. 1951, *Ap.J.* , **113** 441.
- Bates, D. R. 1986a, *J.Chem.Phys.* **85**, 624.
- Bates, D. R. and Morgan, W. L. 1987, *J. Chem. Phys.* **87**, 2611.
- Black, J. H. and Dalgarno, A. 1977, *Astrophysical Journal Supplement Series* **34**, 305.
- Brown, R. L. 1977, *Nature*, **270**, 39.
- Brown, R. D. and Rice, E. 1986, *MNRAS* **223**, 405.
- Canosa, A. , Gomet, J. C., Rowe, J. B. and Queffelec, J. C. 1992, *J. Chem. Phys.* **97(2)**, 1028.
- Carlson, T. R. and Roberts, M. J, 1972, *Molecules in Astrophysics*, Academic Press.
- Cowsik, R. and Price, P. 1971, *Physics Today* **24**, No. 93.
- Cravens, T. and Dalgarno, A. 1978, *Ap.J.* **219** , 750.
- Dangarra, J.J., Bunch, J.R., Moler, C.B. and Stewart, G.W. 1979, **LINPACK Users' Guide**, SIAM, Philadelphia.
- Dalgarno, A. and Lepp. S. 1984, *Ap. J.* **287**, 47.

- Dalgarno, A. and Lepp S. 1988a, *Ap. J.* **32.**, 553.
- Dalgarno, A. 1975, in *Frontiers of Astrophysics* ed. Avert, E. H.
- Duley, W. W. and Williams, D. A. 1984, *Interstellar Chemistry*.
- Duley, W. W. and Williams, D. A. 1986, *MNRAS* **223**, 117.
- Eddington, A. S. 1926, *Proc. Roy. Soc A* **111**, 424.
- Friberg, P. (1984), *Ast. Ap.* **132**, 265.
- Farquhar P. R. A, and Miller T. J., 1993, Ref CCP7 News Letter No.18, 6-15.
- Farquhar P. R. A., Millar T. J., and Herbst, E. 1990 *MNRAS* **269**, 641-648.
- Fukui, Y. and Hayakawa, S. 1981, *International Cosmic Ray Conference* .
- Greenberg J. M. 1989, in *Evolution of Interstellar Dust and Related Topics* . eds. A. Bonnet. J. M. Greenberg. S. Aiello (Amestrdam: North Holland) p. 5-52
- Goldsmith, P. F. 1987, in *Interstellar Process*, eds. Hollenbach, D. J., and Thronson, H. A. Jr. (Dordrecht: D.Reidel).
- Gredel, R., Lepp S. and Dalgarno, A., *Ap. J.*, **323**, L137-L139.
- Graff, M.M. 1990, in *Molecular Astrophysics*. ed. Hartquist, T.W. p. 259-272.
- Genzel R., Watson, D. M., Crawford, M. K, and Townes C. H. 1985, *The Astrophysical Journal* **243** 817-826.
- Herbst E. and Leung C. M. 1989, *Astrophys. J. Suppl. Ser.* **69**, 271.
- Herbst, E. 1973, *Astrophys. J. Suppl.* **53**, 41.
- Herbst, E. and Klemperer, W. 1973, *ApJ.*, **185**, 505.
- Herbig, G. H. 1970, *Ap. J.* **162**, 557.
- Hindmarsh A. C. *Odepack, A Systematized Collection of ODE Solvers*, **Scientific**

Computing, R. S. Stepleman et. al. (eds.), North-Holland, Amsterdam 1983. pp. 55-64.

Hirschfelder, J.D. 1941, *J. Chem. Phys.* **9**, 645.

Kramers, H. A. and ter Harr, D. 1946, *Bull. Astr. Inst. Neth.*, **10**, nr. 371.

Jaffe, D. T., Harris, A. I., Silber, M., Genzel, R. and Betz, A. L. 1985, *Ap. J.*, **290**, L59-L62. Jura, M. 1987, in *Interstellar Process*, eds. Hollenbach, D. J., and Thronson, H. A. Jr. (Dordrecht:D.Reidel).

Lang, K. R., 1992, *Astrophysical Data: Planets and Stars* Springer-Verlag.

Larsson, 1995, Private Communication.

Le Bourlot, J., Pineau des Forets, G., Roueff, E. and Schike, P. 1993, *Ap J*

Leger, A. and Puget. J. L. 1984, *Astr. Ap.* **137** L5. , 416, L88.

Lepp S.H., 1992 P.D.Singh(ed.) *Astrochemistry of Cosmic Phenomena*, 471-475.

Lepp, S., Dalgarno, A., and Sternberg, A. 1986, *Ap. J.* **321** , 383.

Leung, C. H., Herbst, E. and Huebner, W. F., 1984, *ApJ. Suppl.***56**, 231.

Litvak M. M. 1970. *Non-Equilibrium Process in the Interstellar Medium Wiley and Sons* (London and New York).

Merrill 1934 *Pub.A.S.P.* **46**, 206.

Millar, T. J. and Freeman, A. 1984a. *MNRASS*, **207**, 405.

Millar, T. J. and Freeman, A. 1984b. *MNRASS*, **207**,425.

Millar, T. J. 1990 T.W.Hartquist(ed.), *Molecular Astrophysics*, 115-131.

Millar, T. M., Rawlings, J. M. C, Bennett, A., Brown, P. D., and Charnley, S. B, 1991 *Astro. Astroph. Suppl. Ser.* **87**, 585-619.

- Omont, A. 1986, *Astr. Ap.* **164**, 159.
- Oppenheimer, M. and Dalgarno, A, . 1975, *ApJ.* **192**, 1974.
- Petzold L. R. *Automatic Selection of Methods For Solving Stiff and Non-stiff Systems of Ordinary Differential Equations*, **SIAM J. Sci. STAT. Comput.** **4** 1983. pp. 136-148.
- Phillips, T.G. and Huggin, P.J. 1981, *Ap. J.* **251**, 533.
- Pineau des Forets, R. Roueff and D. R. Flower 1992 *MNRAS* **258**, Short Communications, 45p-47p.
- Prasad, S. S. and Huntress, W. T. 1980a, *Astroph. J. Suppl.*, **43**, 1.
- Prasad, S. S. and Huntress, W. T. 1980b, *Astroph. J.* **239**, 151.
- Prasad, S. S., and Tarafdar, S. P. 1983, *Ap. J.* **267**, 603 .
- Prasad, S. S, Tarafdar, S. P, Villere, K. R. and Huntress, W. T, Jr. 1987, in *Interstellar Process*, eds. Hollenbach, D. J. and Thronson, H. A. Jr. (Dordrecht:D.Reidel).
- Press, W. H., Teukolsky S. A., Vetterling, W. T. and Flannery, B. P. 1991 *Numerical Recipes in Fortran* *Cambridge University Press*
- Scott, S. 1989, *New Scientist*, **2** December, 53D.
- Scoville, N. Z. Solomon, P. M. and Penzias, A. A. 1975, *Ap.* **J201**.
- Shalabiea, O.S. and Greenberg, J.M. Greenberg 1994, *A and A*.
- Shaver, P. A. 1976, *Astr. Ap.* **49** 149.
- Solomon, P. M. and Klemperer, W. 1972, *Ap. J.* **178**, 389.
- Spitzer, L. 1968, "Diffuse Matter in Space" (Interscience, New York).
- Sternberg, A., Dalgarno, A., and Lepp, S. 1987, *Ap. J.*, **32**, 383.

- Stief L. J., Donn, B., Glicker, S., Gentie.,E. P., and Mental J. E. 1972, *Ap. J.*, **171** 21.
- Suzuki, H. 1979, *Prog. Theor, Phys*, **62**, 936.
- Swade, D. A. (1987), Ph. D. Dissertation, University of Mass. .
- Swings, P. and Rosenfeld, L. 1937, *ApJ*. **86**, 483.
- Thompson, J. M. T. 1982, *Instabilities and Catastrophes in Science and Engineering*. John Wiley and Sons.
- Vetterling, W. T., Press, W. H., Teukolsky, S. A. and Brian, B. P. in 1993, *Numerical Recipes [Fortran] Second Edition* (Cambridge University Press).
- Weinreb, S., Barrett, A. H., Meeks, M. L. and Henry, J. C, *Nature* **200**, 829 (1963).
- Weinreb, S. Technical Report 412, Research Laboratory of Electronics, M. I. T. 1963.
- Zwillinger 1992 in *Handbook of Differential equations* (Academic Press Inc. : Boston) page 16.
- Ziurys, L. M. and Turner, B. E. (1986), *Ap. J. Lett.*) **302**, L31.